TIME-RESOLVED FLUORESCENCE STUDY OF THE UPPER GI TRACT

DEVELOPMENT AND APPLICATION OF TIME-RESOLVED FLUORESCENCE SPECTROSCOPY ANALYSIS WITH SPECIMENS OF THE UPPER GI TRACT

By:

MICHELLE L. LEPALUD, B.Sc.

A Thesis Submitted to the School of Graduate Studies In Partial Fulfillment of the Requirements for the Degree Master of Applied Science

McMaster University

MASTER OF APPLIED SCIENCE (2012) McMaster University
(Biomedical Engineering) Hamilton, Ontario

TITLE: Development and Application of Time-Resolved Fluorescence Spectroscopy Analysis with Specimens of the Upper GI Tract

AUTHOR: Michelle L. LePalud, B. Sc. (University of Guelph)

SUPERVISOR: Professor Qiyin Fang

NUMBER OF PAGES: XIII, 133

ABSTRACT

Current gold standard practices for the diagnosis of tissue disease involve invasive tissue biopsies subjected to a time consuming histopathological examination process. An optical biopsy can offer a non-invasive diagnostic alternative by exploiting the properties of naturally occurring light-tissue interactions. A time-resolved fluorescence spectroscopy instrument (355 nm excitation) has previously been developed by our lab to capture the fluorescence response of gastrointestinal tissue (370-550 nm in 5 nm increments, 25 ns at 1000 ps/pt). Measurements were conducted ex-vivo during routine upper gastrointestinal tract biopsies on duodenum, antrum, stomach body, and esophageal tissue. The work currently presented is focused on protocol development for tissue handling, measurement collection, clinical data management, fluorescent decay modeling using Laguerre based deconvolution, instrument performance evaluation, and k-means based classification.

Descriptive parameters derived from spectral (total signal intensity) and temporal (lifetime and Laguerre polynomial coefficients) analysis were used to evaluate the data. It was found that data were only compromised when the total signal intensity for the peak wavelength 455 nm fell blow 19.5 V·ns. The data did not exhibit any signs of photobleaching or pulse width broadening that would have otherwise distorted the lifetime from its true fluorescence response. Data for diseased tissue were limited so the clinical diagnosis was used to classify normal duodenum tissue from normal esophageal tissue. Over 400 pairs of parameters demonstrated k-means can identify duodenum tissue with 87.5 % sensitivity and 87.5 % specificity or better. With some dimensional axis transformations these results could be improved. The lifetimes are not factors here but the relative intensity and decay shape were. Protocols can be applied to diseased or other tissue types with little adaptation. Just a single set of parameters may hold the key to help surgeons choose optimum locations for traditional biopsies or perhaps one day replace them altogether.

ACKNOWLEDGEMENTS

The supervision and guidance granted by Dr. Qiyin Fang has provided me with invaluable experience that I will carry forward into the workforce and as I move through life. His superior knowledge of clinical biophotonics research in both the United States and Canada has taught me how to approach any biomedical problem from all angles. This includes viewing problems and solutions in the eyes of not just the scientific engineer but of the patient and clinician as well. I have developed a sound appreciation for the time and patience it takes to develop such cutting edge technology. With that said there are many people I would like to thank for assisting me personally with my research.

First and foremost, this research would not be possible without collaboration from Dr. Frances Tse, MD and Associate Professor in the Division of Gastroenterology. A special thank you goes out to Dr. Joesph Hayward and Dr. Hubert de Bruin for serving on my committee. Several students have assisted with the data collection including Mr. Mowly Krishnamoorthy, Mr. Derek Cappon, and Ms. Zhaojun Nie. Mr. Peter Jonasson, technologist at the Department of Engineering Physics, was there to get us back up and running when the instrument experienced a major electronic circuit board failure.

Lastly, I thank my parents for their unconditional love and support during my pursuit for higher education. They have made many sacrifices to provide my brother and I with access to post secondary education. To all my friends, family, and coworkers, it's been quite the journey. Thank you for adding balance and perspective to my life. It is a privileged to have had this opportunity and I would not be standing where I am today without you all.

TABLE OF CONTENTS

LIST OF FIGURES vii

LIST OF TABLES xi

LIST OF SYMBOLS, ACRONYMS, AND ABBREVIATIONS xii

CHAPTER 1: INTRODUCTION **1**

1.1: Clinical Relevance 1

1.2: Optical biopsy and its Application to Address the Clinical Problem 3

1.3: Instrumentation 8

1.4: Signal Deconvolution 14

1.5: Laguerre Expansion Technique – Basic Theory 17

1.6: Current Work 20

REFERENCES 23

CHAPTER 2: METHODS **26**

2.1: Clinical Procedures 27

2.1.1: Research Ethics *27*

2.1.2: Clinical Data Collection *29*

2.2: Data Processing 34

2.2.1: Pre-Processing and Laguerre Deconvolution *34*

2.2.2: Data Management *38*

2.3: Data Analysis 40

2.3.1: Overview *40*

2.3.2: Hypothesis Testing *42*

2.3.3: Statistical Methods Required to Compare Individual Parameters *44*

2.3.4: Classification Methods *46*

2.3.5: K-Means *49*

REFERENCES 54

CHAPTER 3: DATA EVALUATION **56**

3.1: Clinical Results 57

3.2: Data Assessment 59

3.2.1: Amplitude Saturation *63*

3.2.2: Lower Signal Detection Limits *67*
3.2.3: Photobleaching and Repeated Measurements *76*
3.2.4: Increased Fluorescence Intensity during Shorter Wavelengths *79*
3.3: Results of Data Evaluation 83
REFERENCES 93
CHAPTER 4: RESULTS AND DISCUSSION 94
4.1: Patient Averages 95
4.2: K-means 101
REFERENCES 112
CHAPTER 5: CONCLUSION 113
REFERENCES 119
APPENDIX A: Operation of the TR-FS Instrument for Clinical Study 120
APPENDIX B: Sample Note Collection 121
APPENDIX C: α Calculation 122
APPENDIX D: Values for Figures 4.2 and 4.3 124
APPENDIX E: Results of the Lilliefors Normality Test 128
APPENDIX F: Matlab Code for K-means Classification Using GI Data 129

LIST OF FIGURES

Figure 1.1: Anatomic Regions of the Stomach. This Figure was published in Shackelford's surgery of the alimentary tract, Vol. II, Zuidema GD, Yeo CJ (editors), Anatomy and physiology of the stomach, Page 3, Copyright Elsevier (2002). [2], With Permission. 2

Figure 1.2: AOTF TR-FS Instrument Diagram, Figure 1.3 from Reference [25]. The acronyms and parts are listed in Table 1.1. 11

Figure 1.3: TR-FS system used for ex-vivo clinical data collection. All the contents except for the computer monitor, keyboard, fiber probe and stand in Figure 1.2 fit inside a moveable cart of size 3.5' x 2' x 2'. The fiber probe delivers excitation light through a single fiber (600 μm core diameter) that is surrounded by a ring of 12 (200 μm core diameter) collection fibers. Shown inside the cart are the oscilloscope with built in computer (1), pulse generator (2), MCP-PMT (3), an uninterruptible power supply (4), AOTF spectrometer (5), and the laser with fiber coupling (6). 12

Figure 1.4: The first five Laguerre functions for $\alpha = 0.97$ at 25 ps/pt sampling rate. 19

Figure 2.1: Flowchart for the processing of the tissue fluorescence response collected when the laser has been fired on one tissue spot. The data is averaged to reduce signal noise and truncated to increase processing speed during Laguerre deconvolution. The final result is a set of seven descriptive parameters to be used during tissue classification. 35

Figure 2.2: An example is taken from Patient 15 at 440 nm where the α value of 0.96 creates three obvious inflection points in the decay curve compared to when α was fixed at 0.97. 37

Figure 2.3: The Squared Euclidean and City-Block "Manhattan" centroid to point distance calculations. 51

Figure 3.1: Time-domain and spectral data for paper fluorescence. On the left, the time-domain data are plotted for all 37 wavelengths. On the right is the area under each time-domain curve plotted as a function of wavelength. 61

Figure 3.2: Time-domain (left) and spectral data (right) for P16 body tissue. One data set (T4) was chosen to represent the time-domain data for all wavelengths. Each normalized spectral data set typically has complete overlap with one another, except sometimes during shorter wavelengths as with this sample here. The GI data plotted has a shape similar to the fluorescence by the paper sample in Figure 3.1. 61

Figure 3.3: Patient 6 body tissue time-domain (left) and spectral data (right). In P06, some of the data is distorted (ex. T3) by the instrument's jitter when collecting the data as indicated by the jumps in observed fluorescence signal. Also, the peak wavelength was found to be blue shifted 5 nm and was corrected during the re-calibration process. 62

Figure 3.4: Patient 4 represents most of the data from Patients 2 to 6. There was no consistency in the instrument's ability to measure incoming signal as the normalized spectral data do not overlap. 63

Figure 3.5: Saturation of the instrument by a strong signal is reviewed using P13 as an example. A) T1 maximum signal is nearly four times greater than the other data collected. B) When normalized, the change in fluoresce observed across all wavelengths is maintained. C) The time-domain data is compared between T1 and T5 at three different wavelengths 435 nm, 455 nm, and 475 nm. D) Signal broadening is not observed when the data is normalized in the time-domain. 65

Figure 3.6: Simulated signal with PMT saturation. The saturated signal decays much slower (5 ns) than what an expected GI signal does (2.6 ns).....66

Figure 3.7: Patient 14 has a data set where background noise is dominant. SNR at 455 nm is 11 dB. The space below the zero mark in the time-resolved data (left) makes a negative contribution to the spectral integration while the space above the zero line is positive. The steady-state data (right) have three negative I_λ at I_{380}, I_{385}, and $I_{\lambda 525}$. 68

Figure 3.8: Patient 25 as an example of a weak data set. The SNR at 455 nm (left) is 19 dB. Steady-state information (right) is not a smooth curve but rather erratic and the weak signal is enough to make the I_λ positive at all wavelengths. 69

Figure 3.9: Patient 7 duodenum spectral data where T4, T5, and T6 are consecutive measurements on the same spot location but taken at two different voltages. Some changes in the shorter wavelengths are reflected in the normalized data after the third measurement (T6). This spot also shows increased fluorescence from 370-455 nm and visible absorption around 415 nm when compared to three other spots on the specimen (T1-T3).....77

Figure 3.10: Patient 7 esophagus spectral data where T1 and T2 are consecutive measurements on the same spot at the same PMT voltage (2200 mV). The variations depicted in the above spectral shapes between 435-470 nm are commonly found in other patients that do not have any spot locations repeated. 78

Figure 3.11: All of the P15 data sets show a 20% increase in fluorescence around 400 nm when compared to P08. 80

Figure 3.12: Patient 7 duodenum lifetimes are plotted with the averages of all tissue A ± 1 SD (N = 132). Data sets T4, T5, and T6 show increased fluorescent signals in Figure 3.9 when compared to T1-T3 but for the most part their lifetimes are all within the ± 1 SD of the averages. 82

Figure 3.13: Average lifetimes for data sets with increased fluorescence (black circles) are greater than those without (blue x) but overlap within ± 1 SD. 82

Figure 3.14: Signal to noise ratio and extracted lifetime relationship at 455 nm. 86

Figure 3.15: Lifetime distributions for normal duodenum and normal esophagus at 455 nm. 86

Figure 3.16: Signal to noise ratio increases linearly with the integrated spectral intensity. Examples are shown at both 455 nm and 505 nm for normal duodenum and normal esophagus. 87

Figure 3.17: Lifetime distributions for normal duodenum and normal esophagus at 505 nm. 88

Figure 3.18: Signal to noise ratio and extracted lifetime relationship at 505 nm. 88

Figure 3.19: R^2 values calculated at each wavelength plotted as a function of SNR and integrated spectral intensity for a sample data set taken from P15 duodenum tissue. The R^2 approaches 1 as the signal increases. 90

Figure 3.20: R^2 values for each wavelength corresponding to the P15 duodenum sample in Figure 3.19. The R^2 improves rapidly to values > 0.85 (385-520 nm) from the end wavelengths. From Figure 3.19 this range is where the SNR is > 20 dB. 91

Figure 4.1: Normalized integrated intensity (top) and lifetimes (bottom) are plotted for the four biopsy locations using only the patients with a normal diagnosis. The data is averaged over 16 (A), 3 (C), 13 (B), and 16 (D) patients to ± 1 SE. 96

Figure 4.2: Comparison of normalized spectra (I_λ) from the esophagus to the duodenum (left) and body (right). The ± 1 SE bars are too small to be represented for most λ on this graph. Values are tabulated in Appendix D. 97

Figure 4.3: The average lifetimes and LEC-j for normal duodenum and normal esophagus are plotted with ± 1 SE. Values are tabulated in Appendix D. 99

Figure 4.4: Examples of k-means clustering results from Tables 4.4 and 4.5. The clusters are not homogeneous and well separated despite good sensitivity and specificity. 107

Figure 4.5: Examples of k-means clustering results from τ-λ or LEC-j vs. LEC-j have resulted in classifications that have poor sensitivity or poor specificity. Notice that most of the LEC-0_{390} are in a in a range where a dimensional transformation is not required to match values of LEC-2_{430}. 108

Figure 4.6: An example of improved sensitivity and specificity from k-means clustering when LEC-2_{510} values are multiplied by 10 to match the dimension of $I_{505/455}$. A) The data points are plotted using the clinical results. B) Results of the K-means classification without any axis dimension transformations. C) The LEC-2_{510} axis dimension has been transformed by 100. The result is lower SN but slightly improved SP. D) The LEC-2_{510} axis is transformed by a factor of 10 instead of 100 which results in the best SN and SP of the GI tissue fluorescence study. 110

Figure 4.7: Dimensional transformation of LEC-1_{520} causes shifting of the theoretical centroids creates top-bottom segregation instead of left-right clusters. 111

LIST OF TABLES

Table 1.1: Parts list for TR-FS Instrument. 11

Table 2.1: Clinical Standard Operating Procedure for Ex-Vivo Tissue Handling 31

Table 3.1: Histological Diagnosis for Patients 1 to 28. 58

Table 3.2: Comments for the Histological Diagnosis of Patients 1 to 28. 59

Table 3.3: SNR and Lifetimes for Normal Duodenum (A) and Normal Esophageal (D) Tissue. 72

Table 3.4: The SNR and Lifetimes for Normal Duodenum (A) and Normal Esophagus (D) Data that have $I_\lambda < 20$ V·ns. 73

Table 3.5: The SNR and Lifetimes for Normal Duodenum (A) and Normal Esophagus (D) Data that have Lifetimes > ± 2 SD. 74

Table 3.6: Entire Patient Data Sets (Tissues A-D) Removed. 83

Table 3.7: Data Excluded from Normal Duodenum (A) and Normal Esophageal (D) Tissue. 84

Table 4.1: The dimensional multipliers are presented for each parameter along with the approximate range and median values derived from Figures 4.2 and 4.3. 100

Table 4.2: A comparison between the multipliers 10 and 100 on the LEC-j (j = 1, 2) using the normalized integrated spectra (I) and lifetime (τ) medians 100

Table 4.3: Rank-Sum Test Results from Normal Esophagus and Duodenum. 103

Table 4.4: The K-means Results for Untransformed Data (Part 1). 105

Table 4.5: The K-means Results for Untransformed Data (Part 2). 106

Table 4.6: The K-means Results for Transformed Data. 109

LIST OF SYMBOLS, ACRONYMS, AND ABBREVIATIONS

A	Duodenum
α	System dependent parameter describing the rate of asymptotic L^{α} decline
AOTF	Acousto-Optic Tunable Filter
B	Antrum
C	Body
D	Esophagus
dB	Decibels
d(n)	Distortion from the MCP-PMT detector response
e	Euler's Number (2.71828…)
f_i	Theoretical fitted value
FAD	Flavin Adenine Dinucleotide
FWHM	Full Width at Half Maximum
GI	Gastrointestinal
h(n) or IRF	Impulse Response Function
H_o	Null Hypothesis
H_1	Alternative hypothesis
I_4	Last order term in the diagonal of the identity matrix
I_λ	Normalized integrated spectral intensity recorded in the time-domain
I_t	The Fluorescence Intensity Measured at Time t.
k	The number of Laguerre Functions (k = 1-5)
kB	Kilobytes
KS	Kolmogorov–Smirnov
l(n)	The undistorted laser profile
$L^{\alpha}(n,j)$	Laguerre Function
L and L^T	Laguerre Matrix [k x M] and its transpose [M x k]
LEC-j or c_j	Laguerre Coefficient of the j^{th} order Laguerre function, j = 0-4
LEC-j_λ	Laguerre Coefficient at a particular order and wavelength
LSIR	Least Squares Iterative Reconvolution
M	Truncated memory length of y(n)
MCP-PMT	Micro-Channel Plate Photomultiplier Tube
ms	Milliseconds
mV	Millivolts
n	The discrete time variable from 0, 1, 2, …, M-1
N	Number of data sets
NADH	Nicotinamide Adenine Dinucleotide Hydride
nm	Nanometers
p	Probability
P	Patient
ps	Picoseconds
pt or pts	Data point(s) during the sampling rate
R^2	Coefficient of Determination

REB	Research Ethics Board
RF	Radio Frequency
s	Seconds
SD	Standard Deviation
SE	Standard Error or Standard Deviation of the Mean
SN	Sensitivity
SNR	Signal to Noise Ratio
SP	Specificity
SSError	Residual Sum of Squares
SSTotal	Total Sum of Squares
τ or τ-λ	Lifetime, may be a value for a specific wavelength
Γ	Sampling Interval
t	Time
T	Data set label (take 1, take 2, etc).
TR-FS	Time-Resolved Fluorescence Spectroscopy
μm	Micrometers
μs	Microseconds
V	Volts
V_{RMS}	Root Mean Square of voltage signal over time.
x(n)	Measured output containing only the convolution of l(n) and d(n)
y(n)	Combined measured output of the system
y_i	Measured data value
y_{avg}	Average measured data

CHAPTER 1: INTRODUCTION

1.1: Clinical Relevance

Current gold standard practices for the identification of gastrointestinal (GI) diseases and cancers involve endoscopic surveillance of the GI tract and extraction of tissue biopsies for a histopathological examination. [1] Not only is this process invasive, it is quite time consuming and expensive. An ideal biopsy tool could gather information without the removal of tissue and deliver the results in real time. The doctor could then interpret the results and get back to the patient that very same day. However, the new biopsy tool must be quick, accurate, and affordable before it can be utilized as a standard practice in the clinic.

A patient who experiences reoccurring problems and discomfort in digestion must first report their symptoms to a general physician. If their symptoms cannot be easily resolved then the patient is referred to a gastroenterologist. These specially trained physicians can provide the appropriate care required with the observations gathered from an endoscopy. Depending on what the symptoms are and what the endoscopist sees using a white light camera, they may remove some tissue specimens (i.e. biopsies) from the upper GI tract depicted in Figure 1.1. [2] Typical biopsy locations come from four major regions of the upper GI tract: the duodenum, antrum, stomach body, and esophagus. Gastroenterologists may also have colonoscopies of the lower GI tract conducted but these locations are beyond the scope of our current study.

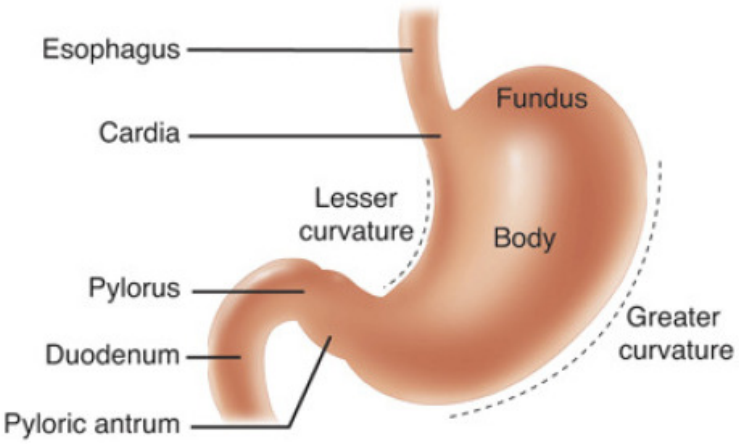

Figure 1.1: Anatomic Regions of the Stomach. This Figure was published in Shackelford's surgery of the alimentary tract, Vol. II, Zuidema GD, Yeo CJ (editors), Anatomy and physiology of the stomach, Page 3, Copyright Elsevier (2002). [2], With Permission.

Biopsies are taken from the mucosa layer of tissue while leaving the deeper submucosa intact. The main reason for this is that the epithelium cells which face the inside of the GI cavity are the most differentiated. It implies that they are highly specialized because they serve different functions along the GI tract and therefore changes in these cells makes the mucosa the most identifiable area for disease. The submucosal layer is composed of connective tissue where cells are more spread out because this layer contains mostly blood vessels, adipose, and nerve cells. Removal of this layer would be more painful to patients and require more time to heal. So sometime after the endoscopy has been completed, a pathologist analyses the specimens under a microscope to look for anatomical differences between normal and diseased tissue. Examples of common findings are chemical cell damage with our without inflammation (gastritis and gastropathy respectively) or types of acidic reflux disease. More serious

conditions include intestinal metaplasia where the cells have mutated to look like the small intestine (ex. Barretts' esophagus) or cancer. [3]

After the biopsies are taken they must be prepared for histology. Regardless of what type of tissue is to be examined, the process usually takes a few days. If the physicians had access to an ideal biopsy technology which provides the results in real-time, they can scan more surface area to search for signs of disease that traditional biopsy grab samples might not always find. If such an ideal technology were to become accepted as a standalone technique where additional histopathological examination was not necessary, any required treatments for the patient could be immediately arranged instead of waiting for histology results. In any case, if the technology allows the patient to have faster access to treatment it may increase the chance of treatment success. Early disease identification is critical for treatment success by stopping abnormal cell development (dysplasia) and preventing neoplastic (uncontrolled) cell growth that could possibly convert into a cancerous situation [4].

1.2: Optical biopsy and its Application to Address the Clinical Problem

With an optical biopsy tool, operators can exploit the properties of light-tissue interactions in order to observe the tissue's health instead of relying upon the microscopic analysis of tissue anatomy from a highly trained and skilled pathologist. The technology's main feature is that it provides a non-invasive way to observe the tissue because it does not require tissue resection. It can be used in-vivo during operating procedures and provide results in a near real-time fashion making it an attractive area for research and

development. There are many types of modalities used in medical diagnostics that collect photons coming from the direction of the tissue but they differ in penetration depth, resolution, and mechanism of tissue interaction. [5-7]

Interactions between light and tissue specimens are quite complex because the tissue is composed of a variety of different molecules, ions, and cellular constituents that can absorb and/or scatter photons. Photon absorption is particularly interesting because incident photons can lose energy to the molecule and re-emit at lower energy wavelengths in a phenomenon called fluorescence. A narrow bandwidth of light can excite multiple cellular components where each one has its own unique emission spectrum because they have different molecular configurations. Endogenous fluorophores are naturally found in tissue and includes molecules such as: metabolites - nicotinamide adenine dinucleotide hydride (NADH), flavin adenine dinucleotide (FAD); and structural components – collagen, elastin. [8] The concentration of each fluorophore depends on the type of tissue studied [3, 8] and each fluorophore has its own unique fluorescent lifetime [9]. For example, cancerous cells are more metabolically active than normal cells because they constantly undergo cell division [3]. If there is a measurable difference in fluorescence between different tissue types, then a diagnosis may be made.

The most common form of optical biopsy technology currently available is the conventional wide field image an endoscopist uses during observational and biopsy procedures. Although the operator is provided with real time feedback, the camera lens is only capable of providing macroscopic resolution. [1, 5, 7] Fluorescence endoscopy is also possible with this method by modifying the camera and source light with both

excitation and emission filters. Filters are chosen specifically to target particular endogenous fluorophores of interest. As a result, the macroscopic locations with high concentrations of the fluorophores are highlighted using a computer defined colour scheme on a two dimensional macroscopic image. [7]

Point spectroscopy can be used to provide more in depth knowledge on the molecular level by quantifying the constituents present in either a steady-state (spectrum) or time-resolved mode. There is also the potential to convert the spectral information into a pixelated "wide field" point-scanned image. [5-7] Examples of microscopic observation techniques include but are not limited to the following technologies. Diffuse Reflectance (or 'Elastic Light Scattering') can be used to derive the scattering and absorption properties of tissue by observing the propagation of incident light through the tissue [7, 10]. Fluorescence spectroscopy studies the concentration of endogenous fluorophores like fluorescence endoscopy but in a single point location [7, 8]. Raman spectroscopy can be used to study the chemical bonds present by observing the inelastic scatter of near infrared photons [11].

There are two other common optical biopsy methods in research that differ from wide-field imaging and point spectroscopy. Confocal Microendoscopy has been used to create two dimensional cross sectional images that are sectioned below the surface area by collecting photons that are only in focus from a single horizontal plane [12]. Optical Coherence Tomography can provide cross-sectional and depth information in a plane vertical to the surface area by using low-coherence interferometry with near infrared light 13]. Even with all these different optical modalities available, no single method has been

shown to be superior as a standalone diagnostic tool [7]. The best solution may be to combine two or more modalities during a procedure to support the diagnosis by confirming the same information [7].

Steady-state fluorescence spectroscopy can be implemented by inserting a fiber optic probe into the working channel of an endoscope or biopsy instrument. It relies exclusively on the total fluorescence intensities observed over a defined period of time to develop a diagnosis protocol. There is however large variability in these spectral measurements when comparing different spatial points within a patient and from one patient to another. [7] Although it is possible to compare relative intensities, it is still difficult to establish an analysis protocol because endogenous fluorophores have overlapping emission spectra [7, 8]. The reality is that one cannot be certain how much influence each endogenous fluorophore species has on the overall contribution to the fluorescence spectral intensities.

Time-resolved measurements in addition to steady-state observations are important because it can allow for identification of molecular species with overlapping emission spectra [7, 14, 15]. Fluorescent lifetimes are intrinsic to each molecule [9] and they are independent of the fluorescent intensity [14, 15]. Therefore the lifetime (or lifetimes) that best describe the fluorescence decay can be used to identify either how much each molecular species dominates the observed decay [14] or find relative changes in an average lifetime from one wavelength to another [15]. Either way fast data acquisition is critical for temporal resolution but the cost of such instruments proves to be a major barrier for this technology to be used in the clinic [15]. There have been a few

groups that have used time-resolved fluorescence spectroscopy (TR-FS) for samples under in-vitro or ex-vivo conditions where tissue specimens are analyzed after excision [16]. In-vivo measurements are necessary to validate an optical biopsy tool because when a tissue is excised the metabolism and morphology change. It is unclear to what extent this change in environment may affect the auto-fluorescent signature of the tissue. [15]

A recent review [15] highlights that many types of tissues have been studied in-vivo using steady-state and/or TR-FS. Anatomical locations include but are not limited to cancers and disease involving the oral cavity, esophagus, colon, brain, skin, eye, lung and arteries. Other tissues such as cervical and breast tissue have been studied using just steady-state fluorescence. The review focuses on just the outcomes of studies involving TR-FS. It was found that several groups could demonstrate that fluorescent lifetimes can be used in contrast to spectral data to characterize diseased tissue and achieve the appropriate diagnosis. [15] Further research in this area could lead to the development of fluorescence spectroscopy diagnostic instruments for practical use in the clinic and perhaps someday lead to acceptance as a standalone technique.

Altogether there have only been two groups [17, 18] that have studied TR-FS specifically targeting the upper GI tract. Pfefer et. al [17] conducted in-vivo TR-FS on esophageal tissue at 337 nm and 400 nm excitation to observe fluorescence between 530 nm and 570 nm on 37 patients. The bi-exponential lifetime parameters lead to unsuccessful tissue classification although they were able to show that at 377 nm the decay of dysplastic tissue is faster than normal tissue. Glanzmann et al. [18] found that under the same excitation (337 nm) the normal esophageal tissue fluorescence from 375-

400 nm had faster decay curves than cancerous tissue but between 465-485 nm it was in fact slower. The findings suggest that large spectral ranges should be used when considering time-domain features although they only sampled one patient.

Ultraviolet and visible light (specifically 300-700 nm) is required to induce tissue auto-fluorescence. Excitation at a 355 nm was chosen in our study because it overlaps with the absorption spectra of NADH, collagen, and elastin. Ultraviolet excitation wavelengths can only penetrate tissue samples up to a depth of 200 μm. [8] The 355 nm excitation is actually ideal for future in-vivo studies because it will not penetrate past the mucosa and into the submucosal layer. The depth of the mucosal and submucosal layers is loosely documented because they can vary significantly depending on their location, health, and function. In the upper GI tract the mucosal layer range for normal stomach tissue is typically between 200 μm and 1500 μm [19].

1.3: Instrumentation

Earlier generations of laser induced TR-FS instruments by our group were much slower than the system used in the GI study. Spectra had originally been obtained using a grating-based monochromatic serial scanner. Mechanical switches inside the monochromator which change the grating limit the speed of data acquisition to about 45s for a 200 nm spectrum with 5 nm increments [20]. If the fluorescence was coupled into a spectrograph instead, it was shown that a custom fiber bundle of different lengths could be used to temporally delay different wavelengths into the detector [21]. Although this parallel setup was much faster (200 ns for five wavelengths 25 nm apart) it is not practical

to increase the data throughput with additional fibers. That fiber coil already contained fibers 5-24 m in length and the additional fibers required would only make the bundle bigger and more fragile. [21]

The next generation TR-FS instrument made use of an acousto-optic tunable filter (AOTF). Technical details about its development and optimization for the GI data collection have been well documented [22-25]. An AOTF is a solid state device capable of altering the Bragg diffraction properties of a birefringent crystal with an acoustic radio frequency (RF) wave induced vibration. It acts as a narrow bandpass filter because the RF changes the refractive index of the crystal selecting the wavelength that will diffract at Bragg's angle of incidence while the others pass through undiffracted. A mirror can be set up to deflect the light from this angle into a photo-detector and thus no mechanical switches are required to select wavelengths when operating an AOTF. [26]

The birefringent property of the crystal allows non-polarized incident light from the selected beam to be diffracted into two first order beams of opposite polarizations but typical AOTF setups only detect use of them [26]. The AOTF was modified with a second mirror to collect light from both beams such that the total light throughput was now comparable to grating-based systems [22]. RFs are modulated within a few microseconds to step though wavelengths such that a 200 nm spectrum (5 nm increments) can be acquired from our instrument in less than 4 s [22]. Therefore the AOTF based instrument can achieve a desirable amount of data acquisition during near real-time clinical applications.

A block diagram of the system is presented in Figure 1.2 while the list of the instrument's components is provided in Table 1.1. Figure 1.3 shows the instrument setup enclosed inside a moveable cart that was used during clinical data collection. In the simplest of terms, a user operates the cart from a program developed in Labview® to configure the AOTF, trigger the laser, and collected the data using a micro-channel plate photomultiplier tube (MCP-PMT). Operation of these components will be discussed briefly as it is essential to understand how the data is collected so it can be processed accordingly. More elaborate instrument documentation can be found in Reference [25].

Fluorescence induced at each wavelength is measured from 11 laser pulses (excitation 355 nm, 350 ps pulse width, 1 kHz repetition rate). A 50 ms time window is allocated for data acquisition at each wavelength to measure 11 consecutive fluorescence decays (11 ms total at 1 ms per pulse) and account for the data acquisition/transfer time required by the oscilloscope. The number of pulses (11) was chosen so that the first pulse could be discarded in the event there was an issue with instrument synchronization while the last 10 fluorescence decays are used to improve signal to noise ratio. The major source of this problem was resolved with an AOTF driver firmware upgrade but there were still some intermittent delays with the direct digital synthesizer chip [25]. That chip is responsible for generating the signaling frequencies that control the timing of all the instrument components. Therefore it is still necessary to discard the first pulse although that data may be reliable (most of the time) after the AOTF firmware was upgraded.

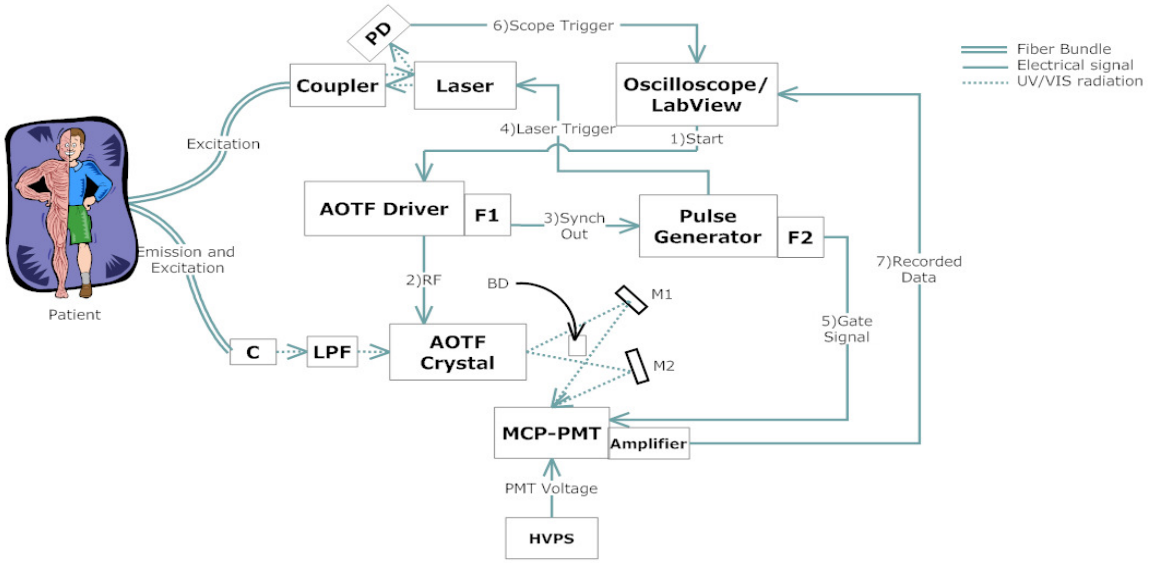

Figure 1.2: AOTF TR-FS Instrument Diagram, Figure 1.3 from Reference [25]. The acronyms and parts are listed in Table 1.1.

Table 1.1: Parts list for TR-FS Instrument.

Digital Oscilloscope (DPO7254, Tektronix Inc, Beaverton, OR, USA)
LabView® (v8.2, National Instruments, Austin, USA)
MCP-PMT (R5916U-50, Hamamatsu Photonics, Tokyo, Japan)
Amplifier (C5594, Hamamatsu Photonics, Tokyo, Japan)
HVPS: high voltage Power Supply (C4840-01, Hamamatsu Photonics, Japan)
AOTF Driver (SN: 0610-AE-7359, Brimrose Corp., Baltimore, USA)
F1: coaxial low pass filter, (BLP-250, Mini-Circuits, Brooklyn, USA)
AOTF Crystal (TEAF5-0.36-0.52-S, Brimrose Corp., Baltimore, USA)
BD: beam dump made of black aluminum foil (Thorlabs) to absorb the diffracted part of the light not desired for collection, the desired wavelength is reflected by 2 concave mirrors **M1** and **M2**
Pulse Generator (QC9512, Quantum Composers, Bozeman, MT)
F2: coaxial low pass filter (BLP-10.7 Mini-Circuits, Brooklyn, USA)
Nd:YAG PowerChip Nanolaser (part no. PV-001525-140, Teem Photonics, Meylan, France)
Coupler: telescopic lens tube with a plano-convex lens with a focal length of 20 mm
PD: external photodiode (DET10A, Thorlabs, Newton, NJ, USA)
Excitation/Emission Fiber: customized silica fiber bundle (50-2632-REV1, CeramOptec GmbH, Berlin, Germany)
C: plano-convex collimation lens (part no. 45098, Edmund Optics, Barrington, NJ, USA)
LPF: long pass filter (LP02-355RU, Semrock, Rochester, NY, USA)
Hospital Grade Isolation Transformer (IS500HG, Tripp Lite, Chicago, USA)
Uninterruptible Power Supply (APC Back-UPS XS 1500VA, American Power Conversion, West Kingston, RI, USA)

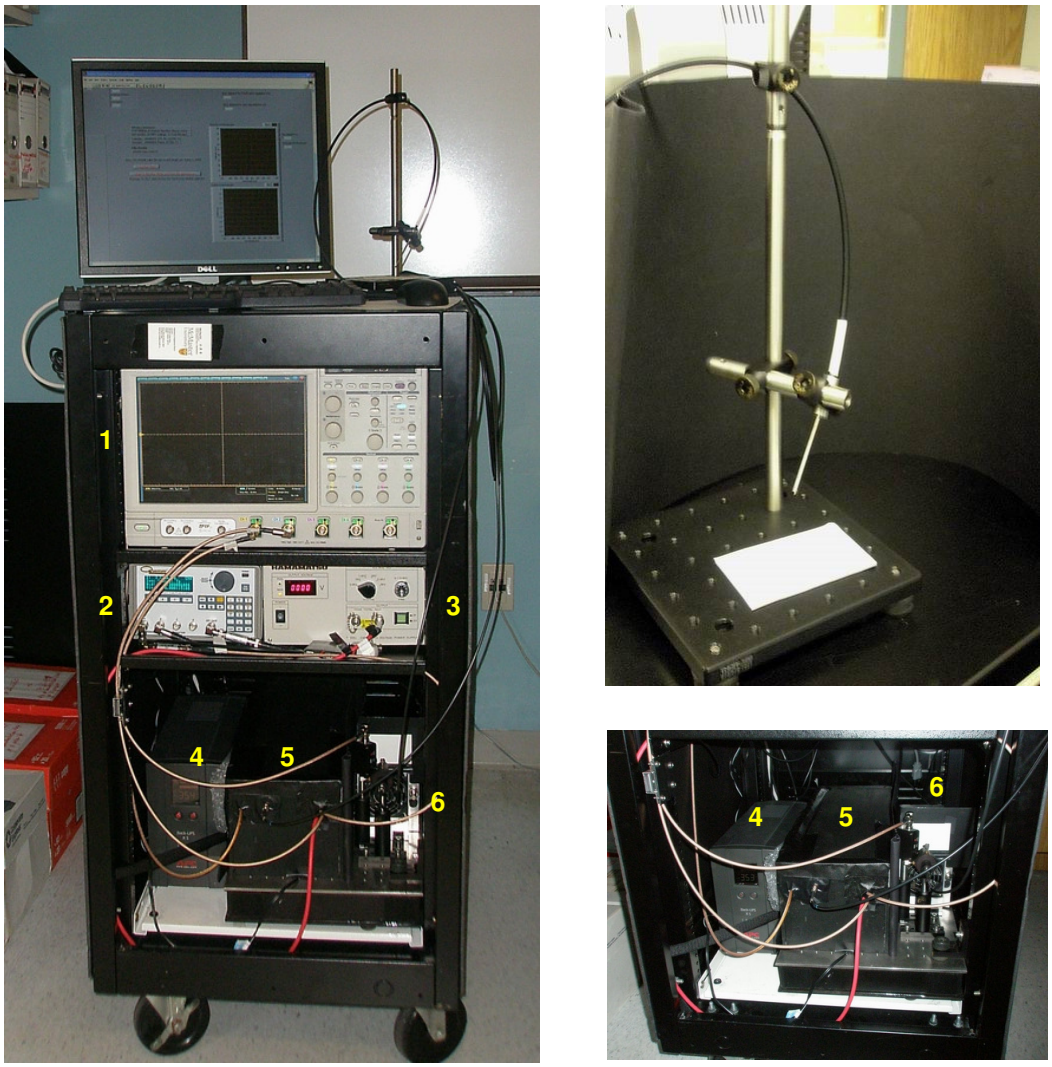

Figure 1.3: TR-FS system used for ex-vivo clinical data collection. All the contents except for the computer monitor, keyboard, fiber probe and stand in Figure 1.2 fit inside a moveable cart of size 3.5' x 2' x 2'. The fiber probe delivers excitation light through a single fiber (600 µm core diameter) that is surrounded by a ring of 12 (200 µm core diameter) collection fibers. Shown inside the cart are the oscilloscope with built in computer (1), pulse generator (2), MCP-PMT (3), an uninterruptible power supply (4), AOTF spectrometer (5), and the laser with fiber coupling (6).

Each laser pulse is sent every 1 ms and the corresponding fluorescence signal detected by the MCP-PMT is recorded by the oscilloscope at 25 ps resolution over a period of 25 ns. This process is repeated until all wavelengths have been collected from 370-550 nm in 5 nm steps. One complete data set can be collected in less than 4 s. It takes the operator about 1.5 s to control the instrument from the computer while the other 2 s is the time it takes for the instrument to measure and record data from all of the 37 wavelengths. Optimal signal resolution was achieved for clinical data when the digitizer was set to a scale range of 2.5 V (500 mV/division) with the shortest sampling rate of 25 ps/pt. Calibration tests showed the lifetimes values for FAD and Fluorescein were within accepted literature values even though the spectral resolution of the AOTF, which increases naturally with the wavelength, was low (1-4 nm) [22, 25]. Therefore wavelength steps of 5 nm are necessary to avoid spectral overlap.

Several artifacts were discovered in the signal and these distortions were removed so that the fluorescent signal could be accurately identified [25]. Out of band RF distortions were noticed if the AOTF was disturbed by vibrations and this was resolved by the manufacturer. Fans were also installed to cool the AOTF driver and stop RF pulse broadening artifacts due to temperature dependent power fluctuations delivered to the crystal. Ringing artifacts (oscillations in the decay signal) were found to be caused by the inherent ringing frequency of the MCP-PMT gating signal. An analogue filter was placed at the output of the pulse generator (F2 in Figure 1.2) to reduce the rise/fall time of the MCP-PMT and consequently the length of ringing, thus eliminating this interference from

the decay. Other electromagnetic interferences were removed by using double shielded co-axial cables, a common ground point, and another filter (F1 in Figure 1.2).

Finally, one last modification was made to the instrument in order to reduce the external trigger jitter. An external photo diode was introduced to trigger the data acquisition because the timing of the laser pulse was significantly unreliable taking anywhere between 50 – 400 μs to generate [25]. Now that the artifacts have been removed and the system components are synchronized, the laser profile was measured to capture the MCP-PMT rise time. The total pulse width measured (350 ps + system response) was about 530 ps [25]. The finite system response will always be present in acquired data. Therefore the intrinsic lifetime response of the sample will need to be extracted from the raw data using a processes referred to as deconvolution.

1.4: Signal Deconvolution

Deconvolution is the act of extracting the sample's intrinsic fluorescence response from any and all distortions in the measured signal y(n). The y(n) is given by Equation 1.1: the unique convolution of the undistorted "h(n)" Impulse Response Function (IRF), the undistorted laser profile "l(n)", and distortion from the MCP-PMT detector response "d(n)". Since the laser profile and IRF are both distorted by d(n), a single laser measurement without an auto-fluorescence response can be used to capture d(n) into a new equation where x(n)=l(n)*d(n) and Equation 1.1 becomes Equation 1.2. Deconvolution can now be performed using the known measurements of y(n) and x(n) in

Equation 1.3 over a sampling interval Γ and a truncated memory length M, where "n" is the discrete time variable from 0, 1, 2, …, M-1. [14, 27]

$$y(n) = h(n) * l(n) * d(n) \tag{1.1}$$

$$y(n) = h(n) * x(n) \tag{1.2}$$

$$y(n) = \Gamma \sum_{m=0}^{M-1} h(m)x(n-m) \tag{1.3}$$

There is, however, one fundamental problem with this theory and the TR-FS instrument. The laser light will not be captured in each y(n) because both the long pass filter and AOTF crystal diffraction will keep it from reaching the MCP-PMT. The d(n) cannot be captured on its own because the response is initiated only by incoming light. Since the duration of the laser is a magnitude smaller than the fluorescent decay, each IRF can be deconvolved relative to the same x(n) and therefore the same l(n). The extracted IRF is very close to the actual IRF minus the same small laser contribution.

The most common way to solve the deconvolution problem is to use a model that assumes the IRF is of a specific form such as a multiexponential decay and find the best solution using non-linear least squares iterative reconvolution (LSIR). The number of decay laws present, as well as their values (lifetimes) and weights (amplitudes) are numerically adjusted until a solution is formed that minimizes the error, by least-squares method, between the y(n) and its theoretical fit [14]. There are two major concerns when it comes to employing this method. The first concern is that multiexponental decays can

have multiple solutions that would satisfy the decay curve. The lifetimes and amplitudes are correlated such that one can be varied to compensate for the other [14]. The second concern is the amount of time that can be spent on computing the parameter solutions only to find out through experimentation and conservative interpretation that they are not actually descriptive of the data [14, 25, 28, 29]. In this regard the fitting parameters cannot be used to describe the fluorophore content of the sample or compute solutions in real time.

The other way to deconvolve the data is to use models that do not require any a priori assumptions about the IRF decay. Some methods include the use of Fourier transformations or solving differential equations to find the best solution [30, 31]. One of each type of deconvolution algorithm (bi-exponential and Laguerre expansion) were tested on preliminary fluorescent data [25]. Laguerre expansion was chosen because the terms in the Laguerre polynomial form an orthonormal basis set having unique and normalized solutions [31]. System dependent parameters in the Laguerre polynomial can be generalized for a particular sample type using LSIR. While those parameters are held constant, the others which are dependent on the individual sample itself can then be determined in a one-step calculation. The computation is so fast and robust that it can be used in real-time to calculate the sample specific descriptive parameters. [28, 29, 31]

The Laguerre deconvolution technique developed by Krishnamoorthy [25] is based on the work done by Marcu's group [28, 29] with a modification to account for wave dependent effects present in our system. The MCP-PMT is a significant upgrade from Marcu's group such that the temporal resolution can pick up on the chromatic

dispersion of the light inside the fiber probe. Fiber probes can cause wavelength dependent temporal shifts where the photons of different colours arrive at the detector at different rates [32]. Although this dispersion is often considered negligible and cannot be seen by sampling at a rate of 100 ps/pt or greater, it can be seen by our sampling rate of 25 ps/pt [25]. The wavelength dependent delay became problematic during LSIR because the x(n) used during recovolution was not in sync with the measured output at any given wavelength [25]. An additional step was added to the Laguerre algorithm that reconvolves each IRF with a shifted x(n) until the best fit is achieved. Basic theory required to understand the implementation of Laguerre deconvolution in this report will be discussed next. Detailed theory including the algorithm code was provided by Krishnamoorthy [25].

1.5: Laguerre Expansion Technique – Basic Theory

In Laguerre deconvolution, the IRF takes on the form of Equation 1.4 with the expansion of discrete Laguerre polynomials (Equation 1.5). For each order "j" the k^{th} Laguerre function, $L^{\alpha}(n,j)$, is weighted by "c_j", the Laguerre Coefficient (LEC-j). The built in exponential functions allow the Laguerre polynomial to describe a physical system that undergoes an asymptotic decay [31]. The system dependent parameter ($0 < \alpha < 1$) is used to govern the rate of asymptotic decline for a given set of $L^{\alpha}(n,j)$. The selection of α depends on the sampling rate and memory length "M". Higher order $L^{\alpha}(n,j)$ also require a longer M to finish converging asymptotically towards zero. The M and α should be chosen such that all $L^{\alpha}(n,j)$ decline close to zero by the end of the y(n). As for

the number of $L^{\alpha}(n,j)$, the amount should be as many as reasonably necessary to model the complexity of the decay function and keep computational time to a minimum.

$$h(n) = \sum_{j=0}^{K-1} c_j L^{\alpha}(n, j) \tag{1.4}$$

$$L^{\alpha}(n, j) = \alpha^{(n-j)/2}(1-\alpha)^{1/2} \sum_{k=0}^{J} (-1)^k \binom{n}{k}\binom{j}{k} \alpha^{j-k}(1-\alpha)^k \tag{1.5}$$

The first five $L^{\alpha}(n,j)$ for a given α (0.97) at our recorded M (1000 pts) and rate (25 ps/pt) is shown in Figure 1.4. When combined these $L^{\alpha}(n,j)$ make a single function h(n) that decays to zero. The 0^{th} order has more influence over the decay shape than the higher orders because it describes the slowest decay process. However, the value of each LEC can drastically change the weight each order has on the overall decay model such that the h(n) might contain local minima as seen in the higher order $L^{\alpha}(n,j)$. These inflection points are not present in the observed y(n) for fluorescent decay and therefore it is critical that the Laguerre fitting algorithm converges to a solution representing a single decay process. Only one 'average' lifetime (τ) is then used to describe the complex biological sample that contains many individual fluorophore lifetimes.

Through a series of lengthy calculations described in [25, 28] the LECs are estimated by the removal of y(n) from each $L^{\alpha}(n,j)$ convolved with x(n). The best solution for our system is found through LSIR, selecting the α and laser shift required to minimize the sum of residuals between the measured output y(n) and the theoretical Laguerre fit to y(n). The LECs are inserted into Equation 1.4 to form the IRF decay curve at each

wavelength where the τ for a single exponential decay (Equation 1.6) is the time the IRF takes to decay to 1/e of its maximum height [14].

$$I_t = I_{t=0} e^{-t/\tau} \qquad (1.6)$$

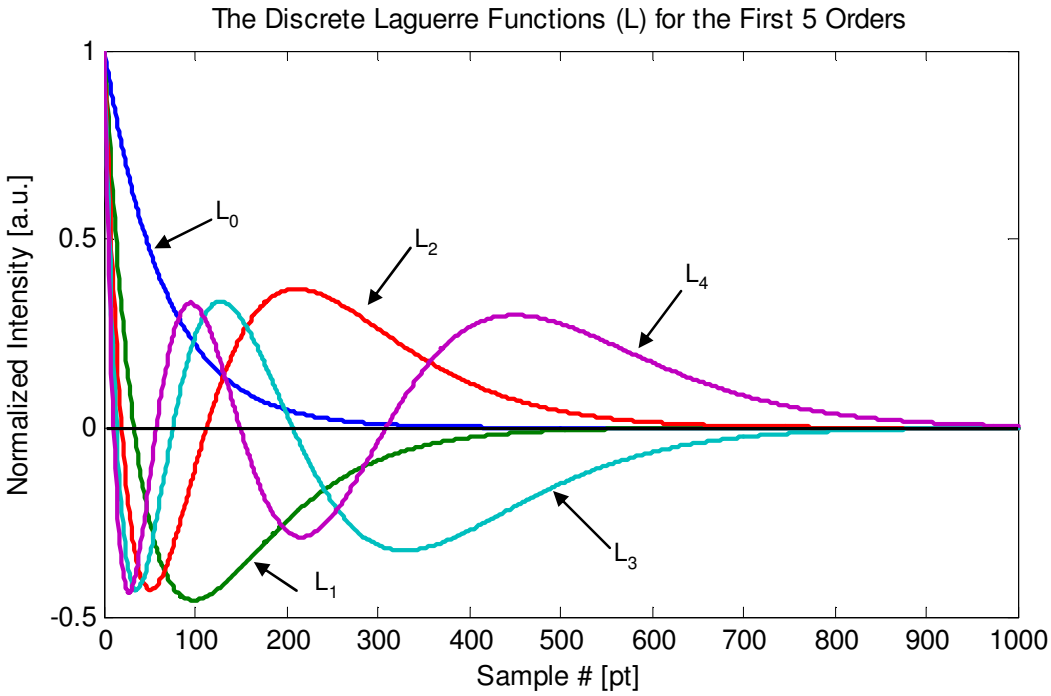

Figure 1.4: The first five Laguerre functions for α = 0.97 at 25 ps/pt sampling rate.

The expanded $L^{\alpha}(n,j)$ are orthonormal meaning that all orders are orthogonal and of the same unit length [31]. The most appropriate solution is obtained when this condition is met for a given sampling rate, M, and α. As a result, the set of LECs are said to be unique or 'normalized' solutions to the set of $L^{\alpha}(n,j)$. No additional normalization is required to compare LEC or τ from one sample or wavelength to another. All five LECs

and the associated IRF lifetime for each wavelength are intrinsic to each individual spot measured on the sample modeled with the Laguerre technique. A fixed α, M, and sampling rate for all wavelengths is required in order to make a comparison between samples because the decay of each $L^{\alpha}(n,j)$ is dependent on these parameters.

To retain orthonormality, the best α and M are the ones that make the Laguerre Matrix (L = [M x k]) of $L^{\alpha}(n,j)$ orthogonal, i.e. when $L^{T}L$ forms the Identity Matrix. Without sacrificing computation time for accuracy, orthonormality is maintained when the last order term in the Identity Matrix (I_4) from the matrix operation $L^{T}L$ is 0.9 or better. It is satisfied (by $I_4 = 0.9441$) for M = 600 pts when $\alpha = 0.97$ during preliminary testing of the GI data. [25] As data was acquired, further testing in Chapter 2 revealed the common α between all GI tissue locations was approximately 0.967. The M was increased to 650 pts ($I_4 = 0.9912$) because it does not noticeably impact the processing speed but it will ensure even more that the Laguerre algorithm provides accurate solutions. Different tissue types can have vastly different tissue compositions because they serve different functions within the body (ex. Brain vs. GI) so α must be optimized for each application and the M adjusted accordingly.

1.6: Current Work

The instrument was fully calibrated for the collection of GI data using the first few patients to trouble shoot and solve any problems. Both the bi-exponential and Laguerre expansion deconvolution algorithms were tested on simulated data, fluorescent dyes, endogenous fluorophores, and the first few GI biopsies. Lifetime results produced by each

method were confirmed with accepted literature values for the dyes and fluorophores demonstrating proof-of-concept. Not only did the Laguerre technique calculate results faster than bi-exponential, it also outperformed the bi-exponential model in noisier environments. [25] Although an optimal α and M were proposed for GI data, more data is required to select an average α and the corresponding M to make the Laguerre results suitable for comparison between different types of GI tissue. The next step is to build a data base of fluorescent measurements from GI patients that can be used to develop a classification system which would successfully identify the tissue type based on the values of its Laguerre parameters.

Protocols for clinical ex-vivo measurements and data management are established in Chapter 2 while the integrity of the data is evaluated in Chapter 3. A single optimized α Laguerre parameter was calculated that best describes the Laguerre function decay for all four GI tissue locations. For the two largest patient groups (normal esophagus and normal duodenum tissue) K-means clustering was used to find pairs of statistically different Laguerre variables (LEC-j_λ, τ-λ) and/or "I_λ" (normalized integrated spectral intensity from the time-domain) that can classify the most GI measurements into their correct clinical diagnosis from histology. Results are presented and discussed in Chapter 4.

At this time, a second generation instrument is under construction. The new instrument will be capable of measuring both diffuse reflectance and TR-FS in the same fiber probe. Eventually the deconvolution and classification algorithms will be added to the instrument so that the tissue type can be identified in real-time from the diffuse reflectance corrected TR-FS signal free from distortions caused by blood absorption.

Before any algorithm can be accepted it must be analyzed statistically and improved over several stages of clinical trials to ensure that auto-fluorescence diagnosis is consistent with the histological tissue identification. Also, to make this diagnostic modality more versatile it must be tested and configured on other types of tissue such as brain tumours or atherosclerotic plaques.

REFERENCES

[1] Jobe BA, Hunter JG, Peters JH. 2009. Esophagus and diaphragmatic hernia. In: Brunicardi F, Andersen D, Billiar T, Dunn D, Hunter J, Matthews J, Pollock RE, editors. Schwartz's principles of surgery [Internet]. 9th ed. New York, NY: McGraw-Hill [cited 2012 Feb 4]. Available from http://www.accessmedicine.com/content.aspx?aID=5031992

[2] Mercer DW, Liu TH, Castaneda A. 2002. Anatomy and physiology of the stomach. In: Zuidema GD, Yeo CJ, editors. Shackelford's surgery of the alimentary tract. 5th ed. Vol. II. Philadelphia, PA: Saunders Elsevier. p 3.

[3] Feldman M, Friedman LS, Brandt LJ. 2010. Sleisenger and Fordtran's gastrointestinal and liver disease. 9th ed. Philadelphia, PA: Saunders Elsevier. 2480 p.

[4] Llombart-Bosch A, Ringborg U, Rutella S, Celis JE. 2011. Cancer - clinical background and key challenges. In: Cesario A, Marcus F, editors. Cancer systems biology, bioinformatics and medicine research and clinical applications. New York, NY: Springer. p 29-93.

[5] Dacosta RS, Wilson BC, Marcon NE. 2002. New optical technologies for earlier endoscopic diagnosis of premalignant gastrointestinal lesions. Journal of Gastroenterology and Hepatology 17(s1):S85-S104.

[6] Wang TD, Van Dam J. 2004. Optical biopsy: a new frontier in endoscopic detection and diagnosis. Clinical Gastroenterology and Hepatology 2(9):744-753.

[7] Wilson BC. 2007. Detection and treatment of dysplasia in Barrett's esophagus: a pivotal challenge in translating biophotonics from bench to bedside. Journal of Biomedical Optics 12(5):051401.

[8] Vo-Dinh T, Cullum BM. 2003. Fluorescence spectroscopy for biomedical diagnostics. In: Vo-Dinh T, editor. Biomedical photonics handbook. Boca Raton, FL: CRC Press. p 28:1-50.

[9] Richards-Kortum R, Sevick-Muraca E. 1996. Quantitative optical spectroscopy for tissue diagnosis. Annual Review of Physical Chemistry 47:555–606.

[10] Mourant JR, Bigio IJ. 2003. Elastic-scattering spectroscopy and diffuse reflectance. In: Vo-Dinh T, editor. Biomedical photonics handbook. Boca Raton, FL: CRC Press. p 29:1-22.

[11] Fenn MB, Xanthopoulos P, Pyrgiotakis G, Grobmyer SR, Pardalos PM, Hench LL. 2011. Raman spectroscopy for clinical oncology. Advances in Optical Technologies 2011:213783.

[12] Paull PE, Hyatt BJ, Wassef W, Fischer AH. 2011. Confocal laser endomicroscopy: a primer for pathologists. Archives of Pathology & Laboratory Medicine 135(10):1343-1348.

[13] Walther J, Gaertner M, Cimalla P, Burkhardt A, Kirsten L, Meissner S, KochE. 2011. Optical coherence tomography in biomedical research. Analytical and Bioanalytical Chemistry 400(9):2721–2743.

[14] Lakowicz JR. 2006. Time-domain lifetime measurements. In: Principles of fluorescence spectroscopy. 3th ed. Singapore: Springer Publishing. p 97-155.

[15] Marcu L. 2012. Fluorescence lifetime techniques in medical applications. Annals of Biomedical Engineering (January 25th 2012 Epub ahead of print):1-28.

[16] Elson D, Galletly N, Talbot C, Requejo-Isidro J, McGinty J, Dunsby C, Lanigan P, Munro I, Benninger R, de Beule p, et al. 2006. Multidimensional fluorescence imaging applied to biological tissue. ln: Geddes CD, Lakowicz JR, editors. Reviews in fluorescence 2006. New York, NY: Springer Science. p 477-524.

[17] Pfefer TJ, Paithankar DY, Poneros JM, Schomacker KT, Nishioka NS. 2003. Temporally and spectrally resolved fluorescence spectroscopy for the detection of high grade dysplasia in Barrett's esophagus. Lasers in Surgery and Medicine 32(1):10-16.

[18] Glanzmann T, Ballini JP, van den Bergh H, Wagnie`res G. 1999. Time-resolved spectrofluorometer for clinical tissue characterization during endoscopy. Review of Scientific Instruments 70(10):4067-4077.

[19] Day DW, Jass JR, Price AB, Shepherd NA, Sloan JM, Talbot NJ, Williams GT, Warren BF. 2003. Normal Stomach In: Morson and Dawson's gastrointestinal pathology. 4th ed. Hoboken, NJ: Wiley-Blackwell. p 91-98.

[20] Fang Q, Papaioannou T, Jo JA, Vaitha R, Shastry K, Marcu L. 2004. Time-domain laser induced fluorescence spectroscopy apparatus for clinical diagnostics. Review of Scientific Instruments 75(1):151-162.

[21] Yuan Y, Papaioannou T, Fang Q. 2008. Single shot acquisition of time-resolved fluorescence spectra using a multiple delay optical fiber bundle. Optical Letters 33(8):791-793.

[22] Yuan Y, Hwang J, Krishnamoorthy M, Ye K, Zhang Y, Ning J, Wang RC, Deen MJ, Fang Q. 2009. High-throughput acousto-optic-tunable-filter based time-resolved fluorescence spectrometer for optical biopsy. Optics Letters 34:1132-1134.

[23] Zhang Y. 2007. Development of a real-time minimally-invasive diagnostic instrument for optical biopsy [dissertation]. Hamilton (ON): McMaster University.

[24] Hwang JY. 2009. Development of an acousto-optic tunable filter based time-domain fluorescence spectrometer with high scanning speed and high throughput for optical biopsy applications [dissertation]. Hamilton (ON): McMaster University.

[25] Krishnamoorthy M. 2010. Optimization of a time-resolved spectroscopy system with an acousto-optic tunable filter employing a deconvolution method based on discrete laguerre functions [dissertation]. Hamilton (ON): McMaster University.

[26] Fellers TJ, Davidson MW. 2009. Olympus Fluoview Resource Center: Acousto-Optic Tunable Filters [Internet]. Olympus Corporation; [cited 2 Mar 2012] Available from: http://www.olympusfluoview.com/theory/aotfintro.html

[27] Ware WR, Doemeny LJ, Nemzek TL. 1973. Deconvolution of fluorescence and phosphorescence decay curves, least-squares method. The Journal of Physical Chemistry 77:2038-2048.

[28] Jo JA, Fang Q, Papaioannou T, Marcu L. 2004. Fast model-free deconvolution of fluorescence decay for analysis of biological systems. Journal of Biomedical Optics 9:743-752.

[29] Maarek JI, Marcu L, Snyder WJ, Grundfest WS. 2000. Time-resolved fluorescence spectra of arterial fluorescent compounds: reconstruction with the laguerre expansion technique. Photochemistry and Photobiology 71:178-187.

[30] O'Connor SV, and Ware WR. 1979. Deconvolution of fluorescence decay curves, a critical comparison of techniques. Journal of Physical Chemistry 83:1333–1343.

[31] Marmarelis V. 1993. Identification of nonlinear biological systems using laguerre expansions of kernels. Annals of Biomedical Engineering 21:573-589.

[32] Buck JA. 2004. Dispersion. In: Fundamentals of Optical Fibers. 2nd ed. Hoboken, NJ: John Wiley and Sons. p 125-184.

CHAPTER 2: METHODS

This chapter begins with an overview of the clinical procedures required to handle the human tissue and collect the data in an ethical manner, protecting both the patients' best interests and the safety of the operators. The TR-FS instrument used in this study was described in Section 1.3. A step by step guide for instrument operation (Appendix A), clinical data collection (Table 2.1), and note taking (Appendix B) will now be provided. Next, the data processing and management strategies are presented. These methods are an extension of the work done by previous students. The α Laguerre parameter described in Section 1.5 was optimized here in Section 2.2.1 for GI tissue.

Finally, the background information required to understand the data analysis is discussed. Several steps were taken to ensure a meaningful classification algorithm was derived for our data. Half of the parameters measured (Chapter 4) did not follow normal sampling distributions. Thus the rank-sum test was used instead of the popular t-test to identify parameters whose measurements from two different tissue locations were statistically different ($p < 0.05$). An unsupervised, non-parametric classification model (K-means) was selected for the GI data that is not influenced by the type of sampling distribution. All calculations were conducted using Matlab®. The identification and removal of outlier measurements from the data pool for the analysis algorithm proved to be quite an extensive task so it will be discussed on its own in Chapter 3.

2.1: Clinical Procedures

2.1.1: Research Ethics

All clinical studies were performed at the McMaster University Medical Center's Endoscopy Unit led by Dr. Frances Tse. Research Ethics applications were prepared by Dr. Fang and Dr. Tse for the project title "An Ex-Vivo Study of Time-Resolved Auto-fluorescence Spectra of Upper GI Biopsy Samples" with Dr. Tse listed as the principle investigator. Ethics boards have been put in place to ensure that the study goals and protocols will protect the health and safety of everyone involved. The Human Tissue Committee, a subcommittee of the Hamilton Health Science/McMaster Faculty of Health Science Research Ethics Board (REB), approved the study project No 08-165T on April 9th, 2008. The initial approval was granted until January 17th 2009 (or one year from the first version submission) and subjected to review upon the anniversary date. Further extensions were given without any required changes for data collection conducted in 2009 and 2010.

As part of the research ethics requirements, patient consent was obtained in writing before each endoscopy procedure by Dr. Tse for use of their tissue specimens in our study using an REB approved form. The consent form explained in basic non-scientific terms that we would shine light onto their tissue only after it has been removed and use the light that shines back to study the sample. The ultraviolet light used would not alter their tissue or affect the outcome of the pathology results. It also explained that their personal information such as their name and address would not be released to us and that they would not be financially compensated for their participation. Since the pathology

evaluation is used for their diagnosis, there is no need to contact patients purely for the outcome of our study. Patients are given the opportunity to withdraw their participation at any time during our study.

The first six patients (P01-P06, measured in three separate experiments) were used to identify any challenges working in a clinical environment. The goal was to perform the fluorescent measurements efficiently without being disruptive to standard endoscopy procedures, hospital staff, and the patients. In this time we were able to streamline the study protocol and test the instrument's sensitivity (signal to noise ratio) on human specimens. While it is not necessary for fluorescence measurements to be conducted in the same room as the procedure, collection took place inside the endoscopy room because of space limitations in the Endoscopy Unit. Most of the patients allowed us to collect data during their procedure but some of the data were collected after the procedure at the request of the patients.

Standard operation procedures were finalized for GI tissue handling, instrument operation, and note taking after the P07-P09 data collection. GI data collection can be completed effectively by two experienced operators where one operator's job is to only handle the tissue while the other operates the computer and records written notes. All of the notes were digitally transcribed and saved as time stamped PDF files for good record keeping practice. Digital copies are backed up on a server in the biophotonics lab. Hardcopies were printed and placed in a binder dedicated to papers containing any information related to this study such as copies of the REB approval and standard endoscopy medical reports from Dr. Tse. All personal identifiable information (name,

birth dates, etc.) has been removed in these notes while the lookup table between the Patient ID (P01, P02, etc.) and the patients' names is maintained by Dr. Tse.

2.1.2: Clinical Data Collection

Endoscopies from Dr. Tse's morning schedule were used to allow us time to setup the cart in the endoscopy unit and finish measurements over the staff lunch break if needed. Sometimes emergency biopsies were scheduled during the break which required us to pack up quickly and leave. On the day of the procedure the first thing to do at the clinic was to double check the planned endoscopy schedule with the charge nurse for any changes. Once the endoscopy schedule had been verified, the cart was moved from Dr. Tse's office to the endoscopy unit.

Before any tissue measurements were performed, the TR-FS instrument described in Section 1.3 was turned on using the procedure described in Appendix A and tested to ensure that it was functioning correctly. First, the laser energy was measured using a power meter (3sigma Laser/Power Energy Meter, 0012-0840, Coherent Inc., Portland, OR, USA) which is calibrated for a 355 nm source (J5-09010K-030-Modified Standard Energy, 1095449, Coherent Inc., Portland, OR, USA). Average laser energy required to produce adequate tissue auto-fluorescence was 3.0 μJ. The second test was to fire the laser on a paper business card to see if its spectrum displayed in Labview matches its known fluorescence spectrum (see Section 3.2). Both the laser energy and paper fluorescence were recorded at the start of each collection day and, if time permitted, before shutting down the instrument. Basic trouble shooting could be performed in the

clinic if either test failed. Laser energy can be tuned by readjusting the focusing lens located directly in front of the laser. Other instrument failures as indicated by a rather noisy paper spectrum collected (with no apparent signal) could be fixed by reloading the Labview software or by verifying that each procedure listed in Appendix A was followed correctly. If the paper signal was drastically different in shape from its relatively stable form, this would be an indication of a major AOTF related malfunction where trouble shooting could only be performed back at the lab or perhaps even the manufacturer.

Table 2.1 presents a step by step procedure for clinical data collection. Disposable supplies such as gloves, absorbent pads, saline, and alcohol wipes required to sanitize our working space and prevent cross-contamination of samples are available in the endoscopy unit. All other materials required in Table 2.1 such as laser equipment, tweezers and a Petri dish were obtained through the Health Sciences Store. The operator designated for tissue handling duty (Operator #1) was required to wear gloves and handle the tissue with tweezers to protect themselves from infection. The tweezers, laser probe, and Petri dish were all sanitized using alcohol wipes after the instrument was setup and after each patient. Gloves and other disposable items were changed only as needed if they had touched anything that had come into contact with the tissue. Since the upper GI tract of a single patient is continuous, disinfecting the equipment between biopsy locations is not necessary by the endoscopist or for our measurements.

Table 2.1: Clinical Standard Operating Procedure for Ex-Vivo Tissue Handling

1. Identify appropriate cases for this clinical study and determine their schedule. (Dr. Tse)
2. On the day of the procedure, visit the clinic first to double check the cases with the charge nurse.
3. Move cart to the endoscopy unit after 8:00 am from Dr. Tse's office (her secretary has the key).
4. Room preparation:
    1. Identify space needed for the TRFS instrument cart.
    2. Obtain a small stainless steel table top cart from the unit nurses.
    3. Obtain supplies:
        - From hospital: Blue pad, needles, gloves, alcohol wipes, 4×4 (absorbent pad), and saline.
        - From our lab: tweezers ×2, Petri dish, laser goggles, metal stand, fiber probe, black cardboard shield, power meter, USB flash drive.
    4. Use alcohol wipes to clean probe (at start), Petri dish, and tweezers. (Clean dish and tweezers after each patient, Step 10)
5. Talk to the nurse in charge:
    1. About what we plan to do.
    2. Ask that they label the cassettes first and don't close them.
    3. We'll put the cassette back closed; they'll put them in the jar of formalin.
6. Take specimens to the cart.
    1. ALWAYS check the labels and that they are labeled.
    2. Put the cassettes on the 4×4 which is on top of the blue pad.
    3. Put a drop of saline on each sample piece.
7. Transfer one specimen to the Petri dish and put another drop of saline on it.
8. Do measurement(s) with probe at 45 degrees, distance 2-3 mm.
9. Move specimen back to the cassette and close it.
    1. [Then go to step 7]
10. Clean the Petri dish and tweezers after we are finished with that patient.
11. Dispose of needles in sharps container and alcohol wipes used in the proper bin. All garbage goes to biohazard; don't put it in the litter bin.
12. At the end, wrap up all disposables in the blue pad and put in the bin.

Operator #1 was required to wear appropriate laser goggles (blocking 355 nm light) when handling the laser probe. A black cardboard shield was placed around the area of the probe stand and Petri dish to protect all other people in the room from any chance of laser reflections as per safety regulations even though special care was taken by the operators when aiming and firing the probe. Saline was used to keep the specimens hydrated, simulating the in-vivo environment as much as possible. It is a sterile 0.9 % sodium chloride solution that is used to clean and hydrate tissue during medical procedures and does not give off a fluorescent signal. Formalin was used by the medical staff to fix the sample in its current biological state and preserve it for pathology. All specimens are labeled based on the following convention: A – Duodenum, B – Antrum, C – Body, and D – Esophagus.

Operator #2 was responsible for operating the instrument, firing the laser under the direction of Operator #1, and recording notes. Enough data sets were collected to represent the visible area of each specimen while it was on the Petri dish without trying to overlap laser spots and achieve acceptable signal strength. Information recorded included notes about the experiment (Appendix B) as well as the file names and if they were new or repeated positions on the specimen. File names included important information about the instrument setup including the PMT voltage in case time did not permit for detailed note taking. Each file name includes the following information: date, patient number, biopsy location and specimen number, PMT voltage, data set or "take" number, and by default the channel number used by the oscilloscope. An example file name is '20091102_P28_B1_V2200_T2_CH1.dat'.

All fluorescence measurements were taken with the probe fixed at an approximate 45˚ angle and close to (~2-3 mm) the sample. The reason for this was to reduce the collection of back reflected laser light which was otherwise found to overpower the strength of the fluorescence signal. Fluorescent light emits isotropically [1] so the measured signal produced by endogenous fluorophore emissions (Section 1.2) should not be affected by the probe placement [2]. Current work includes the production of a new generation optical biopsy system that incorporates the collection of diffuse reflectance measurements. Unlike fluorescent measurements, diffuse reflectance is dependent heavily on probe and fiber position [2, 3] and the new design will require much more consideration and evaluation using tissue phantoms. The focus of this thesis is not to specifically evaluate the probe design experimentally but the evaluation of our data in the following chapters will demonstrate the probe is sufficient to collect data for lifetime extraction using Laguerre deconvolution.

If there was a break between procedures that required us to wait outside for an extended amount of time, the laser trigger was shut off manually so it could not be fired accidentally. The PMT voltage was also turned down to minimize chances of damage and the sample was covered in saline to prevent it from drying out. Upon return, the laser power and/or paper fluorescence was retested before continuing to ensure that there have been no changes to the system that would affect subsequent measurements. After the last biopsy the data was downloaded on to a memory stick by Operator #2 before the cart was shut down and returned to Dr. Tse's office for storage. Operator #1 used alcohol to disinfect the workspace and disposed of all garbage in the biohazards bin. Recorded notes

were transcribed within 24 hours and saved to PDF files. If a standard medical report was obtained from Dr. Tse, the patient name was removed and then the papers were scanned as an extra electronic copy.

2.2: Data Processing

2.2.1: Pre-Processing and Laguerre Deconvolution

The data is collected using the procedure outlined in Section 2.1 with the instrument described in Section 1.3. An overview of the data processing is provided in Figure 2.1. Data were sampled 11 times for every wavelength at a rate of 25 ps/pt for a total of 1000 data points in each frame. The output file saved from the digitizer is a single column of floating-point numbers that requires processing to split it back into 407 (11 x 37) useable frames. The pre-processing code [4] was used to average the data from 10 pulses (discarding the first pulse) at each wavelength, remove any offsets present, and truncate the data to 650 pts (or 16.25 ns). As discussed in Section 1.3, the extra (11^{th}) pulse was added so that the first pulse could be discarded in case the AOTF had not yet stabilized from changing to a new wavelength. Offset removal is a critical component in data analysis because it gives each data set a common baseline allowing one data set to be compared to another and it also reduces error between fitting algorithms and the observed signal [4]. The truncation length was selected (Section 1.5) to improve processing speed without compromising the Laguerre algorithm's ability to provide unique solutions.

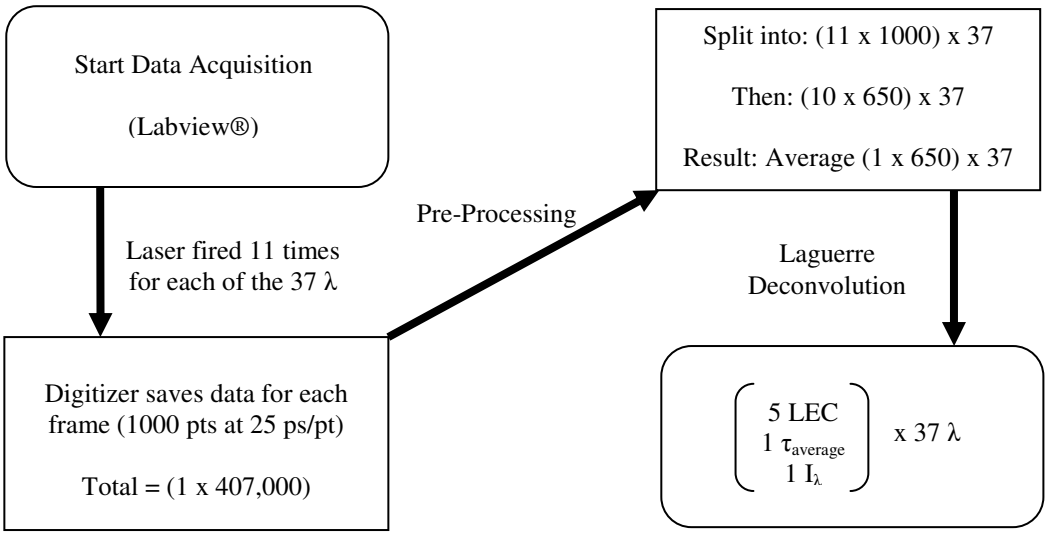

Figure 2.1: Flowchart for the processing of the tissue fluorescence response collected when the laser has been fired on one tissue spot. The data is averaged to reduce signal noise and truncated to increase processing speed during Laguerre deconvolution. The final result is a set of seven descriptive parameters to be used during tissue classification.

The total spectral intensity observed over the 17 ns time period for each wavelength is then calculated from the averaged data using trapezoidal integration to estimate the area under each time-domain curve. It is the integrated spectral intensity 'I_λ' before it has become normalized to a specific wavelength. The resulting file is saved with the same file name replacing the '_CH1.dat' extension with '_pre.mat' so it can be read by Matlab® for further analysis. The I_λ for each of the individual data files were normalized after deconvolution to the wavelength with the highest amplitudes (I_{455}) during the data analysis stage. The signal intensities observed for each data file are dependent on both the tissue composition at that particular spot and the distance between

the fiber probe and tissue. Normalized I_λ allow for the comparison of relative fluorescence signal observed and eliminates the bias.

It was shown in previous work [4] that the empirical Laguerre algorithm performed as well as the bi-exponential fitting algorithm during simulations in a fraction of the computation time. The best α is empirically chosen as the one that minimizes the sum of squared errors where the error is the difference between the data measured and theoretical data curve. Another alpha optimization method using a closed form approach [5] aimed at minimizing a cost function to derive the best alpha did not perform as well as the empirical method during longer lifetime simulations [4]. The motivation behind this cost function for Dr. Jo's group is that it reduced their computation time by 1-2 orders of magnitude to find the optimum α compared to the empirical method [5]. The closed form algorithm, alpha_opt_CF.m in Reference [4], did not yet include any laser shifting mechanism to account for chromatic dispersion inside the fiber probe. An analog to alpha_opt_1f.m (commented as alpha_opt_1g.m [4]) was constructed by Krishnamoorthy using the closed form method called 'alpha_opt_1e.m' but the comparison between methods was not conducted in time for the completion of his dissertation. Since then both the empirical and closed form Laguerre methods have been evaluated for the GI data. The optimization of α will be described next.

Deconvolution was initially conducted to find the optimized alpha and laser shift required for each wavelength on every patient's '_pre.mat' file using alpha_opt_1e.m. The results were saved with the new file extension '_laguerre.mat' and an information variable 'info' was included to record the name of the Matlab function used for the

deconvolution. It was found that α could be as low as 0.94 at the end wavelengths where there is little to no signal recorded while it was most often recorded as 0.96 or 0.97 for the other wavelengths. Review of the optimized α values did not show that the data had a preference for selecting an α of either 0.96 or 0.97. Fixing all the wavelengths to either α value for all data sets produced reconvolved Laguerre functions that resembled single decay curves in some but not all of the data files. An example of an undesirable decay curve is presented in Figure 2.2 when α is fixed to 0.96 instead of 0.97.

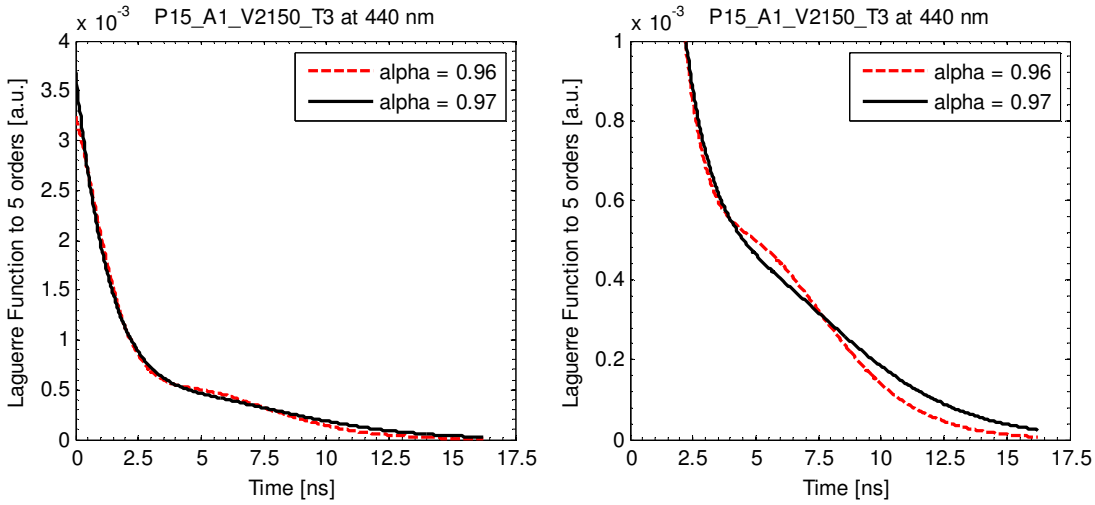

Figure 2.2: An example is taken from Patient 15 at 440 nm where the α value of 0.96 creates three obvious inflection points in the decay curve compared to when α was fixed at 0.97.

The next logical step was to adjust the algorithm so that it runs through α values starting at 0.94 in increments of 0.001 instead of 0.01 to obtain more precise results. Both the empirical and closed form Laguerre methods were used. Neither method was noticeably faster because the laser shifting portion of the algorithm is the limiting time

factor for our system. The computation time required to find the optimized α at each wavelength for one '_pre.mat' file was increased from 6 s to 1 minute when demanding more precision. Therefore five files from each tissue location were selected at random from the patient database because the computation was now 10 times slower. The files selected and their averages at each wavelength are found in Appendix C.

The average α from all tissue locations combined was taken over the range of 390-510 nm because the most variation in α at individual wavelengths takes place outside of this range. Results from both optimization methods were in agreement within 1 SD of each other; 0.968 ± 0.002 for alpha_opt_1e.m and 0.967 ± 0.003 for alpha_opt_1f.m. It suggests that incorporating the laser shifting algorithm into the CF method will provide accurate results but further testing on simpler biological systems, such as simulations and fluorescent dyes, are required to confirm that statement. Since the difference in computation time between the two methods is negligible, there is no advantage to investigate the closed form method further for our instrument. All files in the patient database were deconvolved using alpha_opt_1f.m with a single alpha value of 0.967 for all wavelengths with the file extension label '_lag1f_967.mat'.

2.2.2: Data Management

Laser spots were not registered with histological analysis for this pre-clinical trial feasibility study as that would present another set of challenges working within the clinical environment. The GI study was intended to build upon the previous work done to develop the instrument and demonstrate that the Laguerre deconvolution proof of concept

can be used on human tissue samples. In the next stage, researchers and the pathology staff are working to make a protocol for processing samples marked with tissue dye on larger specimens that come from resected brain tumours. The tissue used for the laser study there is in excess of what is required for the clinical diagnosis and thus allowing the research team time to develop the more involved protocol.

The challenge with the GI biopsies is that they are quite small (typical surface area was about 0.3 x 0.6 cm^2) so often multiple specimens for a biopsy are resected but the pathology is only conducted on one of the specimens. Multiple laser spots, with minimal overlap, were used to collect data until the area of each specimen lying face up on the Petri dish was covered. Even though fluorescent data were labeled specific to each individual specimen, there is no way of knowing which specimen the pathologist selected for their analysis. The best representation of the fluorescent data for each tissue location would be to take the average of all the data sets taken for that patient's tissue location after any outliers have been removed. Outlier data sets include those where the laser missed the sample target or where the instrument's reading was compromised by too high or too low of a signal input. Chapter 3 is devoted to the analysis of the individual data sets collected to identify ones that do not represent tissue fluorescence because of external factors and not the differences in biological composition. Removal of the outlier data before calculating the average patient tissue fluorescence is critical because it will otherwise distort the descriptive statistics from their true values and affect the results of classification models presented in Chapter 4.

One last thing to mention is that the information required to conduct further analysis (such as τ-λ, I_λ , and the LEC-0_λ to LEC-4_λ) was saved into a new file (~169 kB) for two reasons. The first is that having smaller files to work with in Matlab made loading files much faster than individual Laguerre files (~660 kB). The second reason was that these smaller files could be manipulated and sorted into categories (ex. diseased or normal diagnosis) in new folders without jeopardizing the integrity or organization of the original Laguerre files. File names were also shortened by removing the date and adding the extension label '_var.dat' (ex. P28_B1_V2200_T2_var.dat). After some initial data evaluation in Chapter 3 it was found that the time-domain information would be required to do some further analysis. Since the '_var.dat' files had already been categorized by disease it was easier to create a new file (ex. P28_B1_V2200_T2_tdomain.dat) containing just the time-domain information of each wavelength (50 kB) and add them to the categorized data instead of starting from scratch with new '_var.mat' file that included the time-domain information. Matlab scripts were developed and automated to create those new files and to gather the parameter averages after the outlier files were manually removed from the folders.

2.3: Data Analysis

2.3.1: Overview

The parameters available for analysis are the values at each of the 37 wavelengths for the five Laguerre coefficients (LEC-j_λ), average lifetime (τ-λ), and the normalized intensity (I_λ). It is unknown which of these 259 (37 x 7) parameters may differ

significantly from one tissue location to the next as this is the first study of its kind on GI tissue. A simple comparison test is required first to identify potential parameters that statistically differ from one tissue to another and further simplify the data pool for potential classification methods. An ideal classifier can take a measurement from an unknown tissue type and identify it quickly and correctly. The best model can predict the tissue type with 100 % sensitivity (Equation 2.1) and 100 % specificity (Equation 2.2) meaning that there are no results identified as false positives or false negatives respectively. [6]

$$Sensitivity = \frac{\sum True_{positives}}{\sum True_{positives} + \sum False_{negatives}} \qquad (2.1)$$

$$Specificity = \frac{\sum True_{negatives}}{\sum True_{negatives} + \sum False_{positives}} \qquad (2.2)$$

To make the analysis more selective, two parameters that were both identified as being statistically different between two different types of tissue will be used to mark each tissue type in a two dimensional space. The distribution of tissue measurements in a multi-dimensional space should ideally create more separation between each tissue cluster and make it easier to derive a much better defined classification model [7]. All possible pairs of the 259 parameters must be considered. Computation time can be significantly reduced by eliminating those parameters where the tissue samples are not statistically different because it would be impossible to find a classifier that can separate homogeneous data. The following sub-sections of this chapter are dedicated to the

identification of such parameters and the development of a classification system for the GI fluorescence data.

2.3.2: Hypothesis Testing

Before continuing further, a basic review of hypothesis testing is warranted in order to understand the decision making process when interpreting statistical significance. The null hypothesis (H_o) is rejected in favour of some alternative hypothesis (H_1) when the probability of obtaining a test statistic is as or more extreme than the desired confidence level. For example take the t-test, the most popular test for the difference between two independent samples where H_o hypothesizes that both samples have equal means and the alternative H_1 is that they are not equal. If the desired confidence level is 95 %, then H_o is rejected when the probability or 'p-value' is less than 0.05. It means that there is s 5 % chance H_o has been rejected when it's actually true and this is the risk of a false negative result. Note that when the test does conclude that H_o is 'true', it does not imply that the test has proven the mean of the two samples are the same but rather that there is no reason to conclude that they are different. [8, 9] It is important to understand that statistics is not an absolute science but rather one that is developed by studying and modeling events that occur by chance so that one can report and interpret, perhaps even predict, the meaning of events with a quantitative degree of confidence.

Each statistical test developed is based on a certain set of assumptions about the data and its distribution. Violation of any one assumption in a test will jeopardize the integrity of the test results and leave more chance for error when making decisions. In

hypothesis testing the most common assumptions are that the sample outcomes were measured independently from one another, have equal variances, and are normally distributed [8]. Based on the last assumption, tests are divided into two categories: parametric and non-parametric models. Parametric models require more assumptions compared to non-parametric methods and are often preferred because the models are simpler and more precise when the data follow the Gaussian (bell-shaped) normal distribution. Non-parametric tests are designed to make decisions while taking into account that less is known about the sampling distributions and do not rely on a particular distribution to build the test theory. It is to say that they are more versatile but less efficient if there actually is a distribution criteria that can be met. [9]

Most tests available in either case require that the samples are independent and often there are corrections available that can account for unequal and/or unknown variances. Individual fluorescent measurements meet the independence requirement. Data at each wavelength is measured from individual laser pulses and the outcome at each sampling location is not affected by the tissue at another location. The next challenge when searching for meaningful GI data after the removal of outliers is to determine which statistical tests can and should be used to identify differences in tissue fluorescence between samples. The analysis will start by identifying if the most powerful (parametric) tests are applicable to the GI data and then work to select an appropriate method to identify statistically different parameters for tissue classification.

2.3.3: Statistical Methods Required to Compare Individual Parameters

A two sample t-test (where samples are two different tissue locations) would be the best place to start. It can be calculated with or without the assumption that the variances are known and are both equal but each sample must follow a Gaussian normal distribution [9]. Before using the t-test the normality of each distribution must be confirmed. Graphical representation of the data in a histogram can be used to visualize the distribution of the data but it is often too difficult to estimate the skew (tails) and kurtosis (peak rise) of the distribution by simply looking at the graph [7]. In small data sets ($N < 30$) it is near impossible to estimate what the normal distribution should be without some guidance from a mathematical theory [7].

While there are several normality tests available, no single test method is dominant and different software packages will offer different tests [7, 10]. For example SAS® (v.9.2) offers the Kolmogorov–Smirnov (KS), Shapiro-Wilk, and Anderson Darling tests, while Matlab (v.2010) offers KS, Lilliefors, and Jarque-Bera tests. In good practice it is best to try two methods and see if they are in reasonable agreement. In cases where there is a lot of data (such as 259 parameters) using one test to get an idea of how many of the samples are reasonably normally distributed or not is enough to decide if a non-parametric comparison test instead of the t-test should be used. In a search for the popularity of these tests using the Scientific Journal search engines Web of Science and PubMed, KS is the most popular while the others are extremely rare. The vast majority of authors who analyzed data with the t-test did not even report the use of a normality test at all.

The KS test however is arguably an over simplified method used to compare the maximum difference between the cumulative frequency distribution of the sample to the known normal distribution of the population. It is more conservative meaning that it is less likely to reject H_o during borderline decisions. Lilliefors test is a more powerful extension of KS when the population cumulative frequency distribution is unknown and must be estimated. Also its corrections lead to p-values different than the KS which make the test less conservative. [11, 12] The 'lillietest.m' function in Matlab was used to test the normality of each tissue type using the patient averages. As discussed later in Chapter 4, some τ-λ, I_λ, and most of the LEC failed the test ($p < 0.05$) meaning that the data cannot be reasonably fitted to a hypothetical normal distribution. Therefore the non-parametric alternative rank-sum test was used instead of the t-test.

The rank-sum test, known as the Wilcoxon Rank-Sum or Mann Whitney U-Test, uses the rank of the pooled measurements to look for the H_o where the groups have equal medians instead of equal means (i.e. the t-test). To set up the rank-sum test, all of the measurements are ordered lowest to highest and assigned a rank. If the sum of the ranks for each group are close enough to each other ($p < 0.05$) then H_o is true. [6, 13] The rank-sum test does not assume each group has equal variances nor is it dependent on the data satisfying a particular distribution type. However its only fallback is the assumption where the groups to be compared both have the same type of distribution. [13] A two-sample KS test can be used to check this assumption by determining if the maximum difference between these two cumulative frequency distribution is significant ($p < 0.05$) enough to suggest that they follow different distributions [10, 14]. Both tests are available

in Matlab (ranksum.m and kstest2.m) and were used to identify potential parameters for the two dimension separation analysis.

Now if the two groups of interest are in fact very different from each other, then in theory they will have different medians and the rank-sum would be able to detect it regardless of the 2-sample KS test result. Removal of parameters from the rank-sum test whose groups do not have the same distribution, but possibly have different medians, would omit potential parameters that could be used for a successful two dimension classification. All of the parameters were used in the rank-sum test in light of this motive. However, by using the rank-sum test on all of the samples there is still the risk of error of where H_o is kept when it is actually false. The test cannot distinguish a difference between the two samples with different distribution types because co-incidentally they will have the same rank-sum when the samples are pooled together for their rank assignment. To reduce the risk of missing out on these parameters, results of the rank-sum test were cross-referenced with the 2-sample KS test. Any parameters that passed the rank-sum test but failed the 2-sample KS test were included in the classification analysis.

2.3.4: Classification Methods

An unsupervised learning classification algorithm (ex. clustering) is preferential for the GI data because of our small data base available for study. More complex classification models can offer more precise solutions but require the assistance of supervised machine learning. In this case random sub-samples from the population are used to train the classifier until the error in the model is minimized and it converges to a

single solution. It is not an ideal approach to classify the GI data because this process is highly sensitive to change when the sample size is small [15]. Also, many of these supervised methods are parametric models that rely upon several assumptions regarding both the data sampled and its population. One of these assumptions require that the population variance be known because then the variance of random sub-sampling will be stable and make the training classifier more robust [15]. Unsupervised methods are typically non-parametric [15, 16] and are advantageous at this point in the GI study because the behaviour or rather 'the character' of the population distribution can only be truly revealed by acquiring large amounts of data.

On that last note, it is advised to collect as much data as possible within the time and resources available even though there are several ways to justify how much data is enough to draw conclusions [17, 18]. The minimum sample size required by a study needs to be calculated using the initial results of the test in question and not some other related study. Each test completed by a different treatment and/or delivery protocol can present its own influence on the measurements no matter how profound or subtle it may seem. To determine what the minimum sample size should be is often a formula based calculation that depends more on the clinical significance rather than the character of the data. The clinical significance confidence interval is the difference between the two portions (means or categories) being tested that are desired in order to accept the risk of a patient's outcome when treated from a misdiagnosis. [17, 18] Ultimately the calculation of the sample size required to validate the results of a study is the responsibility of a clinical epidemiologist who has been assigned to the research ethics committee.

Researchers must gather enough data to initialize their study and one common way to estimate the starting sample size is to review publications on similar studies. The average pilot study size begins with a minimum of 20 patients so the GI study was targeted at 30-40 patients. Butte et. al [19] has demonstrated that Linear Discriminant Analysis (parametric modeling) can be used to classify brain tumours based on parameters derived from TR-FS and Laguerre deconvolution. However, he is still cautious to point out that they need a sample size much greater than their 42 patients (71 total biopsies) to stay clear of overestimating the classifiers. The main reason cited was that they only selected the biopsies and parameters that would train for the best possible outcomes [19]. GI tissue has not been studied before using Laguerre deconvolution so it is unknown which (if any) parameters can be used effectively to distinguish between different tissue types. Cluster analysis is a popular unsupervised method and will be used to study our parameters for fluorescence signatures.

Typically cluster analysis is reserved for studies where the true object labels and/or number of groups is unknown [16]. However, it can still be used when this information is known because the algorithm was designed not to be influenced by this kind of specific knowledge prior to the analysis. Both the data labels and the number of groups are known for the GI data. In this case the sensitivity and specificity [6] of the object classification in two dimensions can be used to assess the potential of an optical biopsy to be able to distinguish between different tissue types.

If the clusters are not homogeneous and well separated then it is expected that this result would lower the sensitivity and specificity of the test. Heterogeneous data would

have a negative impact on these rates regardless of which classification method was used but to what extent can only be determined by taking the time to implement different models. A more sophisticated classification model from supervised machine learning should be able to improve these numbers provided it was one chosen that can provide a more appropriate fit to the data character. No single classification method is superior to another [15, 16]. It is best to apply several different models to see which one works best to model the data of interest beginning with the simpler, less computationally involved methods first.

2.3.5: K-Means

The simplest unsupervised computational algorithm available is k-means cluster analysis. It is a non-hierarchical way of partitioning the data into classes where the only requirement is that the number of cluster centers or 'k-means' are specified prior to implementing the algorithm. It does not depend on any other prior knowledge about the data character. Clusters can either be estimated when the data graphically appear well separated or they may already be known (as in our case). In contrast, hierarchical methods are used to create cluster trees when the number of clusters is not obvious. [16]

K-means will assign each data point to the closest centroid ('k-mean' value) using the assignment which minimizes the sum of distances to form 'k' initial clusters. Starting point selection for each k-mean centroid is completely arbitrary. Each centroid is then recalculated based on this assignment of data points and then the next iteration begins. The classification of each data point will change if it is now closer to another k-mean.

Once all the data points have been checked or reassigned, each k-mean centroid is recalculated again and the process repeated until the algorithm converges. The k-mean values can then be used for supervised classification where new unlabeled objects are assigned a label based on which k-mean centroid they are closest too. [16]

The k-means analysis was performed on the GI data using the 2-step algorithm available in Matlab (k-means.m). The additional second step can fine tune the centroids to a local minimum after the traditional way of finding k-means (described previously) and thus optimize the chance of finding the global minimums. This step now recalculates the centroid every time one of the data points can be reassigned to reduce the sum of distances from each data point to its centroid. Once all of the points are passed through this process a new iteration begins until none of the points can be reassigned. By default Matlab has included this step in its algorithm although it does not require more than one or two iterations to achieve a local minimum. [20]

Point to centroid distances can be calculated multiple ways depending on if the clusters are roughly spherical with a globular boundary or not. Squared Euclidean distance and City-Block 'Manhattan' are the two most common distance formulas for non-standardized data (Figure 2.3). In most cases the two formulas will yield similar results except for when there are some data (objects) with particularly large centroid to point distances. The Squared Euclidean distance puts more weight on these objects during classification and is recommended for use when the clusters are not globular. Cluster assignment using these distance equations can also be influenced by the dimensions of each axis and may lead to less than desirable clustering results. [21]

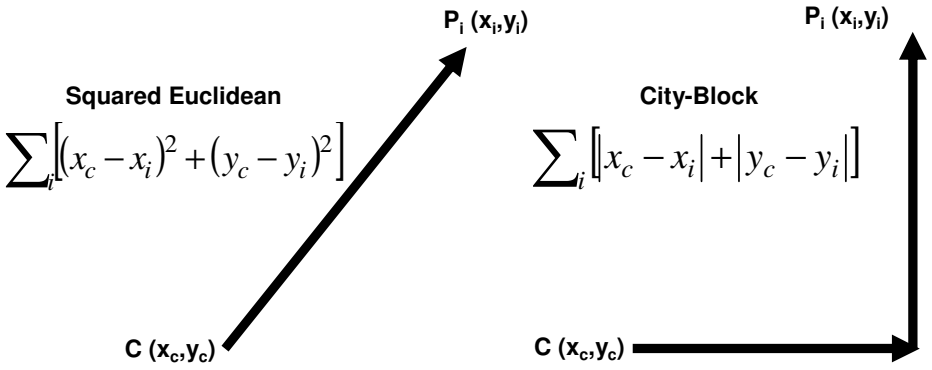

Figure 2.3: The Squared Euclidean and City-Block "Manhattan" centroid to point distance calculations.

Both distance calculations are available in Matlab and by default kmeans.m selects the Squared Euclidean distance. Clusters formed by the parameter pairings roughly do not look globular so the default distance option was used. Some of the parameter pairings had large differences between their dimensions. As an example the values for LEC-3_λ are two orders of magnitude smaller ($1x10^{-2}$) than I_λ. If LEC-3_λ is on the y-axis and I_λ is on the x-axis then the x distance to each centroid will influence the assignment more than the y distance. For pairings where there was at least 1 order of magnitude difference between the dimensions, clustering was performed both with and without dimension transformations. Results for the GI fluorescent data did not reveal a definite answer as to if and when the data should be transformed so that the dimensions are matched. Details are presented and discussed in Chapter 4.

Another disadvantage to clustering is its low precision relative to other classification methods that use training samples because it is sensitive to the initial choice of centroid locations [16]. Ultimately the true global minima can only be found by

repeating the two-step process using several different sets of starting centroids (termed 'replicates') to see which ones produce the best results. Matlab offers an opportunity to run multiple replicates using either pre-defined or randomly chosen initial centroids [20]. Only the k-means solution with the lowest sum of distances from the centroids to their data points is reported back [20]. Each option was tested using two k-mean groups to see how the selection of the starting centroids and number of replicates affected the outcome of results. The sensitivity and specificity with respect to the first group were calculated using the cluster group index results produced by kmeans.m.

Sometimes the computer randomly selected the first centroid from the second half of the data list and the second centroid from the first half. In this case the sensitivity and specificity are very poor because the classification labeling has been reversed where group one has become recognized instead as group two. Random selection of data points using each individual group must be done outside of kmeans.m and used as pre-defined inputs. While this rectified the situation for the most part, it was still a problem when a starting centroid was close enough to the other cluster to cause a reversed classification. Multiple replicates (5, and 10) did not guarantee that Matlab would report the best solution with the correct group label assignment if a solution with the lowest sum of distances happened to be one with a reversed classification.

Since the choice of starting locations is indeed arbitrary, in theory the user can choose any point on the x-y grid to represent the starting locations. The k-means can be steered towards the desired cluster locations because each data's proper classification is known previously from the GI histology results. The average x and y co-ordinate of each

group was used to calculate the actual geographic center (i.e. the 'theoretical centroid') of each cluster making up the pre-defined starting centroid inputs. As the kmeans.m reassigns data points to the other cluster centroid if it is indeed closer, the value of the centroid will be recalculated to reflect this change. Otherwise if the clusters are homogeneous and either well separated or globular, the final centroids will be the same as the input centroids. In preliminary testing it was found that using these averages will produce the best sensitivity and specificity results when used with the Squared Euclidean distance because clusters do not have a defined shape.

REFERENCES

[1] Cohn GE, Domanik R. 2003. In vitro clinical diagnostic instrumentation. In: Vo-Dinh T, editor. Biomedical photonics handbook. Boca Raton, FL: CRC Press LLC. p 19-1:14.

[2] Pfefer TJ, Schomacker KT, Ediger MN, Nishioka NS. 2002. Multiple-fiber probe design for fluorescence spectroscopy in tissue. Applied Optics 41(22):4712–4721.

[3] Papaioannou T, Preyer N, Fang Q, Carnohan M, Ross R, Brightwell A, Cottone G, Jones L, Marcu L. 2004. Effects of fiber-optic probe design and probe-to-target distance on diffuse reflectance measurements of turbid media: an experimental and computational study at 337 nm. Applied Optics 43(14):2846-2860.

[4] Krishnamoorthy M. 2010. Optimization of a time-resolved spectroscopy system with an acousto-optic tunable filter employing a deconvolution method based on discrete laguerre functions [dissertation]. Hamilton (ON): McMaster University.

[5] Dabir A, Trivedi C, Ryu Y, Pandey P, Jo J. 2009. Fully automated deconvolution method for on-line analysis of time-resolved fluorescence spectroscopy data based on an iterative laguerre expansion technique. Journal of Biomedical Optics 14(2):024030.

[6] Riffenburgh, RH. 2006. Statistical testing, risks, and odds in medical decisions. In: Statistics in medicine. 2nd ed. Burlington, MA: Elsevier Academic Press. p 93-114.

[7] Seo J, Shneiderman B. 2010. Multidimensional analysis and visualization on large biomedical data. In: Lee JK, editor. Statistical bioinformatics - for biomedical and life science researchers. Hoboken, NJ: John Wiley & Sons Inc. p 157-184.

[8] Riffenburgh, RH. 2006. Hypothesis testing concept and practice. In: Statistics in medicine. 2nd ed. Burlington, MA: Elsevier Academic Press. p 75-92.

[9] Cho HJ, Seo W. 2010. Statistical testing and significance for large biological data analysis. In: Lee JK, editor. Statistical bioinformatics - for biomedical and life science researchers. Hoboken, NJ: John Wiley & Sons Inc. p 71-88.

[10] Riffenburgh, RH. 2006. Tests on the distribution shape of continuous data. In: Statistics in medicine. 2nd ed. Burlington, MA: Elsevier Academic Press. p 369-386.

[11] Lilliefors HW. 1967. On the Komogorov-Smirnov test for normality with mean and variance unknown. Journal of the American Statistical Association 62:399-402.

[12] MATLAB® v.7.10. 2010. Lilliefors test (lillietest.m). Natick, MA: The MathWorks Inc.

[13] MATLAB® v.7.10. 2010. Wilcoxon rank sum test (ranksum.m). Natick, MA: The MathWorks Inc.

[14] MATLAB® v.7.10. 2010. Two-sample Kolmogorov-Smirnov test (kstest2.m). Natick, MA: The MathWorks Inc.

[15] Ahn H, Moon H. 2010. Classification: supervised learning with high-dimensional biological data. In: Lee JK, editor. Statistical bioinformatics - for biomedical and life science researchers. Hoboken, NJ: John Wiley & Sons Inc. p129-156.

[16] Belacel N, Wang C, Cuperlovic-Culf M. 2010. Clustering: unsupervised learning in large biological data. In: Lee JK, editor. Statistical bioinformatics - for biomedical and life science researchers. Hoboken, NJ: John Wiley & Sons Inc. p 89-128.

[17] Riffenburgh, RH. 2006. Sample size required for a study. In: Statistics in medicine. 2nd ed. Burlington, MA: Elsevier Academic Press. p 115-123.

[18] Riffenburgh, RH. 2006. Sample size required in a study. In: Statistics in medicine. 2nd ed. Burlington, MA: Elsevier Academic Press. p 397-417.

[19] Butte PV, Mamelak AN, Nuno M, Bannykh SI, Black KL, Marcu L. 2011. Fluorescence lifetime spectroscopy for guided therapy of brain tumours. Neuroimage 54(1):S125-S135.

[20] MATLAB® v.7.10. 2010. K-means clustering (kmeans.m). Natick, MA: The MathWorks Inc.

[21] Hill T, Lewicki P. 2007. Cluster analysis. In: Statistics: methods and applications. Tulsa, OK: StatSoft Inc. p 115-126.

CHAPTER 3: DATA EVALUATION

Time-domain fluorescence spectroscopy data collected from human tissue samples are usually noisy and contain a number of artifacts from the clinical data acquisition process. Therefore, it is important to be able to categorize the quality of the data before further analyses are performed. The goal is to establish criteria that can consistently identify outlier data. Such measurements can skew the results and in turn jeopardize the integrity of any generalized conclusions.

The time-domain data was reviewed for any cases where the signal amplitude may have been saturated by inadequate digitizer settings or from excess light build up inside the MCP-PMT. Both steady-state and time-domain data were used to determine the lower signal detection limit of the instrument. If the signal-to-noise ratio (SNR) is poor, the Laguerre algorithm may be incapable of accurately extracting reasonable lifetimes. Also, if the signal is too low, the 8-bit digitizer may not have the sufficient vertical resolution to record the data. Sample photobleaching and the repetition of measurements on the same tissue spot are concerns also addressed in this chapter. Finally, the results were summarized and the list of relevant criteria was applied to tabulate all of the measurements which should be removed from further analysis.

3.1: Clinical Results

The histological diagnosis of each sample location from each patient is shown in Tables 3.1 and 3.2. Patients were labeled in the order that they were sampled however not all of the patients could be included in the analysis and calculations. Samples from two of the 28 patients were from the same person (P12 and P19). Originally the esophageal samples were too small and could not be analyzed by histology or auto-fluorescence. The P19 esophageal biopsy was a successful repeat visit and the results were relabeled in this study to be included as P12 data. Also, the P18 data had to be excluded from our analysis because the medical record number could not be located. For reasons discussed in the next section, patients P01-P06 inclusive were removed from our data set due to instrument sampling errors. Lastly, fluorescence measurements were not recorded for the P26 duodenum because the sample was preserved in formalin immediately after the biopsy and could not be recovered.

In total there are 20 patients available for fluorescence analysis in our data base. Of these 20 patients only some of their tissue locations returned normal biopsy results meaning that there are only 16 duodenum (A), 3 antrum (B), 13 body (C), and 16 esophagus (D) biopsies available for analysis. Most of the diseased antrum tissue (14/17 patients) were found to have various degrees of chemical gastopathy while chemical gastritis was present in the others. Several different conditions ranging from acid reflux to cancer were observed in the other tissue locations but not enough patients (less than 4) to form another diseased group for future analysis.

Table 3.1: Histological Diagnosis for Patients 1 to 28.

Collection Date YMD	Patient	Duodenum A	Antrum B	Body C	Esophagus D
2009-02-23	P01	0	1	0	1
2009-03-06	P02	0	1	0	0
2009-03-09	P03	0	1	1	0
2009-03-09	P04	0	0	0	0
2009-03-09	P05	0	1	0	1
2009-03-09	P06	0	1	0	1
2009-08-31	P07	0	1	1	0
2009-08-31	P08	0	1	0	0
2009-08-31	P09	0	1	1	0
2009-09-14	P10	1	1	0	0
2009-09-14	P11	0	1	0	1
2009-09-14	P12*	0	0	0	0
2009-09-15	P13	1	1	0	0
2009-09-15	P14	0	1	1	0
2009-09-15	P15	0	1	0	0
2009-09-21	P16	0	1	0	0
2009-09-21	P17	0	1	1	0
2009-09-21	P18	NA	NA	NA	NA
2009-09-28	P19*	NA	NA	NA	1
2009-09-28	P20	0	1	0	1
2009-09-28	P21	1	1	0	0
2009-09-28	P22	0	1	1	0
2009-09-29	P23	0	1	0	0
2009-09-29	P24	0	1	1	0
2009-09-29	P25	0	0	0	0
2009-10-19	P26	0	1	0	0
2009-10-19	P27	0	1	1	0
2009-11-02	P28	0	0	0	1

Normal = 0, and Diseased = 1, Diagnosis unavailable = NA.

* P12 esophageal biopsies were non-diagnostic and repeat biopsies were performed on 2009-09-28 (P19).

** Fluorescence results were not obtained for P01 A-D or for P26 A.

Table 3.2: Comments for the Histological Diagnosis of Patients 1 to 28.

Patient	Comments
P01	Antrum has chemical (reactive) gastropathy; Esophagus has mild reflux esophagitis
P02	Antrum has chemical (reactive) gastropathy
P03	Antrum has chemical (reactive) gastrophaty; Body has fundic gland polyp
P04	All are Normal
P05	Antrum has minimal chronic gastritis; esophagus has focal acute esophagitis
P06	Antrum has mild chronic gastritis; esophagus has focal reflux
P07	Antrum has minimal chemical gastropathy; body has minimal chemical gastritis
P08	Antrum has chemical gastrophathy
P09	Antrum and Body have chronic active HP gastritis
P10	Duodenum has mild increase IEL, crypt blunting, architectural distortion with fibrosis; Antrum has mild reactive gastropathy
P11	Antrum has chemical gastropathy; esophagus has mild reflux esophagitis
P12*	Esophagus biopsies were non-diagnostic; repeat with P19*
P13	Duodenum has mild villous blunting; Antrum has chemical gastropathy
P14	Antrum and Body have chemical gastropathy
P15	Antrum has chemical gastropathy; esophagus has mild reflux esophagitis;
P16	Antrum has chemical gastrophaty
P17	Antrum and Body have chemical gastropathy
P18	No Diagnosis Provided.
P19*	P12* is resampled, Esophagus has invasive neuroendocrine cancer
P20	Antrum has mild chemical gastropathy; Esophagus has reflux esophagitis
P21	Duodenum has duodenitis; Antrum has mild chemical gastropathy
P22	Antrum and Body have gastritis
P23	Antrum has chemical gastropathy
P24	Antrum and Body have chemical gastropathy
P25	All are Normal
P26	Antrum has chemical gastropathy
P27	Antrum and Body have HP gastritis
P28	Esophagus has Barrett's with indefinite dysplasia

3.2: Data Assessment

In the data processing stage, steps were taken to reduce the signal noise by removing artifacts and averaging 10 sets of measurements that improved the overall performance of the Laguerre deconvolution algorithm [1]. However, those steps did not include a screening method with upper and lower detection limits for the collection of GI

data. There are a few main causes of outlier data that need to be identified and removed if found present in order to obtain an accurate statistical analysis. Outlier results would be expected when the sample was not in the path of the laser and when there is light saturation inside the MCP-PMT. Other causes arise when the GI signal is quite low in signal amplitude and challenges the performance of fitting algorithms to fit the true signal rather than fit to the noise. All of the data collected were kept for review.

The auto-fluorescence spectral range of human tissue is similar to that of paper with a glossy finish (Figures 3.1 and 3.2). A business card was used to verify that the system was functioning correctly because its spectrum is relatively stable. The program that was developed with Labview was designed to display the maximum intensity profile taken from the last AOTF sweep because it takes less processing power than calculating the I_λ. The spectral shape is nearly identical using these two methods. If the spectral shape of paper displayed in Labview was as expected (based on visual inspection), then the instrument was deemed to be functioning properly and ready for GI data collection.

Problems with the instrument's performance were observed during the first few patients. Transportation of the instrument for the first date shifted the laser components enough making the P01 data collection impossible. Adjustments were made accordingly to realign the laser and the system was tested using paper fluorescence back in the lab. However, during the next two collection dates the erratic and inconsistent spectral shape of GI data raised some further concerns about the instrument's performance. The previous students returned the instrument back to the lab after P06. Every component was retested and recalibrated but they were unsuccessful in determining the exact cause of the

problem. The abnormalities discussed next cannot be reproduced and never occurred in subsequent measurements.

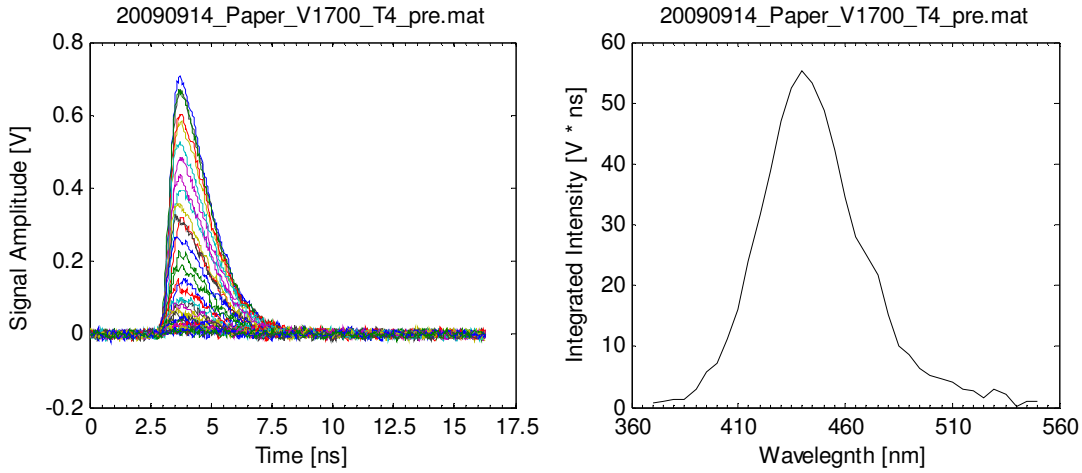

Figure 3.1: Time-domain and spectral data for paper fluorescence. On the left, the time-domain data are plotted for all 37 wavelengths. On the right is the area under each time-domain curve plotted as a function of wavelength.

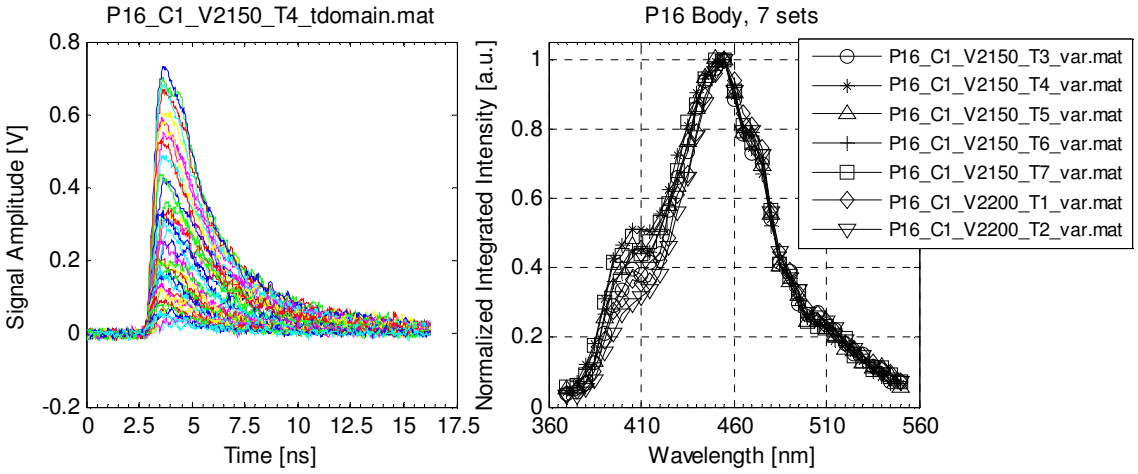

Figure 3.2: Time-domain (left) and spectral data (right) for P16 body tissue. One data set (T4) was chosen to represent the time-domain data for all wavelengths. Each normalized spectral data set typically has complete overlap with one another, except sometimes during shorter wavelengths as with this sample here. The GI data plotted has a shape similar to the fluorescence by the paper sample in Figure 3.1.

The pre-processed time-resolved data were plotted and reviewed from these first few patients (P02-P06). An example is taken from P06 body tissue in Figure 3.3. It was found that the time-resolved signal does indeed resemble the shape of the impulse curves produced by paper and tissue fluorescence but not in the progressive rise and fall pattern of signal strength. The differences are these spikes in measured intensity (ex. 'P06 C1 T3' in Figure 3.3) which are apparent in the steady-state data and are the reasons for raising a concern about the instrument's integrity. Most of the data from P02-P06 can be represented by Figure 3.4 where the instrument lacks the ability to take consistent measurements. Sometimes the instrument was a little more consistent (Figure 3.3) but without the problem or problems identified it is not known to what affect the system had on the outcome of each measurement. All of the data obtained from P01-P06 are excluded from the calculations in this report.

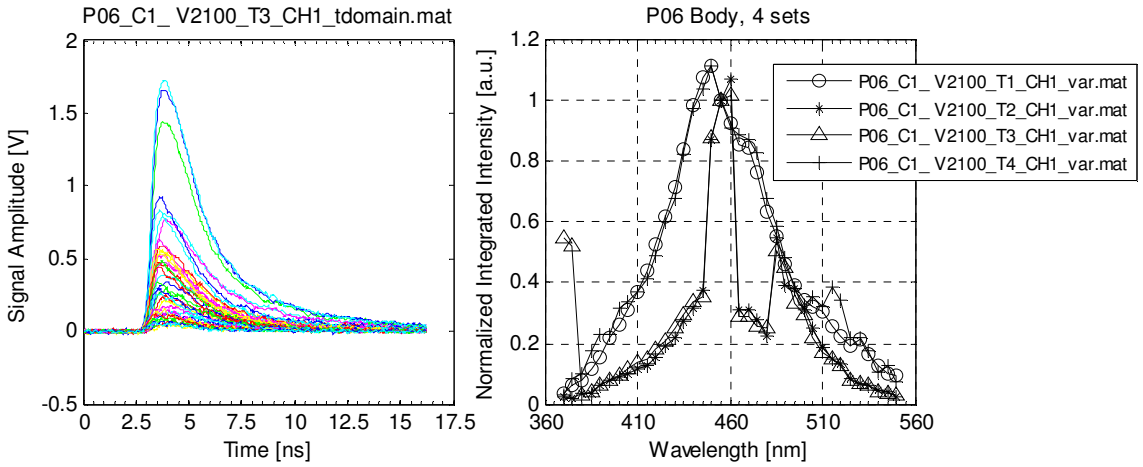

Figure 3.3: Patient 6 body tissue time-domain (left) and spectral data (right). In P06, some of the data is distorted (ex. T3) by the instrument's jitter when collecting the data as indicated by the jumps in observed fluorescence signal. Also, the peak wavelength was found to be blue shifted 5 nm and was corrected during the re-calibration process.

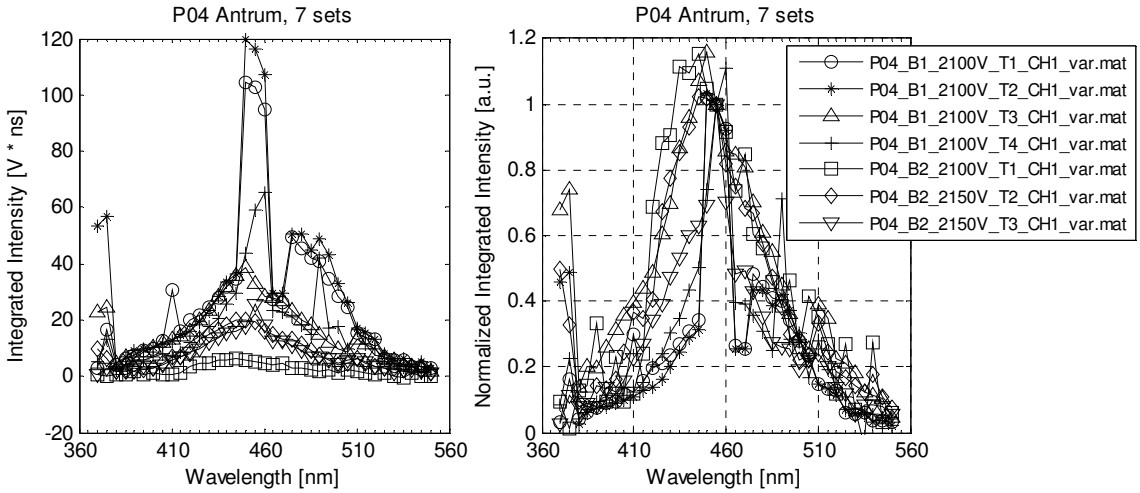

Figure 3.4: Patient 4 represents most of the data from Patients 2 to 6. There was no consistency in the instrument's ability to measure incoming signal as the normalized spectral data do not overlap.

3.2.1: Amplitude Saturation

The initial digitizer vertical scale was set high enough to include the maximum fluorescence intensity observed in GI tissue. If the limits were too low then the digitizer would be saturated such that the signal amplitude would be cut off and the pulse would be square. In other words the measurement is recorded as that cut-off value for any length of time the signal exceeds that maximum limit. The signal could also become saturated if ambient light leaked into the instrument which would increase the observed signal and cause it to saturate the digitizer and/or broaden the observed pulse width. In either case the lifetime features can be influenced by these artifacts and produce erroneous results. If saturation is indeed present in some of the GI data, a square or broadened pulse in the time-resolved data would be obvious during manual visual inspection. The scale used was

from 0 V to -2.5 V (500 mV/division) where the signal amplitude could be adjusted to fit this range by changing the MCP-PMT gain (discussed next in Section 3.2.2). For other tissue types the fluorescence strength may be different and the digitizer scale should be adjusted to capture the signal with maximum vertical resolution before causing saturation. The best vertical resolution is one that can record the signal intensity with enough precision to capture the decay such that an actual curve is observed which would otherwise be lost when each measurement is rounded to a less precise value.

The data with the highest amplitudes ($I_{455} \geq 150$ V·ns.) were checked to see if the maximum time-resolved signal had been cut off. Figure 3.5 shows P13 with the first data set T1 amplified nearly four times higher than the average signal in T2-T6. In Figure 3.5c, time-resolved data was plotted for T1 at 435 nm, 455 nm, and 475 nm where the maximum amplitude is 1.45 V at time point 150 or 3.75 ns. A square pulse was not observed in Figure 3.5 or for any of the high intensity data including the maximum observation of 1.84 V at 3.73 ns for P25 esophagus tissue T4.

Pulse broadening was suspected in cases where the normalized I_λ (to 455 nm) were much greater than other measurements from that same sample or other patients. Some of these samples were targeted first. The full width at half maximum (FWHM) of the time-domain signal looked somewhat wider than usual but evidence of MCP-PMT saturation was not obvious as more extreme broadening was expected (Figure 3.6). For the most suspicious samples the cause of any pulse broadening would be difficult to determine because they are from a patient with a disease that is not found elsewhere in our data base. Manual review of the data in an attempt to quantify evidence of pulse

broadening due to MCP-PMT saturation would be time consuming so the following calculations and analysis was performed in Matlab and Microsoft Excel.

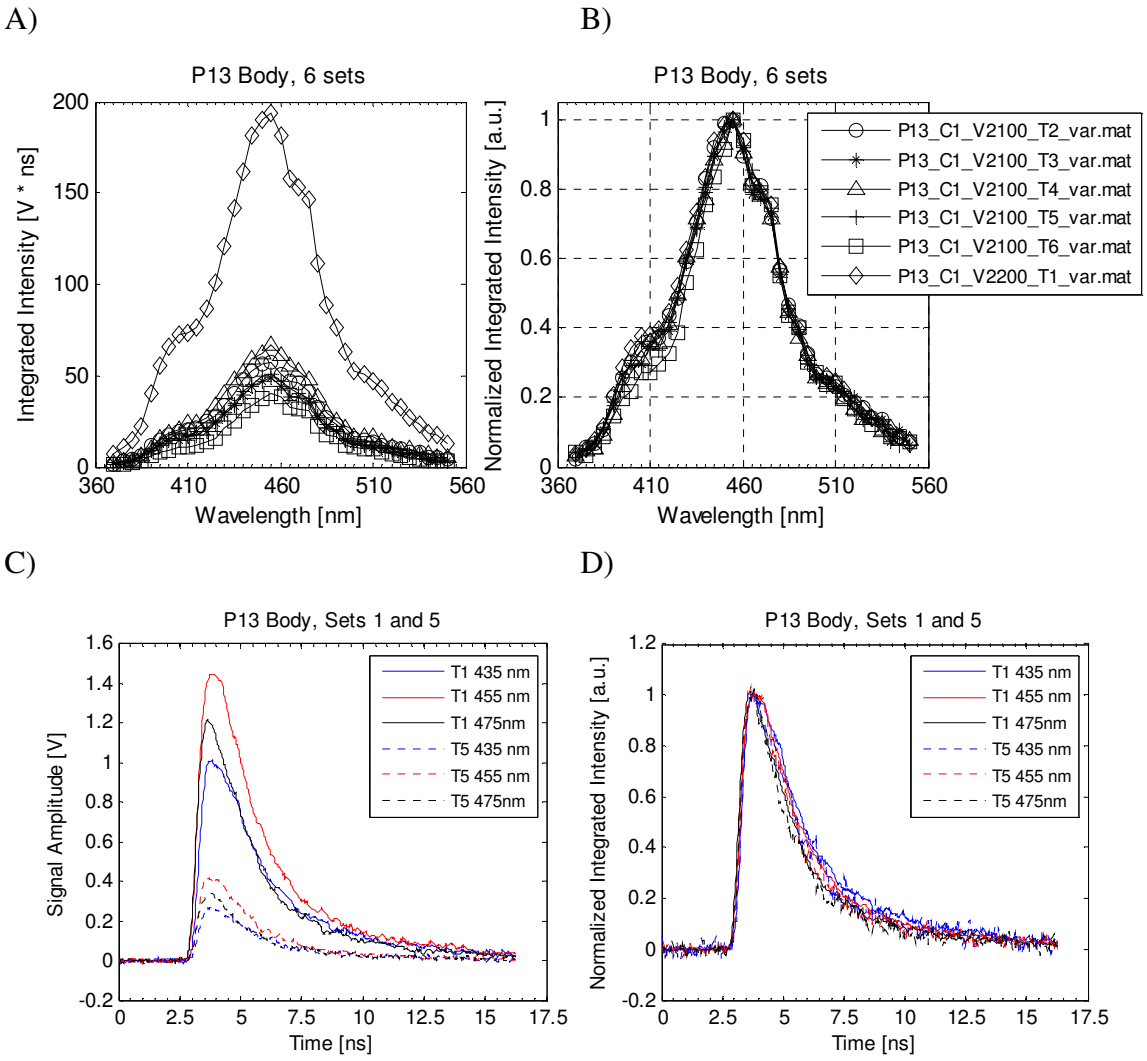

Figure 3.5: Saturation of the instrument by a strong signal is reviewed using P13 as an example. A) T1 maximum signal is nearly four times greater than the other data collected. B) When normalized, the change in fluoresce observed across all wavelengths is maintained. C) The time-domain data is compared between T1 and T5 at three different wavelengths 435 nm, 455 nm, and 475 nm. D) Signal broadening is not observed when the data is normalized in the time-domain.

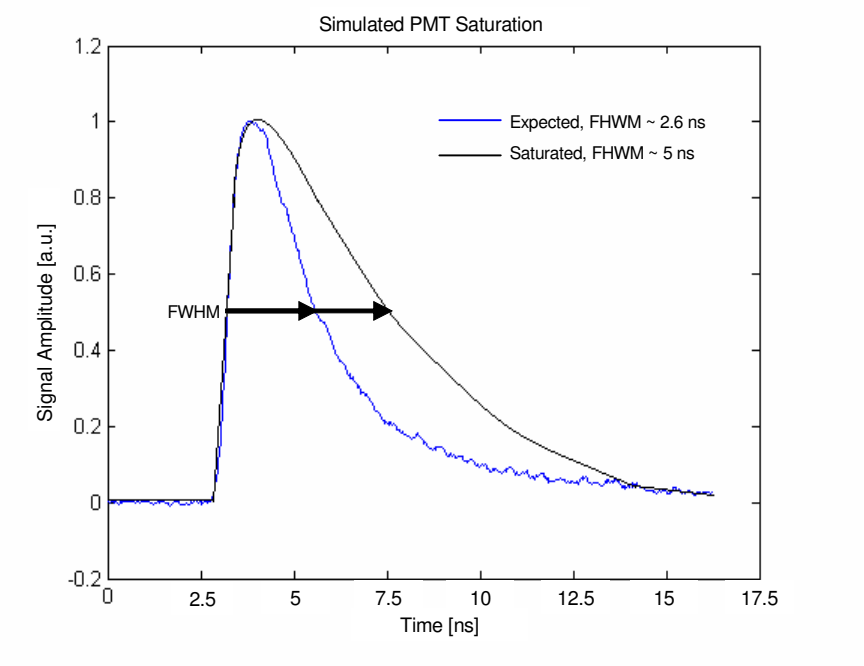

Figure 3.6: Simulated signal with PMT saturation. The saturated signal decays much slower (5 ns) than what an expected GI signal does (2.6 ns).

Since the observed signal is a unique combination of the laser pulse reflection and fluorescent decay, a theoretical formula for calculating the FWHM of this curve distribution does not exist so the FWHM was determined with a less conventional method. A Matlab function add-in available online [2] was used to successfully measure the time taken for the first instant the signal reaches half the maximum to the first instant it drops to half of the max after the maximum point. Microsoft Excel was used to organize the results using conditional formatting to highlight which data sets had FWHM values that are within 1, 2 and 3 standard deviations (SD) of the calculated average for that particular tissue type.

The FWHM of normal duodenum tissue was 2.6 ± 0.6 ns. In the 132 data sets, nine were outside ± 1 SD and only two of them were outside of both ± 2 SD and ± 3 SD. The two outliers P14 T8 (FWHM = 0.64 ns) and P24 T1 (8.4 ns) corresponded to signals of background noise and no visible impulse signal. For normal esophageal tissue the FWHM was 2.4 ± 0.4 ns where 23 of the 107 data sets were outside ± 1 SD with six of them between ± 2-3 SD and two outside ± 3 SD. The two data sets outside the 99% confidence interval (P13 T1 and P26 T2) were both outside -3 SD (0.88 ns and 1.01 ns) so there were no significantly large FWHM values. Also, no pulse broadening was found using the available diseased information and their respective FWHM averages for the categories of 'chemical gastropathy' and 'other diseases'.

3.2.2: Lower Signal Detection Limits

Data with a signal level that is too low may be overpowered by noise and leads to inaccurate lifetime estimation. Upon review of the normalized integrated spectral data it became clear that there is a lower detection ability of the system because the spectral shape was erratic instead of the expected bell shape. Voltage supply to the MCP-PMT was often increased to combat the lack of sensitivity by the system for a low (weak) GI signal. Amplification of the signal in this manner does not affect the signal lifetime decay as seen in Figure 3.5. The time-domain data in T1 taken with 2200 V MCP-PMT voltage was normalized and compared to T5 taken at 2100 V. There is considerable overlap between the two data sets at each wavelength supporting that the MCP-PMT voltage in this range does not affect the temporal shape of the signal but amplifies weaker signals.

In the early stages of the study it was found that data sets without an obvious observed signal pulse could be removed by quick analysis of the steady-state information calculated in the pre-processing code. The I_λ could be negative at a particular wavelength if the time data contained only background noise. Figure 3.7 contains three negative points (at I_{380}, I_{385}, and I_{525}) and the level of background noise overshadows a possible weak impulse signal at 455 nm. No impulse signal was observed in all the cases where the data set contained three or more negative I_λ values. For data with at least some observed impulse signal the I_λ values were all positive. Such a limit was useful to exclude data containing only background noise when making initial comparisons by graphing in Matlab but it cannot remove any data containing signals that challenged the lower detection limit of the instrument (Figure 3.8).

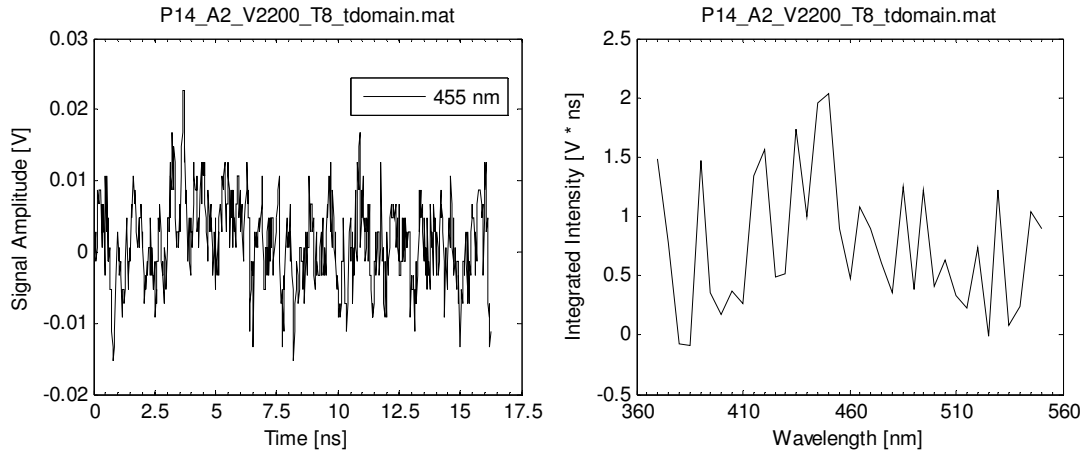

Figure 3.7: Patient 14 has a data set where background noise is dominant. SNR at 455 nm is 11 dB. The space below the zero mark in the time-resolved data (left) makes a negative contribution to the spectral integration while the space above the zero line is positive. The steady-state data (right) have three negative I_λ at I_{380}, I_{385}, and $I_{\lambda 525}$.

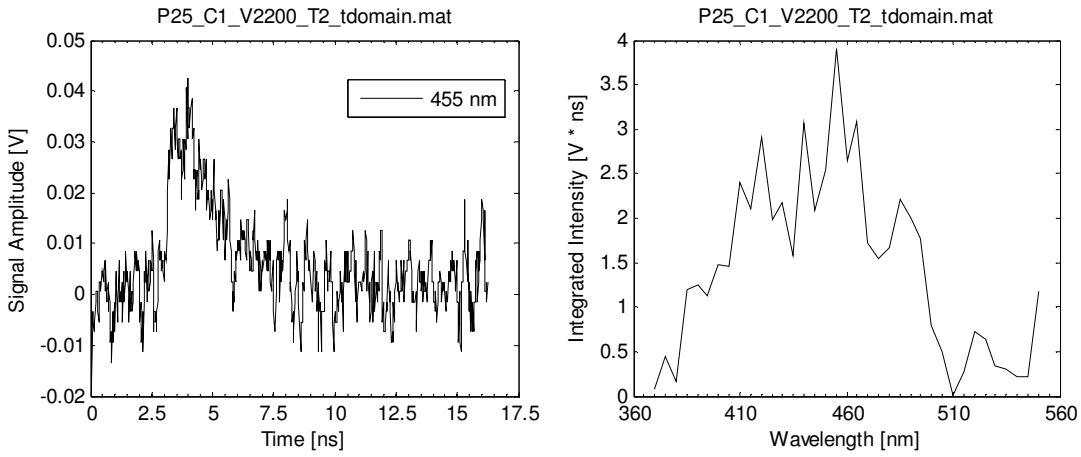

Figure 3.8: Patient 25 as an example of a weak data set. The SNR at 455 nm (left) is 19 dB. Steady-state information (right) is not a smooth curve but rather erratic and the weak signal is enough to make the I_λ positive at all wavelengths.

Visual inspection of the spectral data alone is not sufficient to evaluate the lower detection limit of the system. Another method used to evaluate the strength of the signal was the Signal to Noise Ratio "SNR" (Equation 3.1). The signal and noise were measured at the same point in the instrument (the sample collection reading) so they have the same impedance. Amplitude can then be expressed as the V_{RMS} (Equation 3.2): i.e. the Root Mean Square (RMS) of the voltage measurements (in volts "V") over Time (t). [3]

$$SNR = \frac{Power_{signal}}{Power_{noise}} = \left(\frac{Amplitude_{signal}}{Amplitude_{noise}} \right)^2 \qquad (3.1)$$

$$V_{RMS} = \sqrt{\frac{1}{N} \sum_{N} V(t)^2} \qquad (3.2)$$

Background noise was calculated using the V_{RMS} of 65 time points (or 10% of the data) before the laser was automatically fired. The window of 11-75 points was chosen to start at point 11 to avoid any abnormal noise build up in the instrument at the start of the collection period. The time window ends well before the observed pulse rising edge taking into account the variation in the time (points 85-110) that each wavelength size and speed takes to arrive at the detector. It is important to note that in these fluorescence measurements the signal amplitude of each measurement decays over time and at different rates. Such variations can influence the SNR and make comparisons difficult so the maximum signal should be used [3]. The data point with the maximum amplitude was used to calculate the signal V_{RMS}. To interpret the data, ratios where converted into decibels (dB) by the conversion factor of $10*\log_{10}(SNR)$ [3].

The SNR is largely dependent on the chosen gain of the system by adjusting the MCP-PMT voltage at the time of collection [3] and the ability of the sample type to fluoresce. Data were collected under the direction to achieve a good SNR that was only estimated by looking at the time-resolved data in P07. It was determined that a maximum signal at the peak wavelength of 455 nm should be between 300 mV and 600 mV to get SNR of about 30 dB. On tissue with low signal amplitude the maximum MCP-PMT voltage was limited to voltages of 2250 V because the system response beyond 2300 V was not linear [1] and to protect the instrument from electrical damage caused by long term power exposure. Typical MCP-PMT voltages for tissue were 2150 V or 2200 V while only 1700 V was enough for observing paper.

Anyone comparing SNR from two data sets with different power gain settings should subtract the reference SNR from the data collected using the higher voltage [3]. An example would be as follows:

Sample 1 SNR = 28 dB, MCP-PMT = 2200 V

Sample 2 SNR = 26 dB, MCP-PMT = 2150 V

Reference = $10*\log_{10}(2200/2150) = 0.0998$

Sample 1 SNR = 28 – 0.0998 = 27.9 dB

Therefore when Sample 1 is compared to Sample 2, the Sample 1 SNR is actually equal to 27.9 dB. The maximum reference factor that would have to be considered when comparing tissue data is 0.2996 dB for a 150 V difference. For the purpose of determining a lower cut-off we will see that this small difference is negligible to the outcome of our results.

Evaluation was considered at the first quarter, center, and last quarter of the spectrum (410 nm, 455 nm, and 505 nm) for the two largest tissue groups, normal duodenum and normal esophagus. Table 3.3 shows average SNR and lifetimes calculated for normal duodenum tissue (N = 132) and normal esophageal tissue (N = 107). The largest lifetime SD occurs near the ends of the spectral window when the SNR is less than 20 dB. The SNR at the peak wavelength (455 nm) is always generally quite good, (36 ± 6) dB for duodenum tissue and (33 ± 6) dB for esophageal tissue. On a few occasions there is noticeable variation in spectral shape around 410 nm (ex. Figure 3.2) where phenomena such as blood absorption [4] could possibly have an effect on the outcome of lifetime calculations. To what extent this may be relevant is yet to be determined by

ongoing work which aims to correct for artifacts in the fluorescence measurements by implementing diffuse reflectance analysis. Further study will therefore be performed on data at 505 nm for normal duodenum and esophageal tissue to see if there is a correlation between the calculated lifetime and the SNR for a way to establish possible detection limit criteria.

Table 3.3: SNR and Lifetimes for Normal Duodenum (A) and Normal Esophageal (D) Tissue.

Wavelength [nm]	Wavelength [index]	SNR [dB] Normal A	Lifetime [ns] Normal A	SNR [dB] Normal D	Lifetime [ns] Normal D
375	2	15 ± 5	1.1 ± 11	14 ± 6	2 ± 2
410	9	27 ± 6	1.1 ± 0.3	25 ± 6	1.3 ± 0.6
455	18	36 ± 6	1.1 ± 0.2	33 ± 6	1.1 ± 0.3
505	28	26 ± 5	1.0 ± 0.3	22 ± 5	1.1 ± 0.4
540	35	20 ± 4	1.1 ± 0.5	16 ± 4	1.2 ± 0.7

Normal duodenum and esophagus lifetimes at 455 nm and 505 nm were compared to their respective averages. Table 3.4 lists every normal duodenum and esophageal data set that have an $I_{455} < 20$ V·ns, and very few of these data sets were found to produce lifetimes outside ± 2 SD. At 505 nm SNR's < 20 dB do not affect the Laguerre fitting from producing reasonable lifetimes as only two of the data sets, one from each of duodenum and esophageal, have lifetimes outside ± 2 SD. From this table it can be observed that data sets with similar I_λ and SNR often produce lifetimes within ± 1 SD of the average while on the rare occasion data of similar signal strength can produce two very different lifetimes. For example 'P22 D1 T2' and 'P26 D1 T4' both have similar SNR and I_{455} (7.2 V·ns, 20 dB and 6.9 V·ns, 21 dB respectively) but P26's lifetime of

1.80 ns is outside ± 2 SD and much larger than the P22's lifetime of 0.77 ns. A comparison of the R^2 values from the Laguerre fit indicates that the fitting algorithm is operating optimally on both data sets so it is very probable that the difference is in the tissue composition itself. Without the histological correlation it is impossible to investigate this further and supports the need for exact correlation between fluorescence and histology in future studies. From Table 3.4 it can be concluded that a low signal or SNR for the normal GI data will not result in unreasonable lifetime extraction.

Table 3.4: The SNR and Lifetimes for Normal Duodenum (A) and Normal Esophagus (D) Data that have I_λ < 20 V·ns.

Filename	455 nm			505 nm		
	Integrated Intensity [V*ns]	SNR [dB]	Lifetime [ns]	Integrated Intensity [V*ns]	SNR [dB]	Lifetime [ns]
P09_A1_V2150_T2	19.1	27	0.93	4.2	19	0.60
P12_A2_V2150_T6	16.8	26	0.89	5.3	17	0.79
P12_A2_V2150_T8	17.1	27	0.92	4.9	19	0.72
P14_A2_V2200_T8	0.9	11	**0.49**	0.6	10	0.46
P15_A1_V2150_T1	10.4	24	1.20	4.3	14	0.76
P15_A1_V2150_T3	12.9	24	1.02	3.9	18	1.24
P23_A1_V2200_T1	8.6	21	**2.25**	2.1	14	**1.93**
P24_A1_V2200_T1	1.4	11	**2.18**	-0.9	9	0.38
P24_A2_V2200_T9	12.5	24	0.91	3.1	17	1.06
P09_D1_V2200_T2	19.2	26	0.83	3.8	19	0.61
P10_D1_V2150_T1	17.9	25	1.41	4.2	17	0.54
P13_D1_V2150_T1	0.2	9	**0.37**	-0.5	8	0.33
P13_D1_V2200_T2	7.6	21	1.15	2.9	13	0.44
P14_D1_V2150_T2	7.9	21	0.79	3.0	17	1.23
P14_D1_V2150_T3	11.5	25	0.64	2.7	20	0.52
P22_D1_V2200_T2	7.2	20	0.77	3.1	13	0.65
P23_D1_V2200_T1	15.5	29	0.77	3.4	20	0.84
P25_D1_V2200_T7	19.0	29	0.75	4.5	16	**2.47**
P25_D1_V2200_T9	7.4	22	0.82	2.7	15	1.64
P26_D1_V2150_T1	2.4	17	1.03	1.2	13	1.10
P26_D1_V2150_T2	5.2	21	**2.21**	2.0	12	1.62
P26_D1_V2150_T4	6.9	21	**1.80**	1.5	12	0.84
P26_D1_V2200_T5	11.2	23	1.00	3.0	16	0.78
P26_D1_V2200_T6	16.8	27	1.35	3.3	16	1.79
P26_D1_V2250_T7	17.2	27	1.33	4.6	19	1.86
P26_D1_V2250_T8	19.8	28	0.88	5.3	18	0.76

Lifetimes in **Bold** are outside ± 2 SD, average lifetimes are given in Table 3.3.

Table 3.5: The SNR and Lifetimes for Normal Duodenum (A) and Normal Esophagus (D) Data that have Lifetimes > ± 2 SD.

Filename	455 nm			505 nm		
	Integrated Intensity [V*ns]	SNR [dB]	Lifetime [ns]	Integrated Intensity [V*ns]	SNR [dB]	Lifetime [ns]
P08_A1_V2200_T3	41	35	1.01	11	25	1.89
P11_A1_V2150_T6	34	36	1.17	11	23	**1.72**
P14_A2_V2200_T8	1	11	**0.49**	1	10	0.46
P15_A1_V2150_T5	34	29	**1.93**	10	25	1.59
P23_A1_V2200_T1	9	21	**2.25**	2	14	**1.93**
P23_A1_V2200_T4	38	33	1.25	11	25	**1.65**
P24_A1_V2200_T1	1	11	**2.18**	-1	9	0.38
P24_A1_V2200_T6	154	41	**1.63**	40	33	1.21
P25_A2_V2200_T10	265	50	1.49	72	38	**1.71**
P25_A2_V2200_T5	243	50	**1.62**	69	37	**1.70**
P25_A2_V2200_T8	199	49	1.28	57	35	**1.79**
P28_A1_V2200_T4	50	35	1.17	16	24	**2.31**
P13_D1_V2150_T1	0.2	9	**0.37**	-1	8	**0.33**
P22_D1_V2200_T3	43	34	1.11	10	24	**2.32**
P24_D1_V2200_T1	29	31	**1.93**	8	25	0.58
P25_D1_V2200_T5	170	46	**1.70**	46	32	1.42
P25_D1_V2200_T6	24	31	0.97	6	20	**2.25**
P25_D1_V2200_T7	19	29	0.75	5	16	**2.47**
P25_D1_V2200_T8	105	43	**1.73**	27	30	1.24
P25_D2_V2200_T12	86	41	**1.84**	22	31	1.65
P26_D1_V2150_T2	5	21	**2.21**	2	12	1.62
P26_D1_V2150_T4	7	21	**1.80**	2	12	0.84

Lifetimes in **Bold** are outside ± 2 SD, average lifetimes are given in Table 3.3.

Table 3.5 lists all of the data sets with lifetimes found outside ± 2 SD for normal duodenum and esophagus at 455 nm and 505 nm. Very few filenames overlap with Table 3.4. At first glance it appears that the less desirable lifetimes are produced by mainly large SNRs such as those with > 40 dB at 455 nm and > 20 dB at 505 nm. Upon further consideration there are already some examples which are present in Table 3.5 where the data have very strong signals (ex. 'P25 A2 T8' with 199 V·ns and 49 dB) and a lifetime within ± 1 SD (1.28 ns). It was found in the previous section on Amplitude Saturation

(3.2.1) that none of the data sets with large signals experienced any pulse broadening. There is no trend evident from Table 3.5 that points to a reason for excluding all data above or below a specific SNR.

It is suggested then, on the basis of visual inspection of the spectral data alone, that all data with $I_{455} < 20$ V·ns be removed from all further considerations regarding the patient data analysis. Typically esophageal tissue produced lower I_λ than duodenum tissue and was sometimes less bell shaped (or smooth looking), often requiring a higher MCP-PMT voltage of 2250 V to achieve any reasonable signal. All data sets for normal duodenum and esophagus above this $I_{455} > 20$ V·ns threshold held a consistent and stable spectral shape while anything less was very noisy similar to the example shown in Figure 3.8. Removing data below this threshold from further data analysis will alleviate the influence of noise while keeping most of the data from weaker tissue such as the normal esophageal tissue. Patient 26 is the only one that would lose all of its data under this rule unless it was changed to < 19.5 V·ns so it would get to keep 1 data set (T8, 19.8 V·ns) which has a lifetime within ± 1 SD.

The SNR ratio investigation however may not end here for future studies using the TR-FS instrument. Although the digitizer is very fast (25 ps/pt sampling rate), the vertical resolution of our data is limited by the 8-bit oscilloscope. The instrument could be improved with higher resolution (ex. 12-bit) which would be more sensitive and better able to detect signals from weak samples because it has less digitization noise.

3.2.3: Photobleaching and Repeated Measurements

Laser excitation at 355 nm and intensity of 3.0 μJ were chosen during instrument construction such that it would not be disruptive to the tissue structure and minimize sample photobleaching [5]. In this event, the tissue would loose the ability to fluoresce and it would be evident by observing a rapid decrease in signal acquisition during subsequent measurements. Photobleaching was only observed during paper fluorescence towards the end of the study and was immediately remedied by using a new piece of paper. Typically the same spot on the specimen was not repeated during measurements. If the maximum spectral intensity was < 300 mV, the next measurement was taken either after repositioning the probe closer to the sample or after increasing the MCP-PMT voltage. Often this would improve the signal strength observed but when it did not, the entire sample would give similar low quality auto-fluorescence results.

Repeated spots were performed intentionally on P07 to review the effect of repeated spots (Figures 3.9 and 3.10). It was recorded that duodenum tissue T4, T5, and T6 were all the same tissue location without repositioning the probe or sample. The MCP-PMT voltage for T5 and T6 were 2200 V while T4 was 2150 V. The effects of increased MCP-PMT gain discussed earlier were reflected in the observed increase in I_λ of Figure 3.9 and when normalized, the T4 and T5 steady-state spectra had complete overlap. A third measurement in the same location however started to reveal some changes in tissue fluorescence. The observed intensity in T6 started to decrease and when normalized the spectral shape started to vary from previous measurements T4 and T5. It is possible that minimal photobleaching can be observed after three consecutive measurements but since

the I_λ overlap or are greater than the I_λ of other spots on the sample (when normalized) the effect of photobleaching is considered negligible.

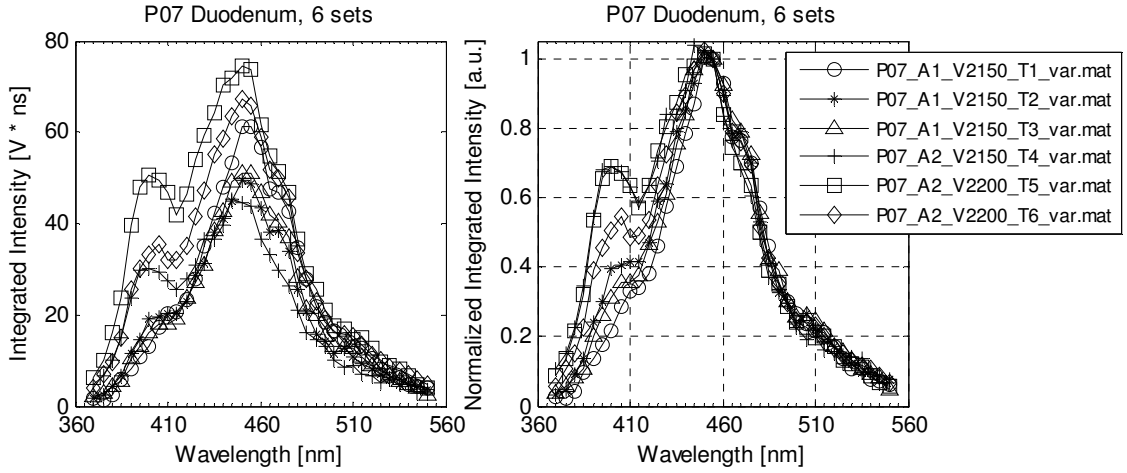

Figure 3.9: Patient 7 duodenum spectral data where T4, T5, and T6 are consecutive measurements on the same spot location but taken at two different voltages. Some changes in the shorter wavelengths are reflected in the normalized data after the third measurement (T6). This spot also shows increased fluorescence from 370-455 nm and visible absorption around 415 nm when compared to three other spots on the specimen (T1-T3).

Some variation can be expected in the spectral shape when measurements are repeated (for example P07 esophageal tissue in Figure 3.10) but this difference is within reasonable limits. It was common for the spectral shape to experience this small type of variation between 435-470 nm in other patients even when the spot locations were not repeated. Small fluctuations in the fluorescent signal can occur because the tissue has not been fixed in a single biological state meaning that the tissue is still living and subject to change. It also means that the fluorophore composition can fluctuate at any location on

the sample at any given moment. Lifetimes from both T1 and T2 are within ± 1 SD of the tissue average showing that these fluctuations are small and very reasonable even though the fluorophore composition cannot be monitored or quantified under the limitations of this feasibility study. Therefore it is not necessary to repeat the same spot more than once.

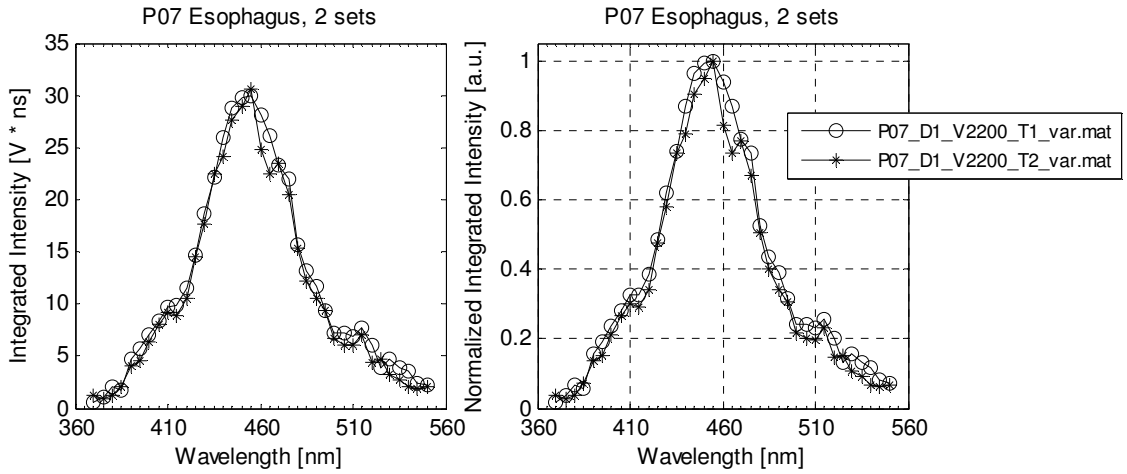

Figure 3.10: Patient 7 esophagus spectral data where T1 and T2 are consecutive measurements on the same spot at the same PMT voltage (2200 mV). The variations depicted in the above spectral shapes between 435-470 nm are commonly found in other patients that do not have any spot locations repeated.

Very few spots have repeated measurements throughout P07-P28 and sometimes these additional notes were not recorded due to time constraints in the clinic. Based on the analysis of this section, it does not matter which of the two repeated spots are removed. The gain was either increased or decreased by the operator in attempt to improve the spectral shape and achieve a maximum measurement between 300-600 mV for an ideal SNR of about 30 dB. Sometimes the student recorded a repeated measurement without

changing the gain or providing a comment. It cannot be assumed in this instance that the laser was repositioned and ultimately changing the spot or they just wanted a second measurement. Regardless, to reduce over counting to the best of our records the first record will be removed for consistency on the basis that instrument adjustments were to be made in attempt to improve the signal quality on the second measurement. All of the remaining data sets will be kept if their I_{455} is less than 19.5 V·ns because it was shown previously (Section 3.2.2) that improving the SNR by increasing the gain does not affect the shape of the time-domain data above this level or effect lifetime extraction.

3.2.4: Increased Fluorescence Intensity during Shorter Wavelengths

As discussed briefly in Section 3.2.2 (Lower Signal Detection Limits), there can be variation in the spectral shape where absorption is sometimes visible around 415 nm. An increased fluorescence between 370-455 nm was often but not necessarily found when the absorption occurred and it was most noticeable from 390-410 nm. Patient 7 duodenum tissue (Figure 3.9) is an example where some of the data reflects this variation while in P15 duodenum tissue (Figure 3.11) all of the data sets show the increased fluorescence. All tissue locations, normal or diseased, were found in some instances to experience this although it was more prominently found to occur within diseased tissue.

It is expected that tissue orientation could very well be the sources of these inconsistencies because the tissue composition will change as the biopsy is sampled deeper into the patient. Recall that a physician's aim is to collect a biopsy that leaves the submucosal layer intact. The submucosal layer is dominated by connective tissue and in

turn this layer requires more fibrous tissue (collagen and elastin) to hold itself together than in the mucosal layer [6]. It is known that the fluorescence emission spectra of these fibrous molecules are greatest around 390 nm and 410 nm [4, 7]. If there are indeed greater concentrations of collagen and elastin present then it would result in larger observed I_λ around these wavelengths.

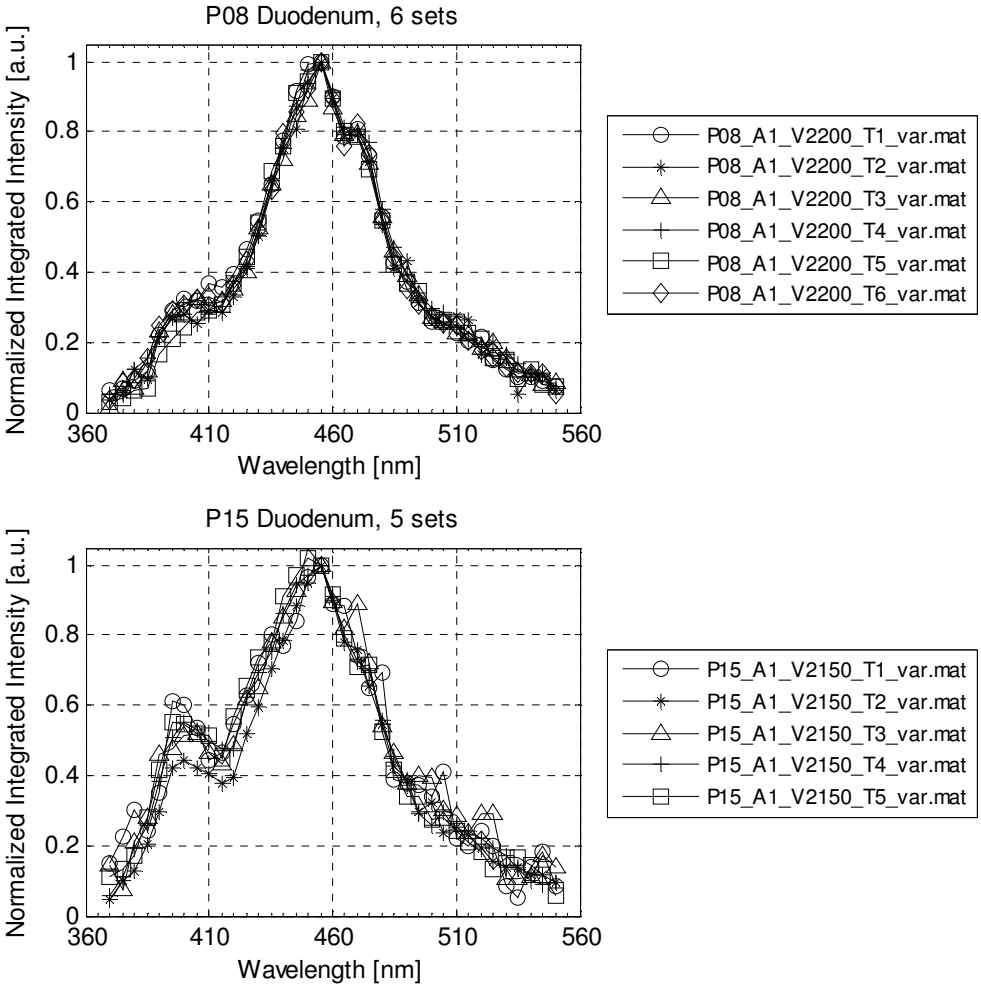

Figure 3.11: All of the P15 data sets show a 20% increase in fluorescence around 400 nm when compared to P08.

Fluorescence measurements have consistent spectral shapes (especially in the normal tissue samples) most of the time because the biopsy was taken from the mucosal layer containing minimal traces of submucosal components. However, without correlation between tissue orientation and fluorescence measurement locations it is difficult to make the assumptions or conclusions about the tissue orientation and composition for our data. Many changes in mucosal tissue structure caused by disease are also accompanied by increased levels of collagen, elastin, and blood [6]. It would be expected that changes in fluorophore concentrations in diseased tissue would become evident in both steady-state and lifetime analysis. Diseased tissue will not be analyzed in this study because there are not enough patients (less than 4) with a similar disease to establish well known lifetimes. Consideration however will be given to one mixed data set (P07) and two opposing sets (P08 and P15) for normal duodenum tissue.

The P07 duodenum data are compared to the overall normal duodenum lifetimes in Figure 3.12. Some of the data sets (T4, T5, and T6) had shown areas of increased fluorescence in Figure 3.9 from 390-455 nm. At 390 nm and 400 nm, both of the T4 and T5 lifetimes are slightly greater than ± 1 SD indicating they have longer lifetimes than the other data sets. Interestingly enough, the T6 lifetime is within ± 1 SD despite coming from the same tissue location. Its lifetime could be shorter due to some minimal photobleaching of the sample or physiological changes because the sample was not fixed. The lifetimes in these shorter wavelengths are not significantly different from the normal duodenum average lifetimes. Also, the average of these data sets (with the greater I_λ) has a ± 1 SD overlap with the other P07 data sets T1-T3 in Figure 3.13. Similarly, the

averages from P08 vs. P15 (Figure 3.13) also overlap with each other within ± 1 SD. Therefore the removal of normal tissue data with increased I_λ in the shorter wavelengths is not necessary as there is no evidence to suggest that there is underlying physiological differences that cause significant changes to the observed lifetimes.

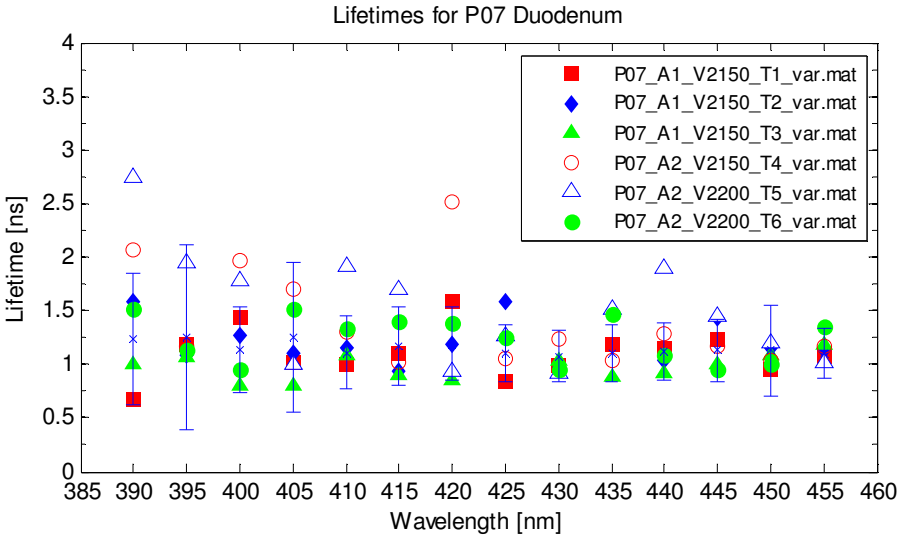

Figure 3.12: Patient 7 duodenum lifetimes are plotted with the averages of all tissue A ± 1 SD (N = 132). Data sets T4, T5, and T6 show increased fluorescent signals in Figure 3.9 when compared to T1-T3 but for the most part their lifetimes are all within the ± 1 SD of the averages.

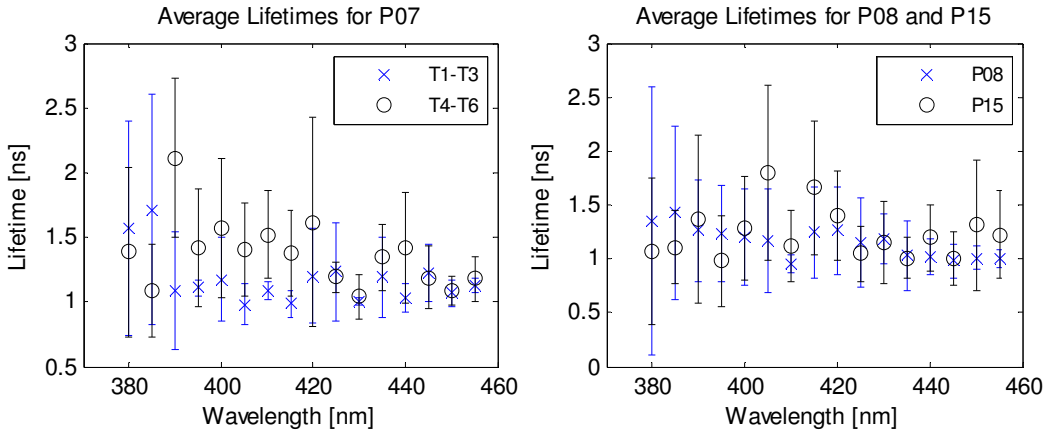

Figure 3.13: Average lifetimes for data sets with increased fluorescence (black circles) are greater than those without (blue x) but overlap within ± 1 SD.

3.3: Results of Data Evaluation

After extensive review of the data in Section 3.2, it is clear that very few data sets should be removed when calculating patient averages and conducting further analysis. Certain patients were excluded entirely from our data base because of obvious reasons summarized in Table 3.6. Saturation in intensity plots was not detected as described in Section 3.2.1 for any tissue using either the manual (visual) inspection of individual time-domain decay data or by searching for samples with a FWHM > + 3 SD of the tissue average. It was found that the detector limits were able to record the entire impulse for all samples where the largest maximum signal observed was 1.5 V for 'P25 A2 T10' (I_{455} = 265 V·ns). It was determined that data sets could only be excluded if their integrated spectral shape are noisy and if the same spot was repeated. All of these data sets listed in Table 3.7 are excluded from all further calculations in the normal duodenum and normal esophageal tissue groups. The arrival of these conclusions and their reasoning are discussed next.

Table 3.6: Entire Patient Data Sets (Tissues A-D) Removed.

Patient	Reason
P01	laser misalignment, no data collected
P02-P06	instrument error, inconsistent measurments
P18	pathological diagnosis unavailable
P19	repeat biopsy from P12

Table 3.7: Data Excluded from Normal Duodenum (A) and Normal Esophageal (D) Tissue.

Filename	First Duplicate	I(455) < 19.5 V*ns	FWHM > ± 3 SD
P07_A2_V2150_T4	X		
P09_A1_V2150_T2	X	X	
P12_A1_V2150_T3	X		
P12_A2_V2150_T6		X	
P12_A2_V2150_T8		X	
P14_A2_V2200_T8		X	X
P15_A1_V2150_T1		X	
P15_A1_V2150_T3		X	
P16_A1_V2100_T1	X		
P17_A1_V2150_T3	X		
P23_A1_V2200_T1		X	
P24_A1_V2200_T1	X	X	X
P24_A2_V2200_T9		X	
P27_A1_V2150_T3	X		
P07_D1_V2200_T1	X		
P08_D1_V2200_T3	X		
P09_D1_V2200_T2		X	
P10_D1_V2150_T1		X	
P10_D1_V2150_T2	X		
P13_D1_V2150_T1	X	X	X
P13_D1_V2200_T2		X	
P14_D1_V2150_T2		X	
P14_D1_V2150_T3	X	X	
P16_D1_V2150_T4	X		
P17_D1_V2150_T1	X		
P22_D1_V2200_T2		X	
P22_D1_V2200_T3	X		
P23_D1_V2200_T1		X	
P23_D1_V2200_T3	X		
P25_D1_V2200_T1	X		
P25_D1_V2200_T7		X	
P25_D1_V2200_T9		X	
P25_D1_V2250_T4	X		
P26_D1_V2150_T1		X	
P26_D1_V2150_T2		X	X
P26_D1_V2150_T4	X	X	
P26_D1_V2200_T5		X	
P26_D1_V2200_T6	X	X	
P26_D1_V2250_T7		X	
P27_D1_V2200_T2	X		

Total Filenames: Tissue A = 14, and Tissue D = 27.

In Section 3.2.2 a low SNR at 445 nm or 505 nm could not be used to identify data sets with unreasonable lifetimes outside ± 2 SD. Figures 3.14 and 3.15 show the extracted lifetime distribution related to SNR 455 nm. Averages and SD were reported in Table 3.3. The distributions are not symmetrical but appear skewed to the right. It should be noted that there is large variation by patient and these distributions may be biased by one patient. At this point in time it provides insight as to what the sampling distribution might look like if we sampled many times (ex. N > 100). The two data sets with lifetimes below 0.5 ns ('P14 A2 T8' and 'P13 D1 T1') are outside ± 2 SD with FWHM outside - 3 SD and can safely be disregarded as data that is mostly noise. Visual inspection of the time-domain data confirms there is no visible impulse at 455 nm. Data sets at 455 nm with lifetimes outside + 2 SD also had extracted lifetimes at 505 nm within ± 1 SD.

The spectral intensity measured at 505 nm is lower than 455 nm in Figure 3.16 and it shows that the instrument response to SNR increases linearly with signal intensity. The extracted lifetimes at these lower signals and SNRs are shown in Figures 3.17 and 3.18 with distributions and limitations similar to the measurements at 455 nm. Averages and SD were reported in Table 3.3. It was found in Table 3.5 that the lifetimes outside ± 2 SD are not always from signals with very high or very low SNR. About half of the esophageal tissue 505 nm data (Figures 3.16 and 3.18) have SNR lower than 20 dB but still have lifetimes within ± 1 SD. Therefore the relationship between SNR and lifetime cannot be used to emplace criteria for disregarding measurements.

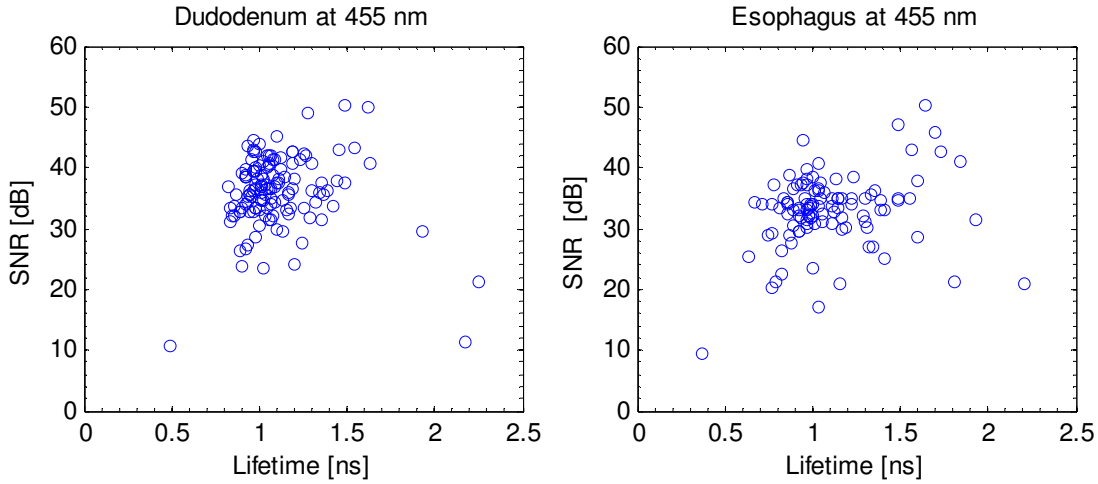

Figure 3.14: Signal to noise ratio and extracted lifetime relationship at 455 nm.

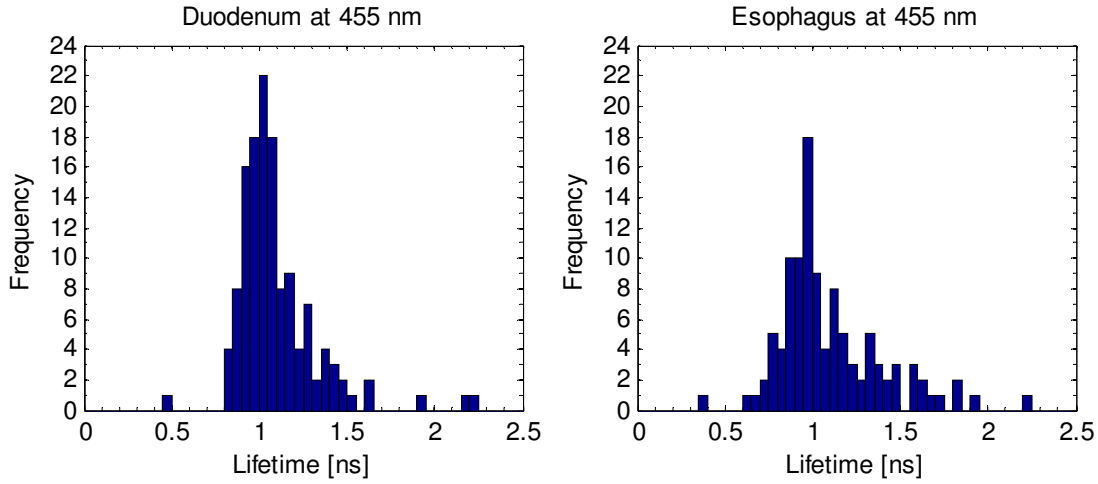

Figure 3.15: Lifetime distributions for normal duodenum and normal esophagus at 455 nm.

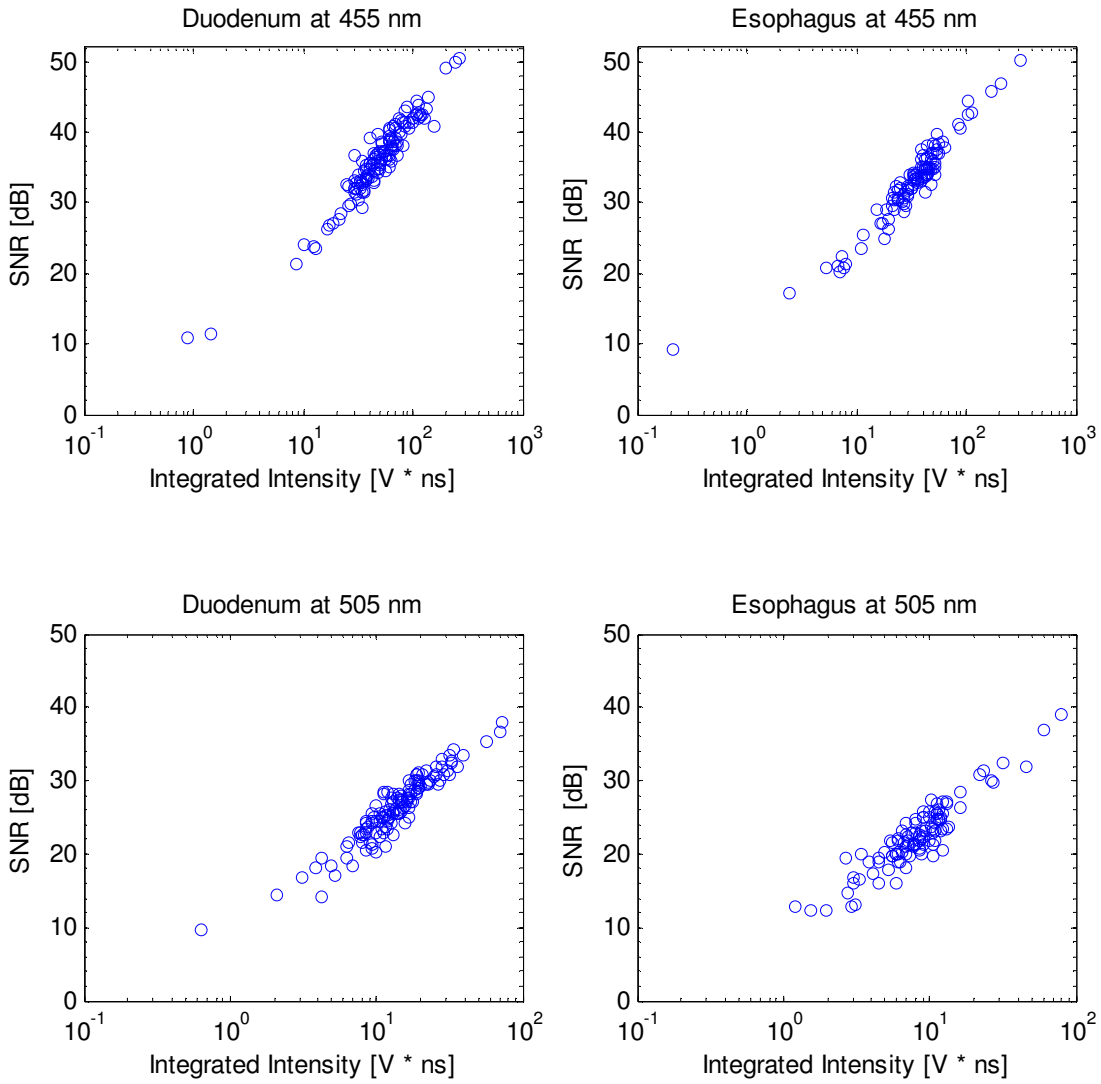

Figure 3.16: Signal to noise ratio increases linearly with the integrated spectral intensity. Examples are shown at both 455 nm and 505 nm for normal duodenum and normal esophagus.

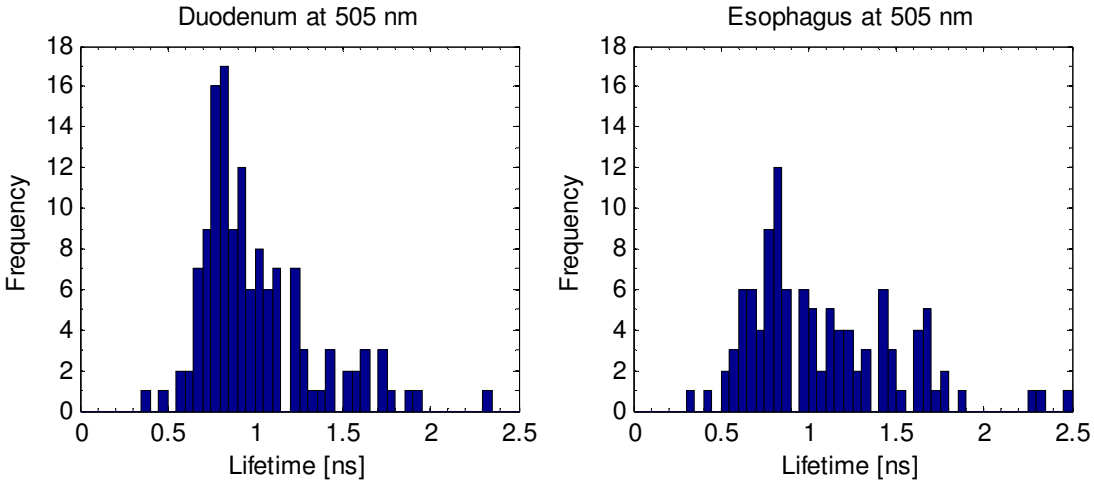

Figure 3.17: Lifetime distributions for normal duodenum and normal esophagus at 505 nm.

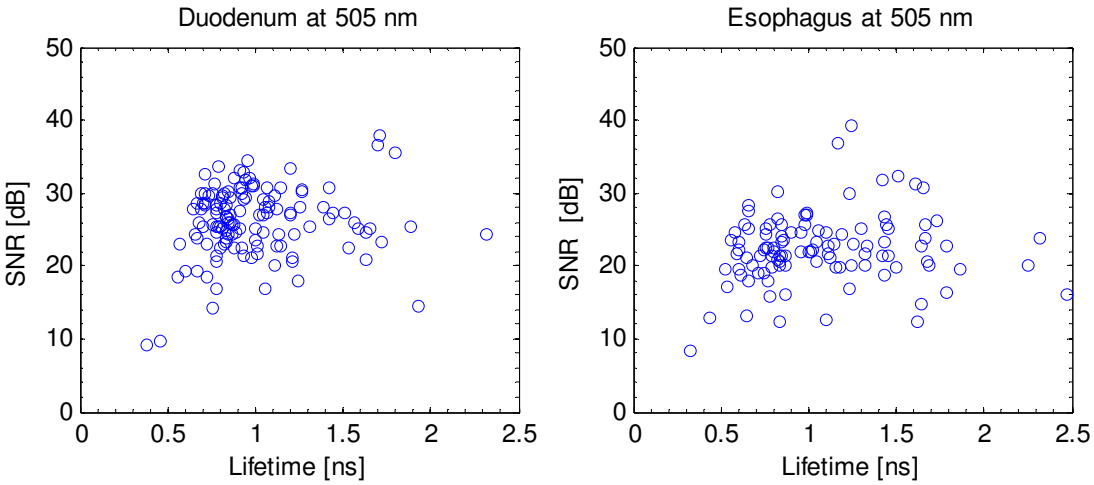

Figure 3.18: Signal to noise ratio and extracted lifetime relationship at 505 nm.

One thing that can be certain though is that the coefficient of determination R^2 (Equation 3.3) will approach 1 as the SNR increases. An example is taken from P15 esophageal tissue in Figure 3.19. In theory an R^2 value equal to exactly 1 indicates that the best possible fit has been achieved because the ratio of the Residual Sum of Squares (SSError) and the Total Sum of Squares (SSTotal) is equal to zero [8]. For that to happen the differences between the measured data (y_i) and a theoretical fit (f_i) have to be very small relative to the differences between y_i and the average measured data (y_{avg}). The range 370-550 nm was chosen to cover most of the auto-fluorescence from tissue. In Figure 3.19 the R^2 improves dramatically (to ≥ 0.87 from 0.4 or 0.6) when the SNR is > 20 dB which corresponds to wavelengths 385-520 nm as shown in Figure 3.20. A good fit is said to have an R^2 of at least 0.8 and a great fit is 0.99 but the R^2 alone cannot be used to assess the quality or accuracy of the model used to fit the behaviour of the data [8].

$$R^2 = 1 - \frac{SSError}{SSTotal} = 1 - \frac{\sum_i (y_i - f_i)^2}{\sum_i (y_i - y_{avg})^2} \qquad (3.3)$$

Recall that the analysis at 505 nm did not suggest that SNR ratios between 10 db and 20 dB provide a signal quality that is insufficient to extract lifetimes with a reasonable SD or lean towards a lower limit for the Laguerre algorithm. In the development of the data processing algorithm [1] it was decided, based on simulations and fluorescent data (NADH, FAD, and P07), that omitting the end wavelengths from both deconvolution and bi-exponential fitting would save processing time knowing this is

where the signal was the lowest at 370 nm, 545 nm, and 550 nm. For the GI data in this report those wavelengths were not involved in deconvolution and therefore not available in any future calculations. The data file in Figures 3.19 and 3.20 was deconvolved separately to get the end wavelengths to demonstrate relationship between the R^2 and the signal quality at each wavelength.

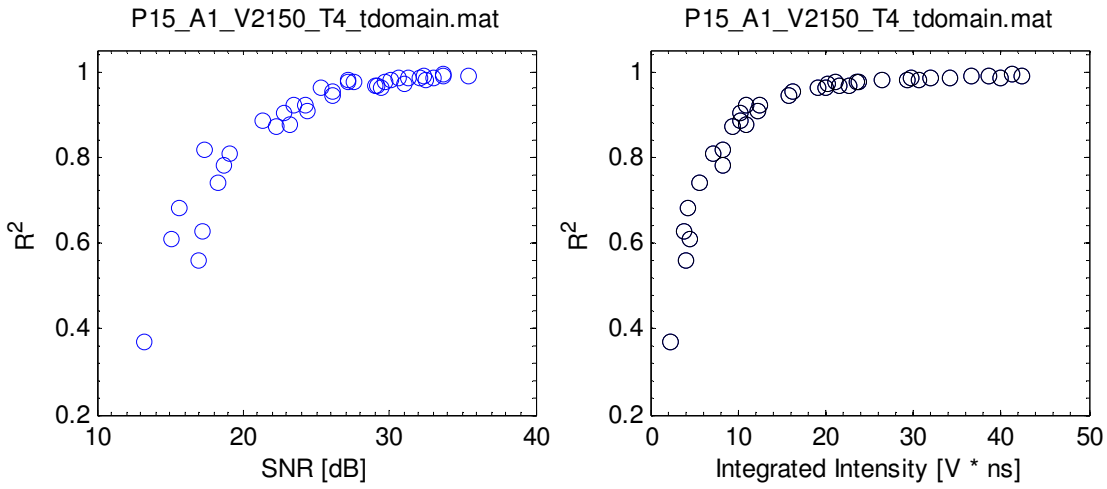

Figure 3.19: R^2 values calculated at each wavelength plotted as a function of SNR and integrated spectral intensity for a sample data set taken from P15 duodenum tissue. The R^2 approaches 1 as the signal increases.

The lifetime and SNR analysis did not reveal that any of the data sets could be removed above or below a particular signal threshold. It is also difficult to exclude data with longer lifetimes (most lifetimes outside ± 2 SD in Table 3.5 were > 2 SD) without knowing the fluorophore content in the tissue. The biological information about the signal is necessary to evaluate the data further to reason if longer lifetimes are indeed a biological relevant signal or abnormalities caused by the instrument. It was obvious that

the spectral data became noisy below I_{455} < 19.5 V·ns. and that the measurements become unstable even though it is not clear to what effect this may have on the observed lifetimes. Since the I_λ ratios can be used to look for tissue signatures, all of the data in Table 3.4 (except for 'P26 D1 T8', I_{455} = 19.8 V·ns) will be excluded from all further calculations. It implies that the lifetimes and Laguerre coefficients from the noisy spectral data will also be disregarded when calculating patient averages. This Table 3.4 includes the data sets mentioned earlier with the FWHM < 3 SD.

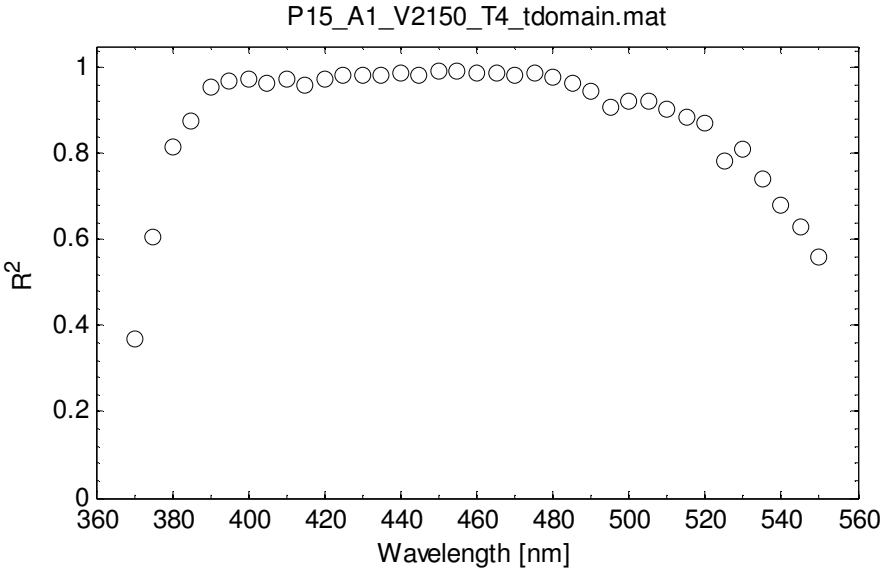

Figure 3.20: R^2 values for each wavelength corresponding to the P15 duodenum sample in Figure 3.19. The R^2 improves rapidly to values > 0.85 (385-520 nm) from the end wavelengths. From Figure 3.19 this range is where the SNR is > 20 dB.

Section 3.2.3 concludes that photobleaching was not observed during two consecutive spot measurements and considered negligible after a third measurement. As long as the I_{455} value was greater than 19.5 V·ns, all of the spectral data regardless of the

MCP-PMT voltage gain can be used in further analysis. However, when there is a spot on the sample whose fluorescence has been measured more than once it introduces bias when calculating the tissue average. A repeated measurement puts more weight on the information coming form that area of the tissue because it was been counted more often than other spot locations. It was decided that the first of every repeated measurement would be removed for consistency and because typically the measurement was repeated by the operator to improve the quality of the signal by increasing SNR. Lastly, in Section 3.2.4 the increased fluoresce intensity that was sometimes observed during the shorter wavelengths did not have extracted lifetimes outside ± 1 SD. Therefore those data sets with possible submucsoal layer exposure to the laser path are not significantly different than all of the other normal samples.

REFERENCES

[1] Krishnamoorthy M. 2010. Optimization of a time-resolved spectroscopy system with an acousto-optic tuneable filter employing a deconvolution method based on discrete laguerre functions [dissertation]. Hamilton (ON): McMaster University.

[2] Egan P. 2009. Full-width at half-maximum (FWHM) of the waveform y(x) and its polarity (fwhm.m). Revision 1.2. Natick, MA: The MathWorks Inc. [cited 2011 Mar 17] Available from: http://www.mathworks.com/matlabcentral/fileexchange/10590-fwhm

[3] Storey N. 2006. Amplification. In: Electronics - a systems approach. 3rd ed. Harlow, England: Pearson Prentice Hall. p 49-91.

[4] Prasad PN. 2003. Photobiology. In: Introduction to Biophotonics. Hoboken, NJ: John Wiley and Sons. p 159-202.

[5] Marcu L, Grundfest WS, Maarek JMI. 1999. Photobleaching of arterial fluorescent compounds: characterization of elastin, collagen and cholesterol time-resolved spectra during prolonged ultraviolet irradiation. Photochemistry and Photobiology 69(6):713-721.

[6] Feldman M, Friedman LS, Brandt LJ. 2010. Sleisenger and Fordtran's Gastrointestinal and Liver Disease. 9th ed. Philadelphia, PA: Elsevier. 2480 p.

[7] Vo-Dinh T, Cullum BM. 2003. Fluorescence spectroscopy for biomedical diagnostics. In: Vo-Dinh T, editor. Biomedical photonics handbook. Boca Raton, FL: CRC Press. p 28:1-50.

[8] McClave JT , Sincich T. 2003. Simple Linear Regression. In: Statistics. 9th ed. Upper Saddle River, NJ: Pearson Prentice Hall. p 509-574.

CHAPTER 4: RESULTS AND DISCUSSION

Now that the erroneous data measurements have been identified in Chapter 3 and discarded from the data pool, the observed tissue fluorescence can be further analyzed without such distortions. The individual parameters (I_λ, LEC-j_λ, and τ-λ) that characterize the individual tissue fluorescence will be used to compare the clinical diagnosis of one tissue type to another. It was noted in Section 2.2.2 that each patient and their biopsy locations have varying amounts of measurements because the total surface area of the specimens was not consistent. Therefore it was necessary to take the average parameter value of the individual measurements to represent the patient's biopsy location before moving forward with any type of analysis.

The new values representing each patient with a normal biopsy diagnosis were averaged to compare the total observed fluorescence, I_λ, of the four biopsy locations at each wavelength. The two largest patient pools available (normal esophagus and normal duodenum) were then compared graphically for any differences between the individual parameters at each wavelength. Data analysis protocols from Section 2.3 were used to select parameters that were statistically different ($p < 0.05$) between the two patient groups in preparation for two dimensional k-means classification. The best results from the k-means classification (with and without the need for dimensional transformations) are presented and discussed in this chapter.

4.1: Patient Averages

In Chapter 3, the clinical diagnosis revealed how many of the patient biopsies were normal. There are 16 duodenum (A), 3 antrum (C), 13 body (B), and 16 (D) normal biopsies out of a possible 20 Patients available for further study (Section 3.1). To make a general comparison between the biopsy locations, the average of the patient's averaged results were taken and reported with the standard deviation of the mean or ± 1 'standard error' ($SE = SD/\sqrt{N}$ [1]) in Figure 4.1 for I_λ and τ-λ. Wavelengths 370 nm, 545 nm, and 550 nm are excluded from the results because the SNR was ≤ 0.6. Erroneous data sets using the criteria derived in Chapter 3 were also excluded from the results. The criteria (summarized in Section 3.3) were data sets that have I_{455} < 19.5 V·ns, a FWHM at I_{455} > ± 3 SD of their tissue average, and the first data set of a spot with repeated measurements.

In Figure 4.1 it is difficult to tell where exactly there may be differences between I_λ except for between I_{380} and I_{410} where the antrum I_λ are greater than all the other tissue. As for the lifetimes, the greatest variation among tissue occurs before 410 nm. The SE values in this region are quite large ranging from ± 0.1 ns to ± 0.3 ns suggesting more data may be required to define what the τ-λ are. From τ-420 to τ-530 there is a clear distinction that the body tissue has shorter lifetimes than all the other tissue. In Figure 4.2 the I_λ were plotted showing just two of the tissue locations at a time. The normalized I_λ shows fairly consistent results for both tissue types with small errors, especially in the longer wavelength region (> 460 nm). There is also more separation between the average values suggesting that these parameters could be significantly different during statistical testing. The focus groups for the k-means clustering however

will be the two largest normal patient groups, esophagus and duodenum, to determine if k-means clustering can be used to classify the data.

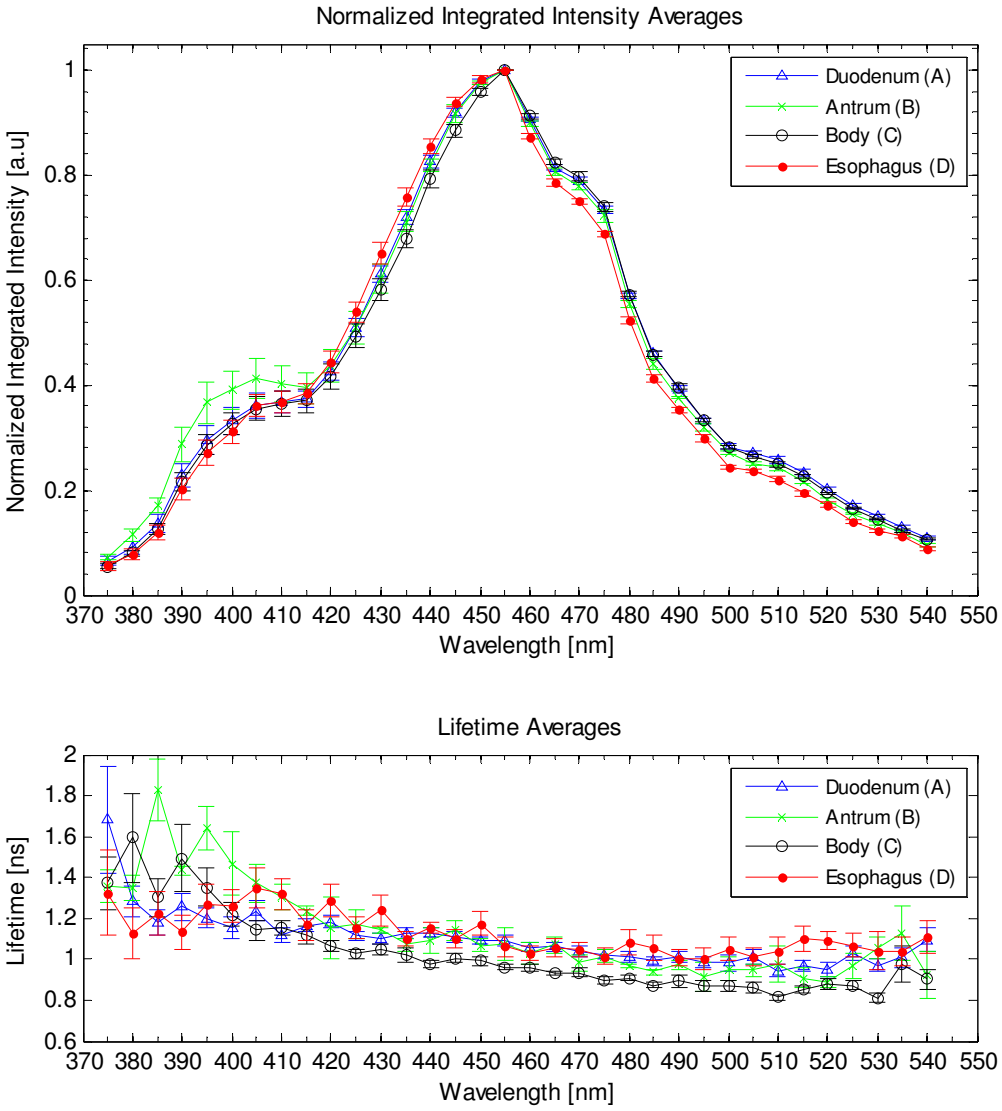

Figure 4.1: Normalized integrated intensity (top) and lifetimes (bottom) are plotted for the four biopsy locations using only the patients with a normal diagnosis. The data is averaged over 16 (A), 3 (C), 13 (B), and 16 (D) patients to ± 1 SE.

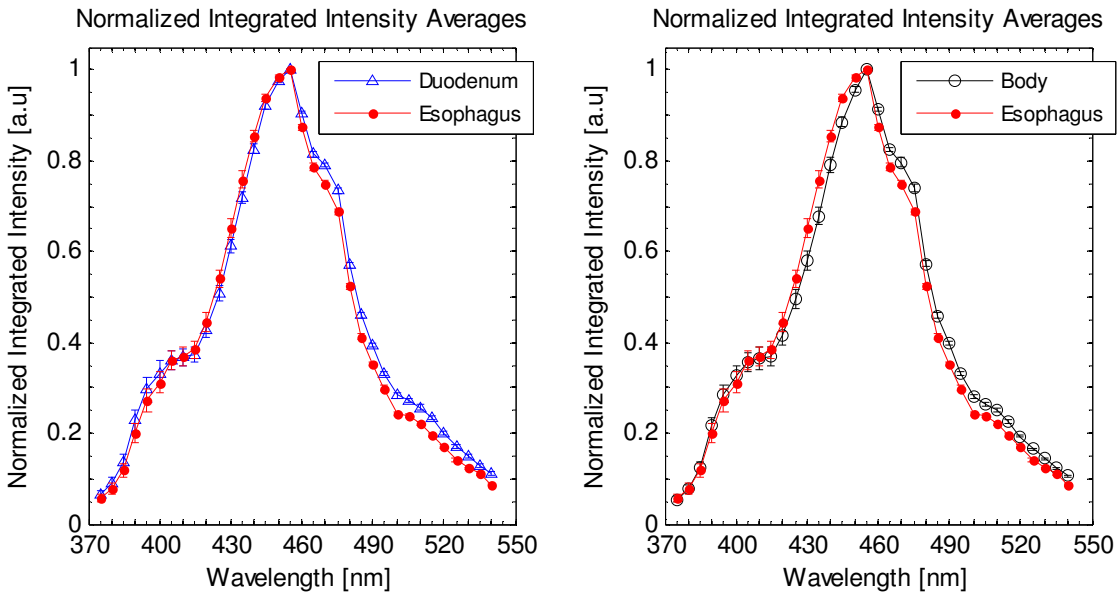

Figure 4.2: Comparison of normalized spectra (I_λ) from the esophagus to the duodenum (left) and body (right). The ± 1 SE bars are too small to be represented for most λ on this graph. Values are tabulated in Appendix D.

The τ-λ and LEC-j_λ for normal esophagus and duodenum are plotted in Figure 4.3. Lifetimes for the esophagus and duodenum were very similar at each wavelength except for around 410 nm and 520 nm where the esophagus displayed longer lifetimes. In Figures 4.1 and 4.3 the lifetimes become shorter, decreasing from about 1.25 ns to 1.0 ns as the wavelengths get longer. Several wavelengths for each LEC-j in Figure 4.3 show promising differences between the two tissue types but ultimately the choices will be narrowed down by mathematical comparison tests instead of graphic extrapolation.

It is apparent in Figure 4.3 that the absolute values of all LEC-j_λ are of a smaller magnitude than both I_λ and τ-λ. Although the LEC-j_λ are indeed unitless, recall from Section 2.3.5 that problems can arise in clustering if the x and y axis dimensions are

mismatched [2]. The squared Euclidean distance (Figure 2.2) may be biased towards assignment of data points to the nearest k-mean in the axis that has the larger dimension [2]. The range of I_λ (~ 0.1-1.0) and τ-λ (~ 0.9-1.2) are close enough to each other that a dimensional transformation is not required to compare them. To get the LEC-j_λ on par with this scale and with each other, the required transformations are listed in Table 4.1. The value of 1 is a tricky number to work around when deciding which dimension should be chosen. When a change in magnitude is applied to small number (i.e. between 1 and 1.5) it creates a negligible change in the difference than if the numbers were any larger. In a quick example: $|1.2 – 0.7| = 0.5$ while $|0.7\text{-}0.12| = 0.58$ and $|2.2 – 0.7| = 1.5$ when $|0.7\text{-}0.22| = 0.48$. The magnitude selection clearly makes significant changes to the difference between two values when they are greater than 2. LEC-2 and LEC-3 are two parameters in our data with high end range values around 2.5 and 2 respectively.

It was found that a reduction in magnitude by a single order on the multiplier provided a more appropriate dimensional match only when LEC-2 and LEC-3 are compared to I_λ. These parameters were flagged for special consideration because their measurements approach values > 1.5. An example using the GI data is worked through in Table 4.2. LEC-2 requires that its dimension be reduced by a factor of 10 when compared to I_λ in order to make the smallest difference between the dimensions. If the 100 factor was not used on LEC-2 when compared to τ-λ then the difference between these two parameters increases by an order of magnitude showing that these dimensions are no longer matched. The same holds true for LEC-3 and its reduced multiplier from 1000 to

100. Also the wider range of I_λ (with values all less than 1) makes the reduced multiplier a better choice than for τ-λ whose range is tight around 1.

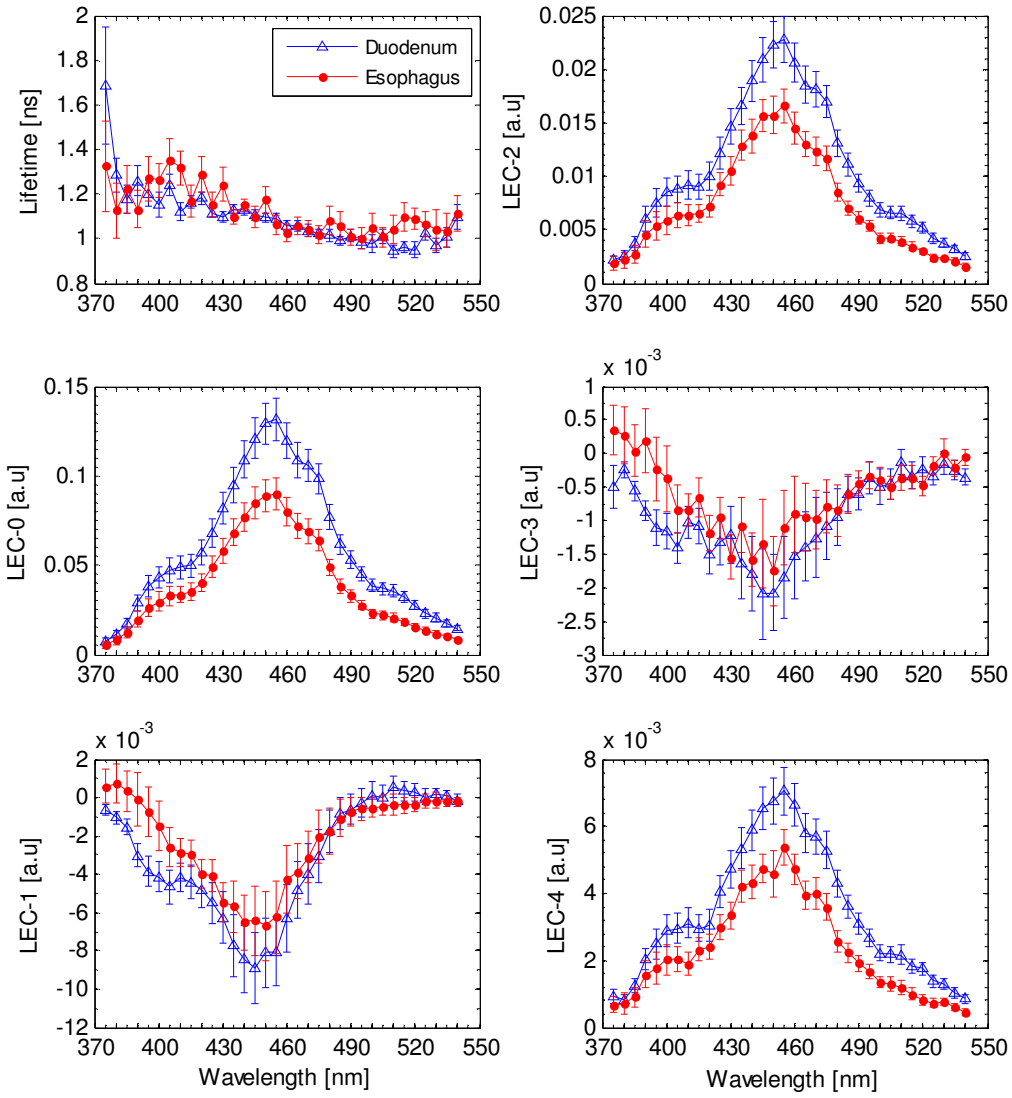

Figure 4.3: The average lifetimes and LEC-j for normal duodenum and normal esophagus are plotted with ± 1 SE. Values are tabulated in Appendix D.

Table 4.1: The dimensional multipliers are presented for each parameter along with the approximate range and median values derived from Figures 4.2 and 4.3.

Parameter	~ Range	~ Median	Multiplier	Median	Maximum
I	0.1 - 1.0	0.5	1	0.5	1.0
τ	0.9 - 1.2	1.1	1	1.1	1.4
LEC-0	0 - 0.150	0.080	10	0.8	1.5
LEC-1	0 - 0.009	0.004	100	0.4	0.9
LEC-2	0 - 0.025	0.012	*100	1.2	2.5
LEC-3	0 - 0.002	0.001	*1000	1.0	2.0
LEC-4	0 - 0.008	0.004	100	0.4	0.8

* A lower multiplier by a factor of 10 may be preferential.

Table 4.2: A comparison between the multipliers 10 and 100 on the LEC-j (j = 1, 2) using the normalized integrated spectra (I) and lifetime (τ) medians.

LEC-j	LEC-j Multiplier	τ Median	LEC-j Median	Absolute Difference	I Median	LEC-j Median	Absolute Difference
LEC-1	100	1.2	0.40	0.8	0.5	0.40	0.10
LEC-1	10	1.2	0.04	1.2	0.5	0.04	0.46
LEC-2	100	1.2	1.20	0	0.5	1.20	0.70
LEC-2	10	1.2	0.12	1.1	0.5	0.12	0.38

Not shown in Table 4.2 is a comparison of a dimensional reduction on LEC-2 with LEC-4 that has the same suggested multiplier of 100 from Table 4.1. Even though the maximum LEC-2 values are about 0.02 a.u., most of wavelengths for both esophagus and duodenum tissues have LEC-2 values that are below 0.015. This range of values is then more consistent with the LEC-1 and LEC-4 suggesting that a reduction in dimension is not necessary here for LEC-2. A LEC-2 dimensional reduction works better for I_λ also because the variability of measurements at each individual λ are much greater for the LEC-j than the I_λ. In this case the multiplier selected should be the one that allows the most overlap between the measurements of LEC-j values. As for LEC-3, its values are on

a dimension of their own and that 1000 multiplier should be used with the other LEC-j's multiplier to match the dimensions. Therefore the lower multiplier is preferential when comparing LEC-2 (and likewise LEC-3) to I_λ only.

So after these initial observations in regards to the measured values and their ranges it can be said that a change in dimension may improve the results at some wavelengths but compromise them more at others. Dimension selection could become more applicable after the rank-sum test has suggested two parameters with wavelengths whose values that fall at the extreme ends of the measured ranges. Changes in the sensitivity and specificity results caused by these transformations (or lack there of) will reveal if the dimension selection is a critical component for k-means clustering of GI fluorescent data. Without over complicating the analysis before it has even begun, clustering will be performed with and without the suggested multipliers from Table 4.1. If clusters turn out to be heterogeneous anyways, a dimensional transformation would not help to separate the overlap and there would be no need for further investigation.

4.2: K-means

Before the K-means classification algorithm was employed, the parameters were analysed using techniques in Section 2.2.3 to identify which individual parameters are statistically different between normal esophagus and duodenum tissue. First it was confirmed that for many of the parameters either the esophagus or duodenum sample group failed the Lilliefors normality test ($p < 0.05$, Appendix E). Most noticeable was the LEC-j where 90% of the LEC-j_λ had either the esophagus and/or the duodenum fails the

normality test. Consequently the 2-sample t-test for equal means cannot be used to compare the tissue because the majority of parameters are not normally distributed. The rank-sum test was used instead where the null hypothesis H_o is tested to see if the two groups have equal medians versus H_1 where they do not.

The results of the rank-sum test in Table 4.3 identify many parameters that do not have equal medians ($p < 0.05$) when normal esophageal tissue is compared to normal duodenum tissue. As discussed in Section 2.3.3 the rank-sum results were cross referenced with the 2-sample K-S test for each parameter because the rank-sum test requires that both groups have the same distribution type. All of the parameters that failed the 2-sample K-S test were picked up as being statistically different by the rank-sum test except for LEC-1_{535}, LEC-2_{375}, and LEC-4_{395}. These three parameters could potentially be useful in a non-parametric classification model (K-means) because they have different distributions despite coincidently having equal medians. Every combination of the parameters in Table 4.3 that found H_1 to be true (value 1 in Table 4.3) along with the other three LEC were used in K-means classification. Two Matlab scripts, fireaway_3.m and GIKmeans_6.m (Appendix F), were created to automate the process.

There are 16 normal duodenum (A) and 16 esophageal (D) data points for each parameter. Recall from Section 2.3.1 that the sensitivity and specificity equations are based upon the number of results that the test identifies as true or false positives and true or false negatives [3]. For our study, let the number of true positives be the amount of data that is correctly identified as duodenum tissue and the number of esophageal tissue correctly identified be the true negatives. In turn any esophageal results classified as

duodenum are said to be false positives while the false negatives are duodenum results that were not identified correctly during the classification.

Table 4.3: Rank-Sum Test Results from Normal Esophagus and Duodenum.

Wavelength [nm]	Integrated Intensity	Lifetime	LEC-0	LEC-1	LEC-2	LEC-3	LEC-4
375	0	0	1	1	0	0	0
380	0	0	1	1	1	0	0
385	0	0	1	0	1	0	0
390	0	0	1	1	1	1	0
395	0	0	1	1	1	0	0
400	0	0	1	0	1	0	0
405	0	0	1	0	1	0	0
410	0	1	1	0	0	0	1
415	0	0	0	0	0	0	0
420	0	0	1	0	1	0	0
425	0	0	1	0	0	0	0
430	0	0	1	0	1	0	0
435	0	0	1	0	0	0	0
440	0	0	1	0	1	0	1
445	0	0	1	0	1	0	1
450	0	0	1	0	1	0	1
455	0	0	1	0	1	0	1
460	1	0	1	0	1	0	1
465	1	0	1	0	1	0	1
470	1	0	1	0	1	0	1
475	1	0	1	0	1	0	1
480	1	0	1	0	1	0	1
485	1	0	1	0	1	0	1
490	1	0	1	0	1	0	1
495	1	0	1	0	1	0	1
500	1	0	1	0	1	0	1
505	1	0	1	0	1	0	1
510	1	0	1	0	1	0	1
515	1	0	1	0	1	0	1
520	1	1	1	1	1	0	1
525	1	0	1	0	1	0	1
530	1	0	1	0	1	0	1
535	1	0	1	0	1	0	1
540	1	0	1	0	1	0	0

The value 0 represents when H_o was found to be true, otherwise the value is 1 when the test has rejected that H_o = the two samples have equal medians.

Sensitivity (SN) will represent the portion of normal duodenum tissue results classified correctly. The specificity (SP) then refers to the portion of normal esophageal tissue that was correctly classified. Both are measured as a percentage where a result of 87.5 % = 14/16, 93.75 % = 15/16 and 100 % = 16/16. The k-means classification is said to be both specific and sensitive if it can identify (test positive) for a high number of tissue diagnosed as normal duodenum that are actually from normal duodenum tissue and not from normal esophagus tissue (false positives). To know how much sensitivity and specificity is required to validate the k-means algorithm would ultimately depend on a much larger sample size and the clinical significance of a patient's outcome when treatment from a misdiagnosis is received (see Section 2.3.4 for further discussion) [4, 5].

A total of 406 two-parameter combinations without dimensional transformations yield both a sensitivity and specificity of 87.5 % or greater. It implies that no more than four data points (two from duodenum and two from esophagus) were classified incorrectly. The number of combinations decreased from 406 to 50 when the results are narrowed down further when no more than two points were falsely classified. There are 13 combinations where the sensitivity and specificity are both 93.75 % and the other 37 occur when one of the sensitivity or specificity is 87.5 % and the other is 100 %. These results are listed in Tables 4.4 and 4.5. Some of these results include the three parameters that passed the rank-sum test but failed the 2-sample K-S test. Examples from these k-means clustering classification results in Figure 4.4 show that clusters can be somewhat heterogeneous and are definitely not the same size or globular.

Where dimensional matching may be required there are only 68 parameter combinations with results of ≥ 87.5% sensitivity/specificity which is down from the 406 pairs observed before. Only three of these 68 pairs have no more than two falsely classified points. These three results (Table 4.6) are new which means they are found only when the dimensions are transformed to what was considered to be a more appropriate match. Some of the 68 combinations produce the same results as the untransformed data but they now only came from I_λ vs. LEC-2 or LEC-4. In either case where dimensions are matched or not, there are no significant combinations involving τ-λ or LEC-j vs. LEC-j. There is too much overlap between duodenum and esophagus clusters to effectively distinguish between tissue types as shown in Figure 4.5.

Table 4.4: The K-means Results for Untransformed Data (Part 1).

Parameter Pairs		Sensitivity	Specificity	Centroid A		Centroid D	
X	Y	(%)	(%)	X1	Y1	X2	Y2
I_460	I_515	93.75	93.75	0.906	0.236	0.873	0.193
I_480	I_540	93.75	93.75	0.575	0.110	0.519	0.088
I_485	I_515	93.75	93.75	0.461	0.236	0.412	0.193
I_500	I_515	93.75	93.75	0.284	0.236	0.242	0.193
I_505	I_515	93.75	93.75	0.273	0.236	0.235	0.193
I_510	I_515	93.75	93.75	0.259	0.236	0.218	0.193
I_515	I_520	93.75	93.75	0.236	0.202	0.193	0.171
I_515	I_530	93.75	93.75	0.236	0.151	0.193	0.122
I_470	LEC-0_460	93.75	93.75	0.793	0.127	0.748	0.073
I_470	LEC-0_465	93.75	93.75	0.793	0.115	0.748	0.065
I_470	LEC-0_470	93.75	93.75	0.793	0.112	0.748	0.063
I_470	LEC-0_475	93.75	93.75	0.793	0.105	0.748	0.058
I_505	LEC-0_490	93.75	93.75	0.273	0.055	0.235	0.031

Spectral parameters I_λ are normalized to I_{455}.

Table 4.5: The K-means Results for Untransformed Data (Part 2).

Parameter Pairs		Sensitivity	Specificity	Centroid A		Centroid D	
X	Y	(%)	(%)	X1	Y1	X2	Y2
I_460	I_505	100	87.5	0.906	0.271	0.868	0.232
I_470	I_470	87.5	100	0.797	0.797	0.750	0.750
I_470	I_540	87.5	100	0.797	0.110	0.750	0.090
I_470	LEC-1_535	87.5	100	0.797	-2.23E-06	0.750	-9.42E-05
I_470	LEC-2_375	87.5	100	0.797	0.0022	0.750	0.0019
I_470	LEC-4_395	87.5	100	0.797	0.0024	0.750	0.0020
I_470	LEC-1_375	87.5	100	0.797	-0.0005	0.750	0.0003
I_470	LEC-1_380	87.5	100	0.797	-0.0009	0.750	0.0004
I_470	LEC-1_390	87.5	100	0.797	-0.0025	0.750	-0.0008
I_470	LEC-1_395	87.5	100	0.797	-0.0035	0.750	-0.0014
I_470	LEC-1_520	87.5	100	0.797	0.0003	0.750	-0.0003
I_470	LEC-2_380	87.5	100	0.797	0.0025	0.750	0.0023
I_470	LEC-2_385	87.5	100	0.797	0.0036	0.750	0.0030
I_470	LEC-2_390	87.5	100	0.797	0.0060	0.750	0.0048
I_470	LEC-2_520	87.5	100	0.797	0.0053	0.750	0.0031
I_470	LEC-2_525	87.5	100	0.797	0.0044	0.750	0.0025
I_470	LEC-2_530	87.5	100	0.797	0.0039	0.750	0.0024
I_470	LEC-2_535	87.5	100	0.797	0.0032	0.750	0.0023
I_470	LEC-2_540	87.5	100	0.797	0.0027	0.750	0.0017
I_470	LEC-3_390	87.5	100	0.797	-0.0008	0.750	0.0000
I_470	LEC-4_410	87.5	100	0.797	0.0031	0.750	0.0020
I_470	LEC-4_440	87.5	100	0.797	0.0060	0.750	0.0044
I_470	LEC-4_445	87.5	100	0.797	0.0066	0.750	0.0049
I_470	LEC-4_465	87.5	100	0.797	0.0060	0.750	0.0040
I_470	LEC-4_475	87.5	100	0.797	0.0055	0.750	0.0036
I_470	LEC-4_480	87.5	100	0.797	0.0044	0.750	0.0027
I_470	LEC-4_485	87.5	100	0.797	0.0037	0.750	0.0023
I_470	LEC-4_490	87.5	100	0.797	0.0032	0.750	0.0020
I_470	LEC-4_495	87.5	100	0.797	0.0028	0.750	0.0017
I_470	LEC-4_500	87.5	100	0.797	0.0022	0.750	0.0014
I_470	LEC-4_505	87.5	100	0.797	0.0022	0.750	0.0014
I_470	LEC-4_510	87.5	100	0.797	0.0022	0.750	0.0012
I_470	LEC-4_515	87.5	100	0.797	0.0019	0.750	0.0010
I_470	LEC-4_520	87.5	100	0.797	0.0018	0.750	0.0009
I_470	LEC-4_525	87.5	100	0.797	0.0014	0.750	0.0008
I_470	LEC-4_530	87.5	100	0.797	0.0013	0.750	0.0008
I_470	LEC-4_535	87.5	100	0.797	0.0011	0.750	0.0006

Spectral parameters I_λ are normalized to I_{455}.

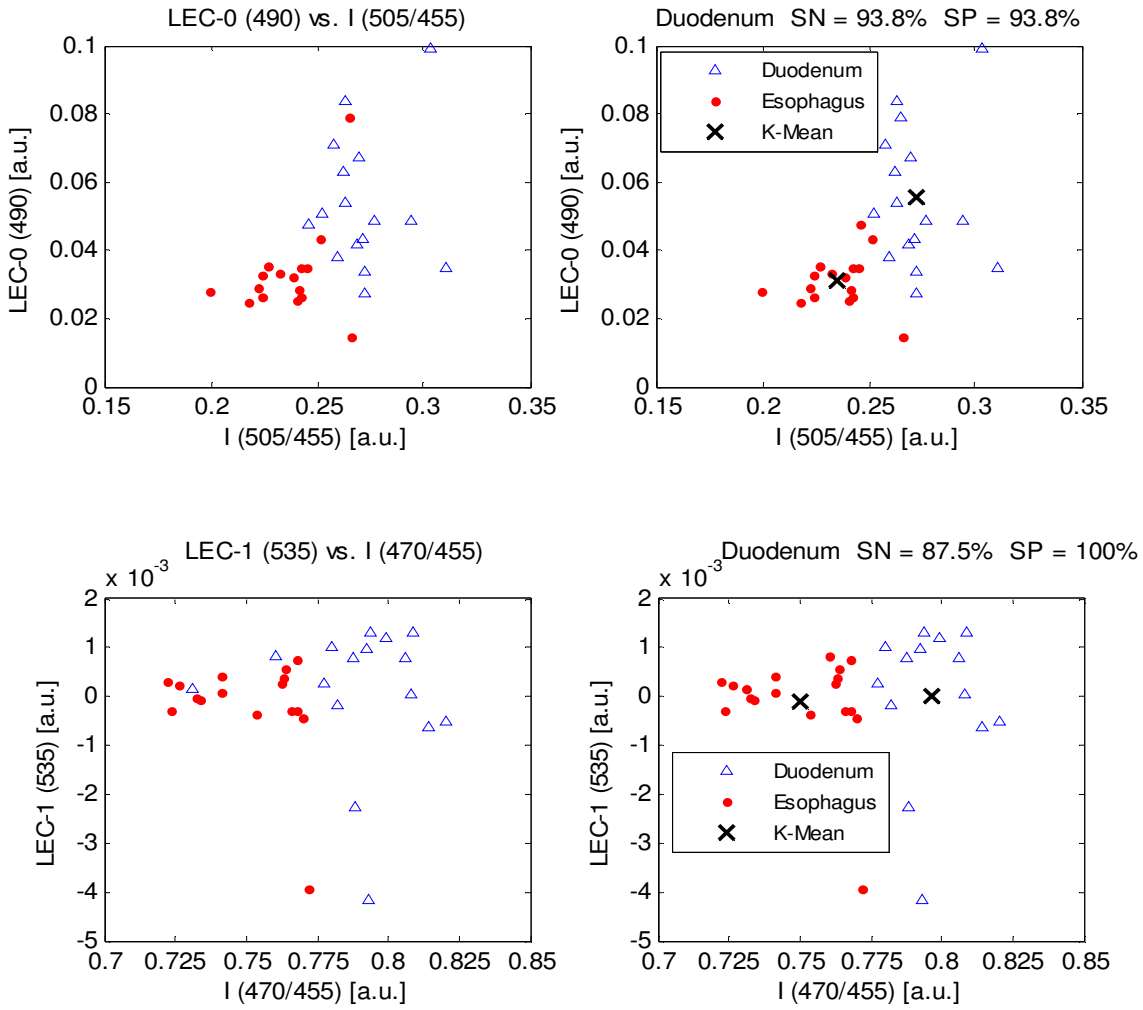

Figure 4.4: Examples of k-means clustering results from Tables 4.4 and 4.5. The clusters are not homogeneous and well separated despite good sensitivity and specificity.

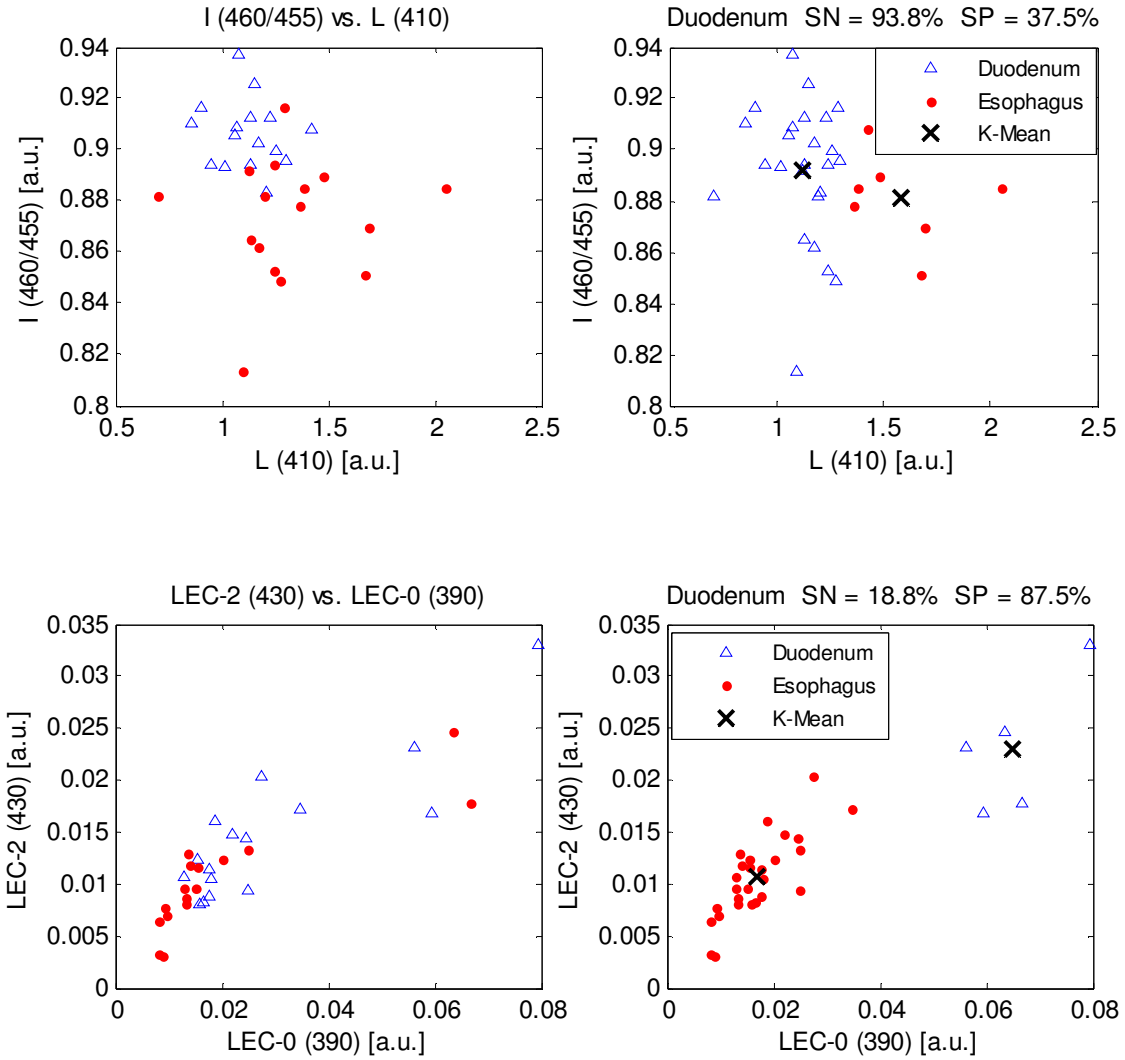

Figure 4.5: Examples of k-means clustering results from τ-λ or LEC-j vs. LEC-j have resulted in classifications that have poor sensitivity or poor specificity. Notice that most of the LEC-0_{390} are in a in a range where a dimensional transformation is not required to match values of LEC-2_{430}.

Table 4.6: The K-means Results for Transformed Data.

Parameter Pairs		Sensitivity	Specificity	Centroid A		Centroid D	
X	Y	(%)	(%)	X1	Y1	X2	Y2
I_460	LEC-2_515	93.75	93.75	0.906	0.065	0.868	0.037
I_505	LEC-2_510	100	93.75	0.271	0.067	0.234	0.036
I_460	LEC-2_510	100	87.5	0.906	0.062	0.873	0.031

The best result from all the parameter combinations with or without dimensional transformations comes from Table 4.6, LEC-2_{510} vs. $I_{505.}$ Before and after classification graphs can be found in Figure 4.6. The dimensional transformation (x 10) allows three more data points to be correctly classified around the border of the two clusters. If the LEC-2_{510} axis was transformed by 1 more dimension (i.e. the 100 multiplier) the sensitivity for the 3 results falls to 50% or lower. Most of the transformations from Table 4.1 when applied altered some but not all of classifications. Transformations generally did not improve the amount of desirable results but it has shown that it is worth the time and consideration.

Axis transformations most often caused one of the centroids to become biased towards the edge of an oddly shaped cluster, lowering the sensitivity and specificity results dramatically. Figure 4.7 is an example from LEC-1 where transformations destroyed all of the reasonably good results with I_{λ}. The theoretical centroid of both clusters in this result (unlike Figure 4.6) shifts with each assignment iteration such that one of them becomes biased towards data points with the smaller values of LEC-1. At the end of the k-means clustering algorithm, the duodenum tissue contains most of the data

points in the top half of the graph because the change in y distance becomes equally as important as the change in x distance when the dimensions are matched.

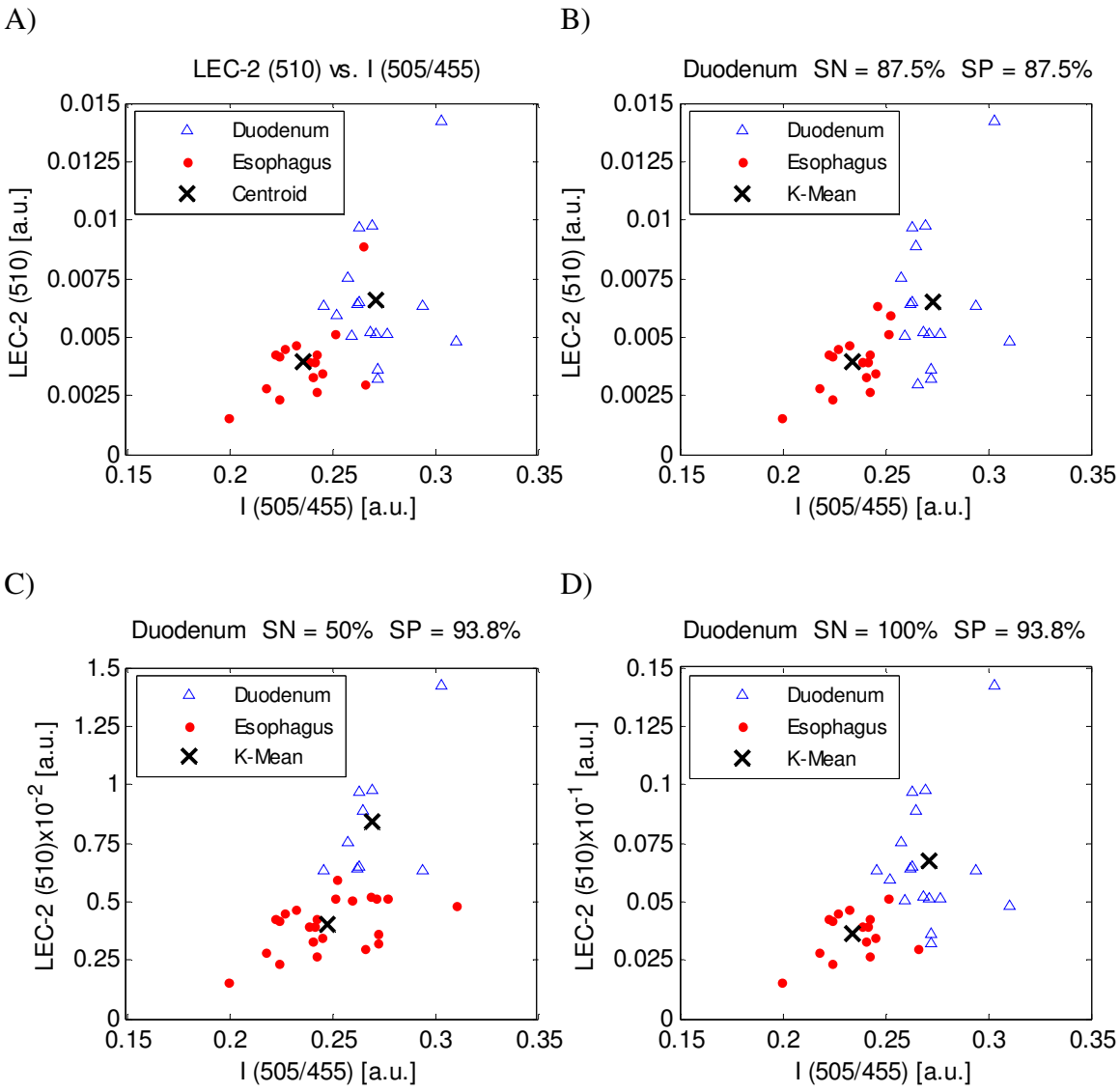

Figure 4.6: An example of improved sensitivity and specificity from k-means clustering when LEC-2_{510} values are multiplied by 10 to match the dimension of $I_{505/455}$. A) The data points are plotted using the clinical results. B) Results of the K-means classification without any axis dimension transformations. C) The LEC-2_{510} axis dimension has been transformed by 100. The result is lower SN but slightly improved SP. D) The LEC-2_{510} axis is transformed by a factor of 10 instead of 100 which results in the best SN and SP of the GI tissue fluorescence study.

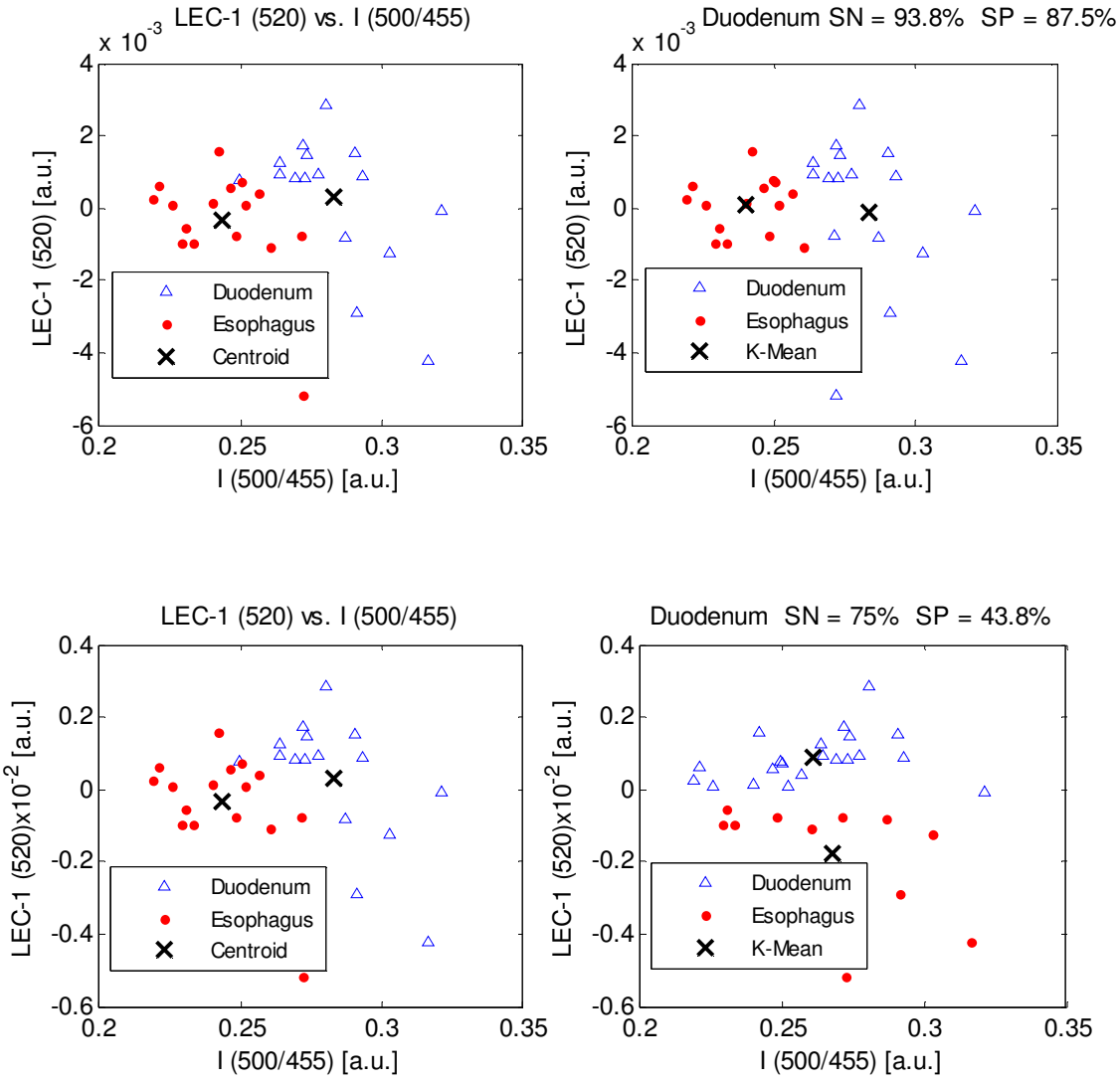

Figure 4.7: Dimensional transformation of LEC-1_{520} causes shifting of the theoretical centroids creates top-bottom segregation instead of left-right clusters.

REFERENCES

[1] Taylor JR. 1997. Statistical Analysis of Random Uncertainties. In: An Introduction to Error Analysis: the study of uncertainties in physical measurements. 2nd ed. Sausalito, California: University Science Books. p 93-119.

[2] Hill T, Lewicki P. 2007. Cluster analysis. In: Statistics: methods and applications. Tulsa, OK: StatSoft Inc. p 115-126.

[3] Riffenburgh, RH. 2006. Statistical testing, risks, and odds in medical decisions. In: Statistics in medicine. 2nd ed. Burlington, MA: Elsevier Academic Press. p 93-114.

[4] Riffenburgh, RH. 2006. Sample size required for a study. In: Statistics in medicine. 2nd ed. Burlington, MA: Elsevier Academic Press. p 115-123.

[5] Riffenburgh, RH. 2006. Sample size required in a study. In: Statistics in medicine. 2nd ed. Burlington, MA: Elsevier Academic Press. p 397-417.

CHAPTER 5: CONCLUSION

The steady-state and time-resolved fluorescence response produced from 355 nm excitation of biopsies from the upper GI tract were collected, processed, and thoroughly evaluated. A set of criteria were derived to single out data deemed to be erroneous so they could be discarded to prevent distortions in the data pool of 28 patients. The clinical diagnosis and k-means classification algorithm were used to identify the tissue diagnosis based on spectral (total signal) and time-resolved (Laguerre based deconvolution [1]) properties of the tissue fluorescence response.

Current gold standard practices for identification of GI disease involve invasive tissue biopsies and require histopathological examination by a trained professional [2]. An optical biopsy can exploit light-tissue interactions without the removal of tissue to arrive at the same diagnosis [3, 4, 5]. Acceptance of an optical biopsy technology into the clinic however requires a highly accurate diagnosis produced in-real time. So far with a limited data pool of 16 normal duodenum and 16 normal esophageal samples we have been able to show that over 400 pairs of fluorescent response parameters can be used to classify these samples with 87.5 % sensitivity and 87.5 % specificity or better. With some minor data manipulation in the form of dimensional transformations can improve these results to be as good as 100% sensitivity and 94% specificity. There is indeed potential that further study into GI tissue can reveal that just one parameter pairing can be measured and used to classify tissue in just a few seconds.

Before the data were acquired for this study, the TR-FS instrument was optimized for clinical data collection by implementing several improvements that maximized the

signal quality which was now free from component interference [1]. The first six patients in this study were used to develop and streamline both data collection and tissue handling protocols. It was found that the instrument error which affected these measurements was unacceptable so they were discarded from any data analysis in this study. Instrument re-calibration resolved the error and all further data collected were scrutinized for several other problems. Descriptive parameters derived from spectral (I_λ) and temporal (τ-λ, LEC-j_λ) analysis extracted from the data [1] aided the evaluation process.

There were four main areas of interest when it came to analysing the integrity of the data. The first two areas were conventional issues dealing with upper and lower instrument signal detection limits. For the data displaying the greatest I_λ, the time-domain signal was reviewed and it was found that nowhere in the data pool did the signal exceed the digitizer's maximum recordable value. Amplitude saturation in the form of extreme pulse width broadening was also not observed in the time-domain as the FWHM did not exceed + 3 SD in each tissue. Some data sets fell below – 3 SD and were directly correlated with samples containing just background noise and no signal.

In an attempt to quantify the lower instrument cut off with an associated SNR value, the τ-λ was used as a measure to determine if the Laguerre deconvolution algorithm was able to fit noisy data. At 505 nm SNRs < 20 dB were not associated with lifetimes outside ± 1 SD. Lifetimes at 455 nm or 505 nm outside of their respective ± 1 SD did if fact happen at any SNR. It is expected that the lifetime response is directly dependent on the tissue fluorophore composition [3]. Without direct correlation between fluorescence and histology it is impossible to investigate the extremely large or small

lifetimes any further. Overall the Laguerre algorithm had demonstrated in this section its robust ability to extract consistent lifetime values under low SNR conditions. There is no conclusive lower detection limit based on SNR and Laguerre lifetimes. On the other hand it was clear based on spectral data that there was in fact an instrument lower detection limit. Spectra with $I_{455} < 19.5$ V·ns had a noisy spectral shape instead of the bell curve observed at all higher signal intensities. Relative I_λ values are an integral part of classification modeling and thus this data could not be placed in confidence. The I_λ with associated τ-λ and LEC-j_λ were removed from the data pool.

The other two main areas of interest arose from variations in the data collection protocol and the spectral data. Some times consecutive measurements on the same sample spot were taken for the sole purpose of increasing the signal quality by adjusting the PCM-PMT gain. It was found that photobleaching could not be observed even after three consecutive measurements were made. Also, the difference in fluorescence between two measurements showed negligible variation confirming that an average of just 10 pulses is enough to articulate the tissue fluorescence response. Average parameters from a single patient location had to be used to represent the diagnosis due to lack of correlation with pathology. Thus the first of every repeated measurement was removed from the data pool because overrepresentation of repeated data can skew the average.

Variations in the spectral data shape with an increased I_λ between 370-455 nm and an absorption around 410 nm seldom occurred in normal esophagus and duodenum tissue. Such a spectral pattern is most attributed to the absorption of blood and the emission of collagen and elastin [6]. It was found that the degree of this variation pattern in the

normal tissue samples had negligible effects on the fluorescent lifetimes. Such a pattern was more exaggerated in some of the diseased tissue samples. The observation supports expectations that diseased tissue have increased levels of collagen, elastin, and blood in the mucosal layer [7]. However it would have been difficult to examine this data and quantify the impact signal attenuation from blood has on the observed fluorescence with only two or three patients in the data pool having the same diseased condition. A larger data pool of diseased patients is required to verify if any corrections to the parameters extracted with the methods used in this study are required.

The two largest specimen pools were normal esophageal and normal duodenum with 16 patients each. The descriptive parameters representing these data pools generally did not follow a normal sampling distribution (Lilliefors test, $p < 0.05$). Thus the rank-sum test instead of the t-test was used to select parameters whose values had significantly different medians ($p < 0.05$) between the esophageal and duodenum groups. There were three parameters identified as having equal medians where the groups did not pass the rank-sum test assumption that they are of the same distribution type (2 sample KS test). Otherwise all other parameters that failed the assumption had measurements that were far enough apart that they were determined to not have equal medians anyways. For completeness, the three parameters were included with the set of rank-sum results for further non-parametric classification analysis.

The k-means classification algorithm was an excellent choice for this initial study because it does not require the groups have the same distribution type or that they are normally distributed. The sheer amount of results from the k-means classification

conducted using different pairs of parameters from duodenum and esophageal tissue is promising. It acknowledges that k-means clustering could become a viable classifier solution for GI tissue based on the parameters extracted from the observed relative wavelength intensities and Laguerre deconvolution of the IRF.

The most significant differences between two normal GI tissue groups stood out in the longer wavelengths after the peak emission I_{455}. The most dominate parameter in k-means classification was $I_{470/455}$ which corresponds to the peak emission of NADH [6]. It suggests that there is a metabolic difference between duodenum and esophageal tissue but this assumption cannot be confirmed from spectral data because the emission spectrum of NADH also overlaps with collagen and elastin [6]. Aside from $I_{470/455}$, differences in the LEC-j parameters with positive terms (j = 0, 2, and 4) also dominated the k-means results. The negative terms in the Laguerre expansion (LEC-1 and LEC-3) are less influential likely because these are the terms in the function that approach asymptotic decay from local minima which are not observed in the IRF. The tissue composition's average fluorophore lifetime (i.e. τ-λ) was not found to be significant in the k-means clustering. It implies that normal esophageal and duodenum tissues have similar fluorophore composition.

There are two drawbacks about the normal GI data in particular that challenge the k-mean method. The first is that the clusters are not homogeneous and the acquisition of data from more patients could reveal greater cluster overlap, lowering the sensitivity and specificity results seen here. The second caution comes as a fall out from the first. The clusters are not globular or well separated and it questions the importance of dimensional

match selection to steer the cluster assignments into their correct shapes. If the cluster boundaries do become more complicated and make k-means classification less viable, it would be time to move on and try some more sophisticated techniques. Advanced classification methods such as those that require machine learning (ex. logistic regression, step-wise linear discriminat analysis, or support vector machine [8]) could work to define linear or nonlinear hyperplane classifiers in two or more dimensions.

In conclusion, a protocol for data analysis was developed such that it is possible to characterize GI tissue fluorescence and use this information to correctly identify the corresponding clinical diagnosis. It is clear that validation of the findings from this study would first require the accumulation of more data for both normal and diseased patients as well as direct correlation between fluorescence location and histology. The signal attenuation effects from blood absorption will have to be investigated to determine what kind of correction if any should be applied to ensure the data is free from such distortions. If a single set of parameters can be used to classify tissue with enough accuracy to satisfy the clinical tolerance then this optical biopsy technology can definitely report the diagnosis on site and in real time. The instrument can be fine-tuned to hone in on just those wavelengths, deconvolve the data, and assign the result a diagnosis based on which k-means it is closest to. This technology not only has the potential to become a very powerful tool in GI diagnostics, it can be very quite versatile. Protocols are applicable to other tissues such as brain and lung with some tweaking of the Laguerre system dependent parameters α and M.

REFERENCES

[1] Krishnamoorthy M. 2010. Optimization of a time-resolved spectroscopy system with an acousto-optic tunable filter employing a deconvolution method based on discrete laguerre functions [dissertation]. Hamilton (ON): McMaster University.

[2] Jobe BA, Hunter JG, Peters JH. 2009. Esophagus and diaphragmatic hernia. In: Brunicardi F, Andersen D, Billiar T, Dunn D, Hunter J, Matthews J, Pollock RE, editors. Schwartz's principles of surgery [Internet]. 9th ed. New York, NY: McGraw-Hill [cited 2012 Feb 4]. Available from http://www.accessmedicine.com/content.aspx?aID=5031992

[3] Vo-Dinh T, Cullum BM. 2003. Fluorescence spectroscopy for biomedical diagnostics. In: Vo-Dinh T, editor. Biomedical photonics handbook. Boca Raton, FL: CRC Press. p 28:1-50.

[4] Wilson BC. 2007. Detection and treatment of dysplasia in Barrett's esophagus: a pivotal challenge in translating biophotonics from bench to bedside. Journal of Biomedical Optics 12(5):051401.

[5] Marcu L. 2012. Fluorescence lifetime techniques in medical applications. Annals of Biomedical Engineering (January 25th 2012 Epub ahead of print):1-28.

[6] Prasad PN. 2003. Photobiology. In: Introduction to Biophotonics. Hoboken, NJ: John Wiley and Sons. p 159-202.

[7] Feldman M, Friedman LS, Brandt LJ. 2010. Sleisenger and Fordtran's gastrointestinal and liver disease. 9th ed. Philadelphia, PA: Saunders Elsevier. 2480 p.

[8] Ahn H, Moon H. 2010. Classification: supervised learning with high-dimensional biological data. In: Lee JK, editor. Statistical bioinformatics - for biomedical and life science researchers. Hoboken, NJ: John Wiley & Sons Inc. p129-156.

APPENDIX A: Operation of the TR-FS Instrument for Clinical Study

1. Plug cart into a wall outlet.
2. UPS Power button On (screen will become red backlit)
3. Top cutout on the side of the cart:
   - Power button for industrial box (if not on already, leave it on so UPS charge is maintained)
   - Red Power button for AOTF driver
   - Chrome toggle switch 'on' for AOFT driver bias voltage
   - Turn key on for the laser power supply
4. Bottom front of cart:
   - Turn on diode (switch in “down” position is “on”, located the backside of the diode)
   - Connect fibre optics probe
5. Bottom cutout on the other side of the cart:
   - Turn on laser switch (back of laser)
   - Turn on laser ready button (do this after connecting the probe)
6. Turn on computer by pressing on/off button on the oscilloscope
7. Turn on delay generator by pressing it's on/off button
8. Press run/stop on delay generator before acquiring data
9. On the computer/oscilloscope:
   - Login using 'user' and the network password
   - Double click 'Tekscope' icon on the desktop (oscilloscope software)
   - Load 'system_hopping_mode_v5' to load Labview and our data acquisition program
10. Turn on PMT and fan:
    - PMT black power switch
    - let voltage=0V and 'Neg' light come on
    - turn on high voltage using the green button
    - use coarse and fine adjustment knobs to set the PMT voltage (do not exceed300V)
    - fan switch is located on white power cord
11. Use Scope Setting 10 on the delay generator to acquire data:
    - Press yellow shift key then “9/Recall” (a music note appears now in upper left display)
    - type in “10”
    - then yellow shift key again then “9/Recall” to save the change (music note disappears)
    - Press Run/Stop (a dot in the upper left display means “Run” mode)
12. Note: Scope setting “6” will allow you to continuously fire the laser controlled manually by pressing Run/Stop.
13. To Turn off the Instrument:
    - Shut down in any instrument order but in reverse detail.
    - Leave the isolation transformer on.
    - Plug the cart back into a wall outlet after cart relocation.
    - Turn on the UPS to recharge it. Do not leave the UPS off with a low charge over a long period of time otherwise it can damage the battery.

APPENDIX B: Sample Note Collection

Ex-Vivo Clinical Testing of the Time-Resolved Laser Induced Fluorescence Spectroscopy (TR-FS) System with Patient 28

Collection Date: November 2nd , 2009 - Patient 28.
McMaster University Medical Centre, Department of Endoscopy
Attendance: F. Tse, Z. Nie, and M. LePalud
Notes by: Z. Nie and M. LePalud

Equipment Notes:
- Used same equipment and data collection method as P07-P09.
- Laser Energy at start: 3.05 μJ with probe perpendicular to the floor (Scope Memory 6).
- Scope settings (Memory 10) were loaded normally for tissue and paper collection.
- Cart was stored in Dr. Tse's office and returned there after endoscopy.

Data Collection Notes:
- Forgot to press Run/Stop before colleting the first trial. Restarting Labview and Tekscope did not fix the problem. Restarted the computer and turned the pulse generator off. Then Labview would collect data.
- Fluorescence of tissue and paper were taken with probe at 45 degrees like always
- Took 3 paper files, all looked normal. 20091102_Paper_V1700_T1_pwrmtr (is actually paper), 20091102_Paper_V1700_T1_CH1.dat and T2 were the other two paper files.
- One endoscopy patient today, biopsies taken at 9:00am.
- P28(U#:XXXXXXXXXX, DOB:XX/XX/XX)
- P28 fluorescence data collected from 9:14 am to 10:03 am.
- Lights were on for A1_T1 to C2_T4. Lights were off from C2_T5 onward.
- Dr. Tse indicated D, E, and F are all Esophagus, sampled at 30cm, 35cm, and 39cm.
- Paper scans T3 to T6 looked normal. Some are strong/weak signals depending on height of the probe.
- The data was copied onto a flash USB drive and loaded onto the lab server.
- Charge Nurse for the day: XXX.

Other Notes:
- Files for P28 are in J:\Data\GI_Ex\GI_P28_20091102 (46 total trials)
- Files labeled Paper are in J:\Data\GI_Ex\GI_P28_20091102 (7 total trials)
- Sample file names: 20091102_P28_B1_V2200_T2_CH1.dat
- These folders have been zipped with the original data files (backups)
- The standard medical report from Dr. Tse was not received, the computer was down to make a printout.

GI_ExpSummary_20091102_P07-P28_bak.xls Notes_P28 03/11/2009 4:13 PM

APPENDIX C: α Calculation

Table 1: Files used to obtain average α values.

Tissue A	Tissue B	Tissue C	Tissue D
P08_A1_V2200_T1	P08_B1_V2200_T1	P08_C1_V2200_T2	P08_D1_V2200_T1
P08_A1_V2200_T2	P08_B1_V2200_T3	P08_C2_V2200_T4	P08_D1_V2200_T2
P17_A1_V2150_T2	P08_B2_V2200_T5	P17_C1_V2200_T3	P17_D1_V2200_T3
P17_A1_V2150_T3	P17_B1_V2200_T3	P17_C2_V2150_T9	P25_D1_V2250_T3
P17_A1_V2200_T6	P26_B1_V2150_T4	P26_C1_V2150_T1	P25_D1_V2250_T4

Table 2: Average α using alpha_opt_1e.m.

Wavelegnth	Tissue A	Tissue B	Tissue C	Tissue D
[ns]	Mean ± SD	Mean ± SD	Mean ± SD	Mean ± SD
375	0.9556 ± 0.0145	0.9586 ± 0.0084	0.9612 ± 0.0124	0.9634 ± 0.0069
380	0.9566 ± 0.0154	0.9692 ± 0.0018	0.9660 ± 0.0068	0.9612 ± 0.0088
385	0.9654 ± 0.0063	0.9598 ± 0.0118	0.9570 ± 0.0112	0.9590 ± 0.0124
390	0.9672 ± 0.0029	0.9628 ± 0.0095	0.9622 ± 0.0074	0.9686 ± 0.0019
395	0.9648 ± 0.0116	0.9682 ± 0.0035	0.9670 ± 0.0062	0.9678 ± 0.0039
400	0.9660 ± 0.0050	0.9694 ± 0.0013	0.9692 ± 0.0011	0.9660 ± 0.0053
405	0.9642 ± 0.0064	0.9672 ± 0.0052	0.9610 ± 0.0123	0.9690 ± 0.0022
410	0.9666 ± 0.0053	0.9664 ± 0.0025	0.9674 ± 0.0024	0.9618 ± 0.0102
415	0.9696 ± 0.0009	0.9652 ± 0.0075	0.9672 ± 0.0036	0.9688 ± 0.0018
420	0.9676 ± 0.0043	0.9662 ± 0.0052	0.9640 ± 0.0022	0.9666 ± 0.0056
425	0.9664 ± 0.0061	0.9618 ± 0.0088	0.9684 ± 0.0030	0.9670 ± 0.0041
430	0.9680 ± 0.0035	0.9686 ± 0.0022	0.9690 ± 0.0014	0.9694 ± 0.0013
435	0.9694 ± 0.0013	0.9688 ± 0.0018	0.9678 ± 0.0029	0.9700 ± 0.0000
440	0.9674 ± 0.0040	0.9684 ± 0.0021	0.9690 ± 0.0017	0.9700 ± 0.0000
445	0.9678 ± 0.0026	0.9684 ± 0.0017	0.9678 ± 0.0019	0.9690 ± 0.0022
450	0.9694 ± 0.0013	0.9686 ± 0.0021	0.9688 ± 0.0016	0.9700 ± 0.0000
455	0.9672 ± 0.0026	0.9678 ± 0.0023	0.9684 ± 0.0026	0.9692 ± 0.0018
460	0.9648 ± 0.0044	0.9692 ± 0.0018	0.9686 ± 0.0017	0.9700 ± 0.0000
465	0.9656 ± 0.0046	0.9680 ± 0.0035	0.9680 ± 0.0019	0.9684 ± 0.0036
470	0.9698 ± 0.0004	0.9700 ± 0.0000	0.9658 ± 0.0058	0.9698 ± 0.0004
475	0.9700 ± 0.0000	0.9676 ± 0.0029	0.9648 ± 0.0059	0.9676 ± 0.0039
480	0.9654 ± 0.0081	0.9670 ± 0.0031	0.9674 ± 0.0024	0.9688 ± 0.0027
485	0.9688 ± 0.0013	0.9658 ± 0.0053	0.9672 ± 0.0024	0.9664 ± 0.0064
490	0.9656 ± 0.0053	0.9644 ± 0.0088	0.9676 ± 0.0029	0.9686 ± 0.0031
495	0.9700 ± 0.0000	0.9668 ± 0.0044	0.9674 ± 0.0036	0.9700 ± 0.0000
500	0.9680 ± 0.0025	0.9624 ± 0.0112	0.9670 ± 0.0045	0.9648 ± 0.0079
505	0.9646 ± 0.0051	0.9678 ± 0.0027	0.9634 ± 0.0117	0.9690 ± 0.0017
510	0.9670 ± 0.0042	0.9674 ± 0.0043	0.9634 ± 0.0131	0.9628 ± 0.0099
515	0.9568 ± 0.0129	0.9642 ± 0.0066	0.9556 ± 0.0125	0.9664 ± 0.0045
520	0.9684 ± 0.0022	0.9552 ± 0.0131	0.9590 ± 0.0083	0.9656 ± 0.0098
525	0.9650 ± 0.0090	0.9566 ± 0.0128	0.9674 ± 0.0032	0.9674 ± 0.0037
530	0.9664 ± 0.0061	0.9682 ± 0.0025	0.9594 ± 0.0096	0.9666 ± 0.0050
535	0.9588 ± 0.0106	0.9640 ± 0.0134	0.9662 ± 0.0036	0.9624 ± 0.0127
540	0.9586 ± 0.0120	0.9618 ± 0.0114	0.9574 ± 0.0101	0.9578 ± 0.0117

Table 3: Average α using alpha_opt_1f.m.

Wavelegnth	Tissue A	Tissue B	Tissue C	Tissue D
[ns]	Mean ± SD	Mean ± SD	Mean ± SD	Mean ± SD
375	0.9556 ± 0.0145	0.9586 ± 0.0084	0.9612 ± 0.0124	0.9634 ± 0.0069
380	0.9566 ± 0.0154	0.9692 ± 0.0018	0.9660 ± 0.0068	0.9612 ± 0.0088
385	0.9654 ± 0.0063	0.9598 ± 0.0118	0.9570 ± 0.0112	0.9590 ± 0.0124
390	0.9672 ± 0.0029	0.9628 ± 0.0095	0.9622 ± 0.0074	0.9686 ± 0.0019
395	0.9648 ± 0.0116	0.9682 ± 0.0035	0.9670 ± 0.0062	0.9678 ± 0.0039
400	0.9660 ± 0.0050	0.9694 ± 0.0013	0.9692 ± 0.0011	0.9660 ± 0.0053
405	0.9642 ± 0.0064	0.9672 ± 0.0052	0.9610 ± 0.0123	0.9690 ± 0.0022
410	0.9666 ± 0.0053	0.9664 ± 0.0025	0.9674 ± 0.0024	0.9618 ± 0.0102
415	0.9696 ± 0.0009	0.9652 ± 0.0075	0.9672 ± 0.0036	0.9688 ± 0.0018
420	0.9676 ± 0.0043	0.9662 ± 0.0052	0.9640 ± 0.0022	0.9666 ± 0.0056
425	0.9664 ± 0.0061	0.9618 ± 0.0088	0.9684 ± 0.0030	0.9670 ± 0.0041
430	0.9680 ± 0.0035	0.9686 ± 0.0022	0.9690 ± 0.0014	0.9694 ± 0.0013
435	0.9694 ± 0.0013	0.9688 ± 0.0018	0.9678 ± 0.0029	0.9700 ± 0.0000
440	0.9674 ± 0.0040	0.9684 ± 0.0021	0.9690 ± 0.0017	0.9700 ± 0.0000
445	0.9678 ± 0.0026	0.9684 ± 0.0017	0.9678 ± 0.0019	0.9690 ± 0.0022
450	0.9694 ± 0.0013	0.9686 ± 0.0021	0.9688 ± 0.0016	0.9700 ± 0.0000
455	0.9672 ± 0.0026	0.9678 ± 0.0023	0.9684 ± 0.0026	0.9692 ± 0.0018
460	0.9648 ± 0.0044	0.9692 ± 0.0018	0.9686 ± 0.0017	0.9700 ± 0.0000
465	0.9656 ± 0.0046	0.9680 ± 0.0035	0.9680 ± 0.0019	0.9684 ± 0.0036
470	0.9698 ± 0.0004	0.9700 ± 0.0000	0.9658 ± 0.0058	0.9698 ± 0.0004
475	0.9700 ± 0.0000	0.9676 ± 0.0029	0.9648 ± 0.0059	0.9676 ± 0.0039
480	0.9654 ± 0.0081	0.9670 ± 0.0031	0.9674 ± 0.0024	0.9688 ± 0.0027
485	0.9688 ± 0.0013	0.9658 ± 0.0053	0.9672 ± 0.0024	0.9664 ± 0.0064
490	0.9656 ± 0.0053	0.9644 ± 0.0088	0.9676 ± 0.0029	0.9686 ± 0.0031
495	0.9700 ± 0.0000	0.9668 ± 0.0044	0.9674 ± 0.0036	0.9700 ± 0.0000
500	0.9680 ± 0.0025	0.9624 ± 0.0112	0.9670 ± 0.0045	0.9648 ± 0.0079
505	0.9646 ± 0.0051	0.9678 ± 0.0027	0.9634 ± 0.0117	0.9690 ± 0.0017
510	0.9670 ± 0.0042	0.9674 ± 0.0043	0.9634 ± 0.0131	0.9628 ± 0.0099
515	0.9568 ± 0.0129	0.9642 ± 0.0066	0.9556 ± 0.0125	0.9664 ± 0.0045
520	0.9684 ± 0.0022	0.9552 ± 0.0131	0.9590 ± 0.0083	0.9656 ± 0.0098
525	0.9650 ± 0.0090	0.9566 ± 0.0128	0.9674 ± 0.0032	0.9674 ± 0.0037
530	0.9664 ± 0.0061	0.9682 ± 0.0025	0.9594 ± 0.0096	0.9666 ± 0.0050
535	0.9588 ± 0.0106	0.9640 ± 0.0134	0.9662 ± 0.0036	0.9624 ± 0.0127
540	0.9586 ± 0.0120	0.9618 ± 0.0114	0.9574 ± 0.0101	0.9578 ± 0.0117

APPENDIX D: Values for Figures 4.2 and 4.3

Table 1: Values for Figure 4.2, Average ± 1 Standard Error.

Wavelength [nm]	Normalized Integrated Intensity (to 455nm)		
	A	C	D
375	0.065 ± 0.008	0.055 ± 0.005	0.056 ± 0.008
380	0.091 ± 0.011	0.080 ± 0.006	0.078 ± 0.011
385	0.137 ± 0.016	0.126 ± 0.011	0.119 ± 0.015
390	0.228 ± 0.023	0.217 ± 0.018	0.201 ± 0.021
395	0.296 ± 0.028	0.286 ± 0.018	0.271 ± 0.024
400	0.333 ± 0.026	0.326 ± 0.021	0.311 ± 0.022
405	0.361 ± 0.023	0.356 ± 0.022	0.360 ± 0.021
410	0.368 ± 0.020	0.365 ± 0.024	0.368 ± 0.021
415	0.374 ± 0.016	0.370 ± 0.022	0.385 ± 0.019
420	0.426 ± 0.016	0.416 ± 0.023	0.445 ± 0.021
425	0.509 ± 0.017	0.494 ± 0.021	0.540 ± 0.020
430	0.613 ± 0.016	0.581 ± 0.021	0.650 ± 0.020
435	0.719 ± 0.014	0.679 ± 0.018	0.759 ± 0.018
440	0.826 ± 0.011	0.792 ± 0.017	0.854 ± 0.014
445	0.920 ± 0.009	0.884 ± 0.012	0.939 ± 0.010
450	0.978 ± 0.006	0.957 ± 0.007	0.983 ± 0.006
455	1.000 ± 0.000	1.000 ± 0.000	1.000 ± 0.000
460	0.906 ± 0.003	0.913 ± 0.006	0.873 ± 0.006
465	0.814 ± 0.005	0.825 ± 0.005	0.785 ± 0.007
470	0.790 ± 0.005	0.797 ± 0.009	0.750 ± 0.005
475	0.734 ± 0.007	0.740 ± 0.008	0.688 ± 0.006
480	0.570 ± 0.006	0.573 ± 0.006	0.524 ± 0.007
485	0.460 ± 0.006	0.459 ± 0.005	0.413 ± 0.006
490	0.393 ± 0.005	0.397 ± 0.004	0.353 ± 0.005
495	0.332 ± 0.005	0.332 ± 0.004	0.299 ± 0.006
500	0.283 ± 0.005	0.281 ± 0.004	0.243 ± 0.004
505	0.271 ± 0.004	0.264 ± 0.004	0.236 ± 0.004
510	0.257 ± 0.006	0.250 ± 0.005	0.220 ± 0.005
515	0.235 ± 0.005	0.226 ± 0.004	0.195 ± 0.005
520	0.201 ± 0.005	0.194 ± 0.003	0.172 ± 0.004
525	0.170 ± 0.005	0.166 ± 0.002	0.140 ± 0.003
530	0.149 ± 0.005	0.144 ± 0.002	0.123 ± 0.003
535	0.129 ± 0.005	0.123 ± 0.003	0.112 ± 0.004
540	0.110 ± 0.004	0.106 ± 0.003	0.088 ± 0.003

Table 2a: Values for Figure 4.3, Average ± 1 Standard Error.

Wavelength [nm]	LEC-0 A	LEC-0 D	LEC-1 A	LEC-1 D
375	0.008 ± 0.001	0.006 ± 0.002	-0.0007 ± 0.0003	0.0006 ± 0.0009
380	0.011 ± 0.002	0.008 ± 0.002	-0.0010 ± 0.0003	0.0008 ± 0.0010
385	0.017 ± 0.003	0.012 ± 0.003	-0.0015 ± 0.0004	0.0004 ± 0.0011
390	0.029 ± 0.005	0.020 ± 0.005	-0.0030 ± 0.0006	-0.0001 ± 0.0014
395	0.038 ± 0.006	0.026 ± 0.005	-0.0039 ± 0.0008	-0.0008 ± 0.0013
400	0.043 ± 0.006	0.030 ± 0.005	-0.0041 ± 0.0008	-0.0015 ± 0.0013
405	0.047 ± 0.007	0.033 ± 0.005	-0.0047 ± 0.0009	-0.0026 ± 0.0011
410	0.049 ± 0.007	0.034 ± 0.005	-0.0042 ± 0.0008	-0.0029 ± 0.0008
415	0.050 ± 0.007	0.035 ± 0.005	-0.0044 ± 0.0009	-0.0029 ± 0.0007
420	0.057 ± 0.007	0.040 ± 0.005	-0.0048 ± 0.0009	-0.0040 ± 0.0007
425	0.068 ± 0.008	0.049 ± 0.006	-0.0055 ± 0.0011	-0.0041 ± 0.0009
430	0.082 ± 0.009	0.059 ± 0.007	-0.0063 ± 0.0013	-0.0055 ± 0.0011
435	0.095 ± 0.010	0.068 ± 0.008	-0.0077 ± 0.0016	-0.0057 ± 0.0013
440	0.109 ± 0.011	0.077 ± 0.008	-0.0084 ± 0.0018	-0.0065 ± 0.0014
445	0.121 ± 0.011	0.085 ± 0.009	-0.0089 ± 0.0019	-0.0064 ± 0.0018
450	0.129 ± 0.012	0.089 ± 0.009	-0.0081 ± 0.0018	-0.0067 ± 0.0018
455	0.132 ± 0.012	0.090 ± 0.009	-0.0080 ± 0.0018	-0.0062 ± 0.0019
460	0.120 ± 0.010	0.080 ± 0.008	-0.0063 ± 0.0017	-0.0043 ± 0.0017
465	0.109 ± 0.010	0.072 ± 0.007	-0.0048 ± 0.0015	-0.0039 ± 0.0014
470	0.106 ± 0.009	0.069 ± 0.007	-0.0039 ± 0.0016	-0.0031 ± 0.0013
475	0.099 ± 0.008	0.064 ± 0.006	-0.0031 ± 0.0014	-0.0020 ± 0.0014
480	0.077 ± 0.007	0.049 ± 0.005	-0.0017 ± 0.0011	-0.0018 ± 0.0012
485	0.062 ± 0.005	0.039 ± 0.004	-0.0009 ± 0.0008	-0.0011 ± 0.0010
490	0.053 ± 0.005	0.033 ± 0.003	-0.0006 ± 0.0008	-0.0008 ± 0.0007
495	0.045 ± 0.004	0.028 ± 0.003	-0.0003 ± 0.0007	-0.0006 ± 0.0006
500	0.039 ± 0.004	0.023 ± 0.002	0.0001 ± 0.0007	-0.0005 ± 0.0005
505	0.037 ± 0.003	0.022 ± 0.002	0.00004 ± 0.0006	-0.0004 ± 0.0005
510	0.036 ± 0.003	0.021 ± 0.002	0.0005 ± 0.0006	-0.0003 ± 0.0005
515	0.032 ± 0.003	0.018 ± 0.002	0.0003 ± 0.0005	-0.0004 ± 0.0004
520	0.028 ± 0.003	0.016 ± 0.002	0.0003 ± 0.0005	-0.0004 ± 0.0004
525	0.023 ± 0.002	0.014 ± 0.001	0.00005 ± 0.0004	-0.0002 ± 0.0004
530	0.021 ± 0.002	0.012 ± 0.001	0.0002 ± 0.0003	-0.0001 ± 0.0004
535	0.018 ± 0.002	0.010 ± 0.001	0.0001 ± 0.0004	-0.0002 ± 0.0003
540	0.015 ± 0.002	0.008 ± 0.001	-0.0002 ± 0.0003	-0.0002 ± 0.0002

Table 2b: Values for Figure 4.3 Continued, Average ± 1 Standard Error.

Wavelength [nm]	LEC-2		LEC-3	
	A	D	A	D
375	0.002 ± 0.000	0.002 ± 0.001	-0.0005 ± 0.0003	0.0003 ± 0.0004
380	0.003 ± 0.000	0.002 ± 0.001	-0.0002 ± 0.0001	0.0003 ± 0.0004
385	0.004 ± 0.001	0.003 ± 0.001	-0.0006 ± 0.0002	0.0000 ± 0.0004
390	0.006 ± 0.001	0.005 ± 0.001	-0.0009 ± 0.0001	0.0002 ± 0.0005
395	0.008 ± 0.001	0.005 ± 0.001	-0.0011 ± 0.0003	-0.0002 ± 0.0005
400	0.009 ± 0.001	0.006 ± 0.001	-0.0012 ± 0.0003	-0.0004 ± 0.0005
405	0.009 ± 0.001	0.006 ± 0.001	-0.0014 ± 0.0002	-0.0008 ± 0.0004
410	0.009 ± 0.001	0.006 ± 0.001	-0.0010 ± 0.0002	-0.0008 ± 0.0002
415	0.009 ± 0.001	0.007 ± 0.001	-0.0011 ± 0.0003	-0.0007 ± 0.0003
420	0.010 ± 0.001	0.007 ± 0.001	-0.0015 ± 0.0003	-0.0012 ± 0.0003
425	0.012 ± 0.001	0.009 ± 0.001	-0.0013 ± 0.0004	-0.0010 ± 0.0003
430	0.015 ± 0.002	0.010 ± 0.001	-0.0012 ± 0.0004	-0.0015 ± 0.0003
435	0.017 ± 0.002	0.013 ± 0.001	-0.0016 ± 0.0005	-0.0011 ± 0.0004
440	0.019 ± 0.002	0.014 ± 0.002	-0.0018 ± 0.0006	-0.0016 ± 0.0004
445	0.021 ± 0.002	0.016 ± 0.002	-0.0021 ± 0.0007	-0.0014 ± 0.0007
450	0.022 ± 0.002	0.016 ± 0.002	-0.0021 ± 0.0006	-0.0018 ± 0.0005
455	0.023 ± 0.002	0.017 ± 0.002	-0.0018 ± 0.0006	-0.0011 ± 0.0006
460	0.021 ± 0.002	0.014 ± 0.001	-0.0015 ± 0.0006	-0.0009 ± 0.0006
465	0.019 ± 0.002	0.013 ± 0.001	-0.0014 ± 0.0005	-0.0009 ± 0.0005
470	0.018 ± 0.002	0.012 ± 0.001	-0.0013 ± 0.0006	-0.0010 ± 0.0004
475	0.017 ± 0.002	0.012 ± 0.001	-0.0011 ± 0.0005	-0.0008 ± 0.0004
480	0.013 ± 0.001	0.009 ± 0.001	-0.0009 ± 0.0004	-0.0008 ± 0.0004
485	0.011 ± 0.001	0.007 ± 0.001	-0.0006 ± 0.0003	-0.0006 ± 0.0003
490	0.009 ± 0.001	0.006 ± 0.001	-0.0006 ± 0.0002	-0.0004 ± 0.0002
495	0.008 ± 0.001	0.005 ± 0.001	-0.0004 ± 0.0002	-0.0003 ± 0.0002
500	0.007 ± 0.001	0.0042 ± 0.0004	-0.0005 ± 0.0003	-0.0004 ± 0.0002
505	0.007 ± 0.001	0.0043 ± 0.0004	-0.0004 ± 0.0002	-0.0005 ± 0.0002
510	0.007 ± 0.001	0.0039 ± 0.0004	-0.0001 ± 0.0002	-0.0004 ± 0.0002
515	0.006 ± 0.001	0.0034 ± 0.0004	-0.0003 ± 0.0002	-0.0004 ± 0.0002
520	0.005 ± 0.001	0.0030 ± 0.0003	-0.0002 ± 0.0002	-0.0005 ± 0.0002
525	0.004 ± 0.001	0.0024 ± 0.0003	-0.0003 ± 0.0001	-0.0002 ± 0.0001
530	0.0038 ± 0.0004	0.0023 ± 0.0001	-0.0001 ± 0.0002	0.0000 ± 0.0002
535	0.0032 ± 0.0003	0.0021 ± 0.0002	-0.0003 ± 0.0002	-0.0002 ± 0.0001
540	0.0026 ± 0.0003	0.0016 ± 0.0002	-0.0004 ± 0.0001	-0.0001 ± 0.0001

Table 2c: Values for Figure 4.3 Continued, Average ± 1 Standard Error.

Wavelength [nm]	LEC-4 A	LEC-4 D
375	0.0009 ± 0.0002	0.0007 ± 0.0002
380	0.0008 ± 0.0001	0.0007 ± 0.0003
385	0.0012 ± 0.0002	0.0009 ± 0.0003
390	0.0020 ± 0.0003	0.0016 ± 0.0004
395	0.0025 ± 0.0004	0.0018 ± 0.0005
400	0.0029 ± 0.0005	0.0020 ± 0.0005
405	0.0030 ± 0.0004	0.0020 ± 0.0004
410	0.0031 ± 0.0004	0.0019 ± 0.0004
415	0.0030 ± 0.0004	0.0023 ± 0.0003
420	0.0030 ± 0.0005	0.0024 ± 0.0004
425	0.0040 ± 0.0005	0.0030 ± 0.0004
430	0.0047 ± 0.0006	0.0033 ± 0.0004
435	0.0053 ± 0.0006	0.0042 ± 0.0005
440	0.0059 ± 0.0006	0.0043 ± 0.0005
445	0.0065 ± 0.0006	0.0047 ± 0.0004
450	0.0067 ± 0.0007	0.0046 ± 0.0007
455	0.0071 ± 0.0007	0.0054 ± 0.0005
460	0.0067 ± 0.0006	0.0047 ± 0.0005
465	0.0058 ± 0.0006	0.0040 ± 0.0004
470	0.0057 ± 0.0005	0.0040 ± 0.0005
475	0.0053 ± 0.0006	0.0036 ± 0.0004
480	0.0043 ± 0.0004	0.0026 ± 0.0003
485	0.0036 ± 0.0003	0.0022 ± 0.0003
490	0.0031 ± 0.0003	0.0019 ± 0.0002
495	0.0027 ± 0.0003	0.0017 ± 0.0002
500	0.0022 ± 0.0002	0.0013 ± 0.0002
505	0.0022 ± 0.0002	0.0013 ± 0.0002
510	0.0022 ± 0.0003	0.0012 ± 0.0002
515	0.0018 ± 0.0002	0.0010 ± 0.0002
520	0.0018 ± 0.0002	0.0008 ± 0.0002
525	0.0014 ± 0.0002	0.0007 ± 0.0001
530	0.0013 ± 0.0001	0.0008 ± 0.0001
535	0.0011 ± 0.0002	0.0006 ± 0.0001
540	0.0009 ± 0.0001	0.0004 ± 0.0001

APPENDIX E: Results of the Lilliefors Normality Test

Table 1: Results form Lilliefors Normality Test for Normal A and Normal D Tissue.

Wavelength	Intgr. Inten.		Lifetime		LEC-0		LEC-1		LEC-2		LEC-3		LEC-4	
[nm]	A	D	A	D	A	D	A	D	A	D	A	D	A	D
375	1	0	0	0	1	1	0	1	1	1	1	1	1	1
380	0	1	0	0	1	1	1	1	1	1	0	1	0	1
385	1	0	1	1	1	1	0	1	1	1	0	1	1	1
390	1	1	0	0	1	1	1	1	1	1	0	1	1	1
395	1	0	0	0	1	1	1	1	1	1	0	1	1	1
400	1	0	0	0	1	1	1	1	1	1	0	1	1	1
405	0	0	0	0	0	1	1	1	1	1	1	1	1	1
410	0	0	0	0	0	1	1	0	1	1	1	1	1	1
415	0	0	0	0	0	1	1	0	0	1	1	0	1	0
420	0	0	0	0	0	1	0	0	0	1	0	0	1	0
425	0	0	0	0	0	1	0	0	0	1	1	0	0	0
430	0	0	0	0	0	1	1	0	0	0	1	1	0	0
435	0	0	1	0	0	1	1	1	0	0	1	1	1	0
440	0	0	0	0	0	1	1	1	0	0	1	1	0	0
445	0	0	0	0	0	1	1	1	0	1	1	1	1	0
450	0	0	0	1	0	1	1	1	0	0	1	1	0	0
455	0	0	0	0	0	1	1	1	1	1	1	1	1	1
460	0	0	0	0	0	1	1	1	0	0	1	1	0	1
465	0	1	0	0	0	1	1	1	1	1	1	1	1	1
470	0	1	0	0	0	1	1	1	1	0	1	0	1	1
475	0	0	0	0	0	1	1	0	0	1	1	0	0	1
480	0	1	0	1	0	1	1	1	1	1	0	1	0	1
485	0	0	0	1	0	1	1	1	0	0	1	1	1	0
490	0	0	0	0	0	1	1	1	0	1	0	0	0	0
495	0	0	0	0	0	1	1	1	1	1	0	0	1	0
500	0	0	1	0	0	1	1	1	1	1	0	0	1	1
505	1	0	0	1	0	1	0	1	0	1	0	0	0	1
510	0	1	0	0	0	1	0	1	1	0	0	0	1	0
515	1	0	0	0	0	1	0	0	1	1	0	0	0	1
520	0	0	0	0	1	1	1	1	1	1	0	1	1	0
525	0	0	0	0	1	1	0	1	1	1	0	0	0	1
530	0	0	0	0	1	1	0	1	1	0	0	0	1	0
535	0	0	0	1	1	1	0	1	0	0	1	1	1	0
540	0	0	1	0	0	1	1	1	0	0	0	1	0	1

If H_o is true then H = 0, otherwise H = 1 when the test rejects that the data sampled follow a normal distribution.

APPENDIX F: Matlab Code for K-means Classification Using GI Data

Fireaway_3.m

```
%% Parameters (P1 & P2) are loaded and sent to the function GIKmeans_6.m
if they both failed the rank-sum test. The k-means results from all the
possible combinations are saved into a single file at the end.

close all
clear all

load results_ranksum_spec.mat h_all
P1=h_all;
P1_name='I';
load all_spec_thesis.mat
xA=tissueA.spec_intgr_norm;
xD=tissueD.spec_intgr_norm;

load results_ranksum_lift.mat h_all
P2=h_all;
P2_name='Lifetime';
load all_lifet_thesis.mat
yA=tissueA.lifet;
yD=tissueD.lifet;

%% Use for loading file names containing LEC.
%
% for L=0 %or 0:4
%     f1=strcat('results_ranksum_cc_',int2str(L));
%     load(f1)
%     P1=h_all;
%     P1_name=strcat('LEC-',int2str(L));
%
%     f2=strcat('all_cc_',int2str(L),'_thesis.mat');
%     load(f2)
%     xA=tissueA.lag_cc;
%     xD=tissueD.lag_cc;
%
%     %for k=L:4 %don't repeat 0-1 and 1-0 etc., j=1:35.
%     k=L; %use when j=i:35
%         f3=strcat('results_ranksum_cc_',int2str(k));
%         load(f3)
%         P2=h_all;
%         P2_name=strcat('LEC-',int2str(k));
%
%         f4=strcat('all_cc_',int2str(k),'_thesis.mat');
%         load(f4)
%         yA=tissueA.lag_cc;
%         yD=tissueD.lag_cc;

%% Code is the same for all parameter types.
```

```
outfile=strcat(P2_name,'_vs_',P1_name,'_all.mat')
W=[370:5:550];
results_all=[];
labels_all=[];
Centers_all=[];
true_false_all=[];
km_results_all=[];
starts_all=[];

 for i=2:35
        if P1(i) == 1
            temp_xA=xA(:,i);
            temp_xD=xD(:,i);
            P1_w=num2str(W(i));

            %for j=2:35 %use when P1 and P2 files are different
            for j=i:35 %don't repeat 2-35 and 35-2 etc.
                if P2(j) == 1
                    temp_yA = yA(:,j);
                    temp_yD = yD(:,j);
                    P2_w=num2str(W(j));

[starts,true_false,Centers,km_results,results,labels] =
      GIKmeans_6(P1_w, P1_name, P2_w, P2_name, temp_xA, ...
                                temp_yA, temp_xD, temp_yD,j);

                    pause(1)
                    close all

                    results_all=[results_all; results];
                    labels_all=[labels_all; labels];
                    Centers_all=[Centers_all; Centers];
                    true_false_all=[true_false_all; true_false];
                    km_results_all=[km_results_all; km_results];
                    starts_all=[starts_all; starts];

                end % P2(j)==1
            end %for j=2:35
        end %if P1(i)==1
end% for i=2:35

save(outfile, 'results_all', 'labels_all', 'Centers_all',...
    'true_false_all', 'km_results_all', 'starts_all')
close all

%    end %for k=0:4   %% end loop for a LEC file names as P2
%L=L+1;
%end %for L=0:4       %% end loop for a LEC file names as P1
```

END Fireaway_3.m

GIKmeans_6.m

```
%% Data from P1 & P2 are received and are used to conduct K-means
classification. The sensitivity and specificity are then calculated. The
before and after clustering results are plotted and saved while the
results are passed back to Fireaway_3.m.


function [starts, true_false,Centers,km_results,results,labels] =
GIKmeans_6(P1_W, P1_name, P2_W,...
    P2_name, temp_xA, temp_yA, temp_xD, temp_yD,J)


%% labels for plots
temp_P1=([P1_name,' (',P1_W,')']);
temp_P2=([P2_name,' (',P2_W,')']);

x_name=([temp_P1,' [a.u.]']);
y_name=([temp_P2,' [a.u.]']);
name_A='Tissue A';
name_D='Tissue D';

% label_1=strcat('L_',P1_W);
% label_2=strcat('L_',P2_W);
label_1=strcat(P1_name,'_',P1_W);
label_2=strcat(P2_name,'_',P2_W);


%% setup data in format required for kmeans.m
W=[370:5:550];

[m,n]=size(temp_xA);
[j,k]=size(temp_xD);

GROUP=[repmat(name_A,[m 1]); repmat(name_D,[n 1])];

XY= [temp_xA temp_yA ; temp_xD temp_yD];

k=size(XY,2); %# of columns in XY=# of clusters

%% run K-means using the average P1 and average P2
kmean1=[mean(temp_xA) mean(temp_yA)];
kmean2=[mean(temp_xD) mean(temp_yD)];

SPTS=[kmean1; kmean2];

opts = statset('Display','off');

[idx,C,SUMD,D] = kmeans(XY,k,'Distance','sqEuclidean',...
    'start',SPTS,'Options',opts);
```

```
% %% run K-means with random starting points
%
% rep=5; % picks 5 random sets, selects best answer as final result
%
% for i=1:rep
%     kmean1=XY(randsample((1:m),1),:); % 1st kmean from A
%     kmean2=XY(randsample((m+1:m+j),1),:); % 2nd kmean from D
%     start_means=[kmean1; kmean2];%
%     SPTS(:,:,i)=[kmean1; kmean2];%
% end %for
%
% %disp(SPTS)
% %opts = statset('Display','iter'); % or 'final'.
%
% [idx,C,SUMD,D] = kmeans(XY,k,'Distance','sqEuclidean',...
%     'start',SPTS,'Options',opts);
%

%% Sensitivity and Specificity Calculations

% Let A (or parameter 1) be the True Positive.
A1=0; % A1 = # of sample 1's belonging to cluster 1, True +ve
A2=0; % A2 = # of sample 1's belonging to cluster 2, Flase -ve
D1=0; % D1 = # of sample 2's belonging to cluster 2, True -ve
D2=0; % D2 = # of sample 2's belonging to cluster 1, False +ve

 for w=1:m
    if idx(w)==1
        A1=A1+1; % true +ve
    else
        A2=A2+1; % false -ve
    end
 end

 % for the second half of "idx" belonging to sample 2.
 for w=m+1:m+j
     if idx(w)==2
         D1=D1+1;  % true -ve
     else
         D2=D2+1;  % false +ve
     end
 end

sens_A=A1/(A1+A2)*100; % sensitivity for A=tp/(tp+fn) i.e. portion of
                       % A's correctly idetified as As.
specif_A=D1/(D1+D2)*100; % specificity for A= tn/(tn+fp) i.e. portion of
                         % D's correctly identifed as D's
% measures of performance are
pos_rate=A1/(A1+D2)*100; %positive predictor value for the tp/(tp+fp)
neg_rate=D1/(D1+A2)*100; %tn/(tn+fn), the negative rate is the portion
      %of the negative tests found that are actually true negatives.
```

```
%% PLOTTING

% if (sens_A >=90 && specif_A >=90)%% || (sens_A >=93 && specif_A >=87)
pos1=[0.1 0.15 0.37 0.715]; % horizontal
pos2=[0.58 0.15 0.37 0.715]; % horizontal
pos3=[200 200 720 325];% for Matlab v.2010
figure(J)
% plot A and D categorized from histology
subplot(1,2,1,'Position',pos1)
     plot(temp_xA, temp_yA, 'b^','MarkerSize',5)
        hold on
    plot(temp_xD, temp_yD,'r.','MarkerSize',12)
        v=axis;
            %gscatter(XY(:,1),XY(:,2),GROUP,'br','^*',5);
        xlabel(x_name,'Interpreter','none');
        ylabel(y_name,'Interpreter','none');
%        legend(name_A,name_D,'Location','NorthEast')
%            set(legend,'FontSize',8,'Interpreter','None')
        title([temp_P2,' vs. ',temp_P1]);
        box('on');
% plot A and D categorized by K-means
subplot(1,2,2,'Position',pos2)
    plot(XY(idx==1,1),XY(idx==1,2),'b^','MarkerSize',5)
        hold on
    plot(XY(idx==2,1),XY(idx==2,2),'r.','MarkerSize',12)
    plot(C(:,1),C(:,2),'kx','MarkerSize',10,'LineWidth',2)
    plot(C(:,1),C(:,2),'ko','MarkerSize',10,'LineWidth',2)
        xlabel(x_name);
        ylabel(y_name);
%        legend(name_A,name_D,'K-Mean','Location','NorthEast')
%            set(legend,'FontSize',8,'Interpreter','None')
        title([name_A,'  SN = ',num2str(sens_A,3),...
                  '%  SP = ',num2str(specif_A,3),'%']);
        %set(gca, 'Xlim', [v(1) v(2)], 'Ylim', [v(3) v(4)]);
        axis(v)
        set(gcf, 'Position', pos3);

pause(1) %pause 1 sec. so video card can catch up

outname=strcat(label_1,'_',label_2,'__',num2str(sens_A,3),'_',...
      num2str(specif_A,3),'.bmp');

saveas(figure(J), outname, 'bmp')

results= [sens_A specif_A pos_rate neg_rate];
labels=[{label_1} {label_2}];
km_results=struct('idx',idx,'kmeans_centroids',C,'SUMD',SUMD,'D',D);
Centers=[C(1,1) C(1,2) C(2,1) C(2,2)];
true_false=[A1 A2 D1 D2];
starts=[SPTS(1,1) SPTS(1,2) SPTS(2,1) SPTS(2,2)];


END GIKmeans_6.m
```